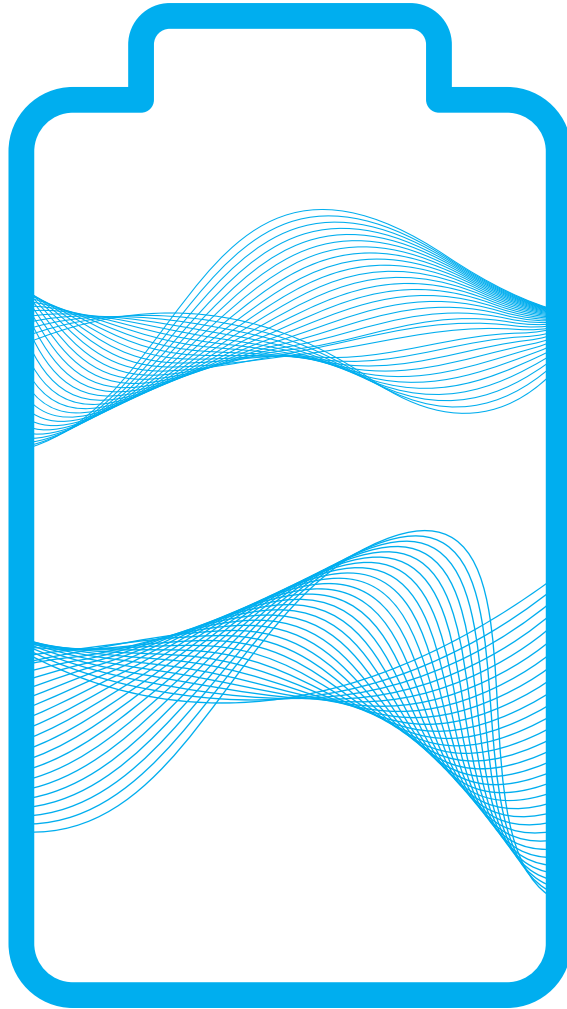


QUANTUM BATTERY IMPLEMENTATION

On the Quantum Inspire platform



Author: Milou van Nederveen
Supervisor: dr. Miriam Blaauboer
Master thesis, February 2024

QUANTUM BATTERIES

THE IMPLEMENTATION OF A QUANTUM BATTERY ON THE
QUANTUM INSPIRE PLATFORM



Department of Quantum Nanoscience
Opening the quantum world for innovation

Master Thesis

Submitted to the
Delft University of Technology
on February 7, 2024

for the purpose of obtaining the degree of Master of Science

to be defended publicly on
February 14, 2024 at 10:30 AM

by

Milou VAN NEDERVEEN

Thesis committee:

Dr. Miriam Blaauboer,	Delft University of Technology, <i>supervisor</i>
Dr. Christian Andersen,	Delft University of Technology
Dr. Stephan Eijt,	Delft University of Technology

An electronic copy of this master thesis is available at

<https://repository.tudelft.nl/>.

The code and data of this master thesis are available at

<https://github.com/mvannederveen/quantum-battery-thesis>.

ACKNOWLEDGEMENTS

The thesis that is lying in front of you embarks on the end of my journey as a student, which I started at the University College Twente in Enschede, continued as an exchange student at the University of New South Wales in Sydney, and am now graduating as an Applied Physics master student at the TU Delft.

First and foremost, I want to express my gratitude for the guidance and support of dr. Miriam Blaauboer during this project. Aside from being a knowledgeable expert in this field, you truly have been a mentor to me, who gave me inspiration, support and motivation. Our weekly meetings were always moments to look forward to, where our lively discussions often led to new insights. This helped a lot with pushing the content of this project, and also always keeping the joy in doing so. It is my goal to follow in your footsteps and attain both your deep understanding of physics and your kindness towards the humans around you.

I want to thank my family, who have always supported me in exploring what I am passionate about. I am blessed to have such incredible parents, Gea Lentz and Sander van Nederveen, and the best brother one could ask for, Jord van Nederveen. Thank you for supporting me in this journey, and for being there for me through all the phases.

I also want to thank all of my teachers from my bachelor the University College Twente for teaching me to take risks and always go for 'it'. Ruud van Damme and Jennifer Herek, a special thank you for your support and guidance in becoming a physicist as a university college student. In very unique ways, you are both big inspirations to me. My appreciation also goes to the teachers of the master of Applied Physics - for teaching me with your in-depth understanding of physics.

This thesis challenged me to combine my interest in more fundamental theoretical physics with real systems - which I believe to be very important for making an impact in the real world. I want to thank Giuseppe Ruggero Di Carlo for all his help with Quantum Inspire, it has truly added a lot to this thesis.

I would like to extend my appreciation to dr. Christian Andersen and dr. Stephan Eijt, I am honoured to have both of you on my committee, and want to thank you for taking the time to evaluate this thesis.

I want to acknowledge Giulia Gemme for her elaborate answers to my questions about her publications, Mert Bozkurt for our discussions on quantum thermodynamics, and Max Werninghaus & Ricard Ravell for answering my questions about their work on Quantum Optimal Control. Camille de Valk, thank you for teaching me the skills of Qiskit during my internship at Capgemini, this has been one of the main pillars for getting started with this project.

I am incredibly grateful for the friends I have made along the way and the friends that have stuck with me since even before. Thank you to every single one of you. To all my friends from Delft, Enschede, Australia, Austria, Portugal - and anywhere in between.

Thank you for always believing in me, reminding me of my potential during moments of doubt, and for the endless joy in the meantime. Xenia Una Mainelli & Natasha Birari, from our Aquarium study sessions to our shared journey to Delft, both of you have been invaluable to me. Living with my current housemate, Alycia Danckaarts, has been a true blessing during this thesis. Thank you for the good and positive energy in the house, for always helping and supporting me when I need it, and for all of our crazy funny moments. Jess Thomson, thank you for our endless voice message conversations during the time of this thesis, which kept me reflecting and moving forward. Tessa Küppers, Linde Holwerda and Emily van Beek, our friendships go way back, and I feel such gratitude that you are still in my life - and shall continue to be. Smit Chaudhary and Yannik Wotte, our shared curiosity about physics and the resulting discussions have always helped me stay inspired and passionate about it.

And last but not least, I want to thank you - for reading this thesis! Your interest in my work means a lot to me, and I hope you find the content interesting and engaging. I am always available for further questions or discussions. Enjoy reading!

Milou van Nederveen
Delft, February 2024

ABSTRACT

Quantum Batteries (QBs) are quantum-mechanical devices for energy storage, gaining interest due to a potential quantum advantage in power. Recently, the first experimental implementations of QBs were realised. This study characterises the superconducting transmon qubits of Starmon-5 as QBs using the Quantum Inspire platform. In addition to direct charging of a QB, our focus is on charger-mediated energy transfer and parallel charging of an array of transmon qubits. The figures of merit include the average stored energy, the charging time and the charging power.

The results from direct charging of the qubits align with existing literature. Charger-mediated energy transfer is demonstrated through the characterisation of the CNOT gate as an interaction gate, gaining the same amount of stored energy, but with a significant increase in the charging time, resulting in a lower charging power. Furthermore, our findings demonstrate that parallel charging of an array of qubits preserves the quality of direct charging of the individual qubits.

To our knowledge, this work presents the first results of charger-mediated energy transfer in real quantum devices. Charger-mediated energy transfer can be interesting for specific applications such as quantum metrology, where preserving the quantum state is critical. Additionally, this is the first demonstration of parallel charging of superconducting transmon qubits in the QB context, giving promising results for the scalability of superconducting transmon qubits as QB. Our study paves the way forward to implementing quantum batteries for energy management in quantum technologies, a near-term future application of quantum batteries.

CONTENTS

Acknowledgements	iii
Abstract	v
Nomenclature	xi
List of Symbols	xiii
1. Introduction	1
1.1. Background and Relevance	1
1.2. State-of-the-art	2
1.3. Research goals	4
1.4. Thesis structure	5
2. Theoretical Background	7
2.1. Quantum Thermodynamics	7
2.1.1. Work Extraction	7
2.1.2. Ergotropy and passive states	8
2.1.3. Charging, storage, and transfer of energy	9
2.2. Quantum Battery	10
2.2.1. One quantum system	10
2.2.2. An array of n quantum systems	10
2.2.3. Entanglement boost of power	11
2.2.4. Faster charging: global versus local charging	13
2.2.5. Quantum advantage	15
2.2.6. Role of interaction order	15
2.3. Transmon Theory	17
2.3.1. Superconducting transmon qubits	17
2.3.2. Circuit Quantum Electrodynamics	20
2.4. Charging Protocols	22
2.4.1. Direct charging	22
2.4.2. Charger-mediated energy transfer	23
2.5. Optimal Charging	26
2.5.1. Pulse design	26
2.5.2. Quantum optimal control	26
2.6. Figures of merit	29
3. Quantum Battery implementation on the Quantum Inspire	31
3.1. Starmon-5 in Quantum Inspire	31

3.2.	Quantum battery framework	32
3.3.	Charging via RX gate	33
3.4.	Quantum battery implementation	34
3.5.	Charging of q0, q1, q2, q3, q4	35
3.6.	Figures of merit	36
3.7.	Discussion	36
4.	Charger-mediated energy transfer in Quantum Inspire	39
4.1.	Charger mediated energy transfer framework	39
4.2.	CNOT gate for energy transfer	40
4.3.	Charger-mediated energy transfer implementation	42
4.4.	Figures of merit	43
4.5.	Discussion	44
5.	Charging of multiple qubits	47
5.1.	Parallel charging	47
5.1.1.	Parallel charging framework	47
5.1.2.	Parallel charging using RX gates	48
5.1.3.	Parallel charging implementation	48
5.1.4.	Figures of merit	48
5.1.5.	Discussion	50
5.2.	Collective charging	52
5.2.1.	Nearest-neighbour coupling	52
5.2.2.	Multi-qubit coupling	53
6.	Conclusions and Outlook	55
6.1.	Conclusion	55
6.2.	Future Outlook	55
A.	Modular pulse shape compared to the RX gate the IBM Quantum Platform	69
A.1.	Motivation	69
A.2.	Results	69
B.	Towards optimising the charging pulse of a quantum battery	73
B.1.	State-to-state transfer	73
C.	Code and circuits	77
C.1.	Qiskit, Quantum Inspire, and IBM Quantum	77
C.2.	Direct charging of a single QB in Quantum Inspire	78
C.2.1.	Packages	79
C.2.2.	Functions	79
C.2.3.	Code	80
C.2.4.	Circuit	81
C.2.5.	Data plot	82
C.2.6.	Data Analysis	83
C.2.7.	Fitting the data	84

C.3. Charger-mediated energy transfer in Quantum Inspire	85
C.3.1. Code	85
C.3.2. Circuit	86
C.4. Parallel charging in Quantum Inspire	86
C.4.1. Code	87
C.4.2. Circuit	88
C.5. Modular pulse shaping compared to the Rx gate on the IBM Quantum Plat- form	89
C.5.1. RX Gate	89
C.5.2. Modular Pulse Shape	90
C.6. Optimisation of state-to-state transfer on IBM Brisbane	93
C.6.1. Optimisation	94
C.6.2. Implementation on IBM Quantum Platform	98
D. Data	99
D.1. Direct charging of a single QB	99
D.2. Charger-mediated energy transfer	103
D.3. Parallel charging	105
D.4. Modular pulse shaped and RX gate on IBM Mumbai	107
D.5. Optimised pulse on IBM Brisbane	107

NOMENCLATURE

- CNOT** Controlled-NOT gate
- CZ** Controlled-Z gate
- MNR** Metric-Noise-Resource
- NISQ** Noisy Intermediate-Scale Quantum era
- QB** Quantum Battery
- QED** Quantum Electrodynamics
- QEI** Quantum Energy Initiative
- QHO** Quantum Harmonic Oscillator
- QOC** Quantum Optimal Control
- QSL** Quantum Speed Limit
- RES** Renewable Energy Sources
- TLS** Two-Level-System

Operators are denoted with a hat $\hat{}$ on top of the symbol.

The Pauli-X, -Y, and -Z matrices denote a π rotation around the respective axis. The convention is shown below.

$$X = \hat{\sigma}_x = \begin{bmatrix} 0 & 1 \\ 1 & 0 \end{bmatrix}, \quad Y = \hat{\sigma}_y = \begin{bmatrix} 0 & -i \\ i & 0 \end{bmatrix}, \quad Z = \hat{\sigma}_z = \begin{bmatrix} 1 & 0 \\ 0 & -1 \end{bmatrix}$$

LIST OF SYMBOLS

E_s	Stored Energy (eV)
g	Coupling constant between qubit and modes of the external field
\hat{H}	Hamiltonian
J	Nearest-neighbour coupling constant
P_c	Charging Power (eV/ms)
\hat{V}	External drive field, potential field
Γ	Quantum advantage in power
Δ	Energy level splitting (eV)
θ	Angle (rad)
λ	Classical control parameter of external field, pulse shape
$\hat{\rho}$	Density matrix, quantum state, active state
$\hat{\rho}^*$	Maximally active state
$\hat{\sigma}_\rho$	Passive state
τ	Charging time (ns)
ψ	Wave function
ω_0	Resonance frequency (GHz)
$\hat{\omega}_\beta$	Gibbs state
\hbar	Reduced Planck constant, $\hbar = \frac{h}{2\pi}$ (1.054·10 ⁻³⁴ J·s)
\mathcal{W}	Ergotropy (eV)

1

INTRODUCTION

1.1. BACKGROUND AND RELEVANCE

Imagine the smallest and most fundamental battery in the universe. Quantum Batteries (QBs) are quantum mechanical systems that can be used for the storage and transfer of energy [1]. At this scale, quantum phenomena such as superposition, entanglement and interference start playing a non-trivial role [2]. Due to their quantum nature, QBs hold great promise for faster charging and work extraction, offering a quantum advantage over their classical counterparts [1, 3, 4].

There are several reasons to study QBs. Firstly, the study of QBs offers insights into quantum thermodynamics, increasing our understanding of the laws of thermodynamics at the quantum scale. Secondly, the size of electronic devices is ever-decreasing, adhering to Moore's law. This is approaching the quantum scale, making it important to understand the functioning of QBs for miniature technologies. Thirdly, QBs hold promise for improving future battery technologies. This can have a wide range of applications in different devices, from medical devices and phone batteries to electric vehicles. It is particularly important for tackling the climate crisis. Energy storage systems are a key element in the global energy transition, where Renewable Energy Sources (RES) like wind and solar energy face challenges due to fluctuations in production. This is relevant for Sustainable Development Goal 7: ensuring access to affordable, reliable, sustainable and modern energy for all [5].

The quantum advantage of power is confined to operating at the quantum scale. This restricts the practical application of QBs in daily technologies due to two major reasons. First of all, the typical energy scale where quantum phenomena come into play is the order of $\sim eV$, which is extremely small. More concretely, this means you would require the energy of about 10^{23} QBs to fully charge the battery of an everyday smartphone. Secondly, to use the effects of quantum phenomena, the quantum system must be completely protected from any external noise to avoid any decoherences. This requires cooling the system down to temperatures near absolute zero¹. The necessary cryogenic fridge has substantial energy costs, which poses a

¹Currently, room temperature quantum computers are being explored as well. Examples include photonic qubits [6], neutral atoms [7], and nitrogen-vacancy (NV) centres in diamond [8]. Although these hardware platforms each have their challenges to overcome, choosing room-temperature

concern for sustainability [9]. Hence, it is important to clarify that the quantum advantage shown in QBs does not result in a direct enhancement of everyday batteries.

Instead, a near-term application of QBs is energy management in quantum technologies, reducing their energy cost. Operations at the quantum level can have a major effect on the macroscopic energy cost [10]. For example, implementing a single-gate operation involves not just the microwave pulse that implements the qubit rotation. Instead, it also involves the energy cost of the classical computer, the control electronics, and the translation of the signal [10]. Hence, it can be expected that reducing energy consumption at the quantum level has a major impact on the macroscopic resource cost as well. In line with this, QBs can be useful for managing energy at the quantum level within quantum technologies. For example, by managing energy transfer locally on a quantum computer chip, the waste of energy inside the cryogenic fridge can be minimised. Furthermore, quantum properties like phase and entanglement can be retained during energy transfer by using quantum systems as batteries. This can be particularly interesting for energy transfer in quantum metrology systems. This research is aligned with the Quantum Energy Initiative, a community of experts in research, industry and other organisations, intending to investigate and reduce the resource cost of quantum technologies consciously.

To conclude, the study of QBs has both fundamental and practical relevance. In the end, a better understanding of energy storage at the quantum scale can help us create better systems for energy storage.

1.2. STATE-OF-THE-ART

The field of quantum thermodynamics investigates how properties such as work, heat, and temperature start to behave at the quantum scale [11]. Thermodynamics considers large, macroscopic systems in equilibrium. Quantum mechanics deals with finite-size, non-equilibrium systems, where fluctuations and randomness are unavoidable. Combining the two fields has led to new insights, and the rise of quantum machines which exploit the principles of quantum thermodynamics to perform useful tasks [12, 13]. Examples include the quantum heat engine [14], the quantum refrigerator [15], and the quantum battery [1].

In 2004, Allahverdyan, Balian and Nieuwenhuizen studied maximal work extraction from finite quantum systems [2]. This is performed through a cyclic process, via only unitary operations. The maximally extractable work from a quantum state is called ergotropy. The ergotropy depends on two quantities: the initial density state, and the passive state. The initial density state describes the state of the initial system. A passive state is defined as the state from which no more work can be extracted. The ergotropy then depends on the difference between the energies of these two respective states.

Suppose a system is initially off-equilibrium and then gets coupled to work sources. The laws of thermodynamics state that the maximal extractable work is

quantum hardware for QB implementation can make it a truly sustainable option in the future, and provide the quantum advantage without additional energy costs.

determined by energy and entropy. This is encapsulated by the so-called Gibbs state. The Gibbs state is the thermal equilibrium state, and therefore the passive state of the system. In quantum thermodynamics, both entropy and eigenvalues of the state must be preserved. This confines the transformation to unitary operations, and due to this, reaching the Gibbs state is not always possible [2]. Remarkably, it was suggested that the creation of quantum correlations may allow the ergotropy of a finite system to get closer to the thermodynamic bounds [2].

This led to the introduction of the concept of a quantum battery (QB) by Alicki & Fannes in 2013 [1]. A QB is a d -dimensional quantum-mechanical system that can be used to reversibly store energy in and extract energy from. This work suggested that entanglement generation could allow for more work extraction [1]. Subsequent work showed that the same amount of work can be extracted by increasing the number of steps without generating entanglement [16]. Avoiding entanglement then allows for the same amount of extractable work, yet increases the charging time (or the time it takes to extract work). Hence, entanglement can increase the power of a battery [16]. The quantum advantage is defined as the difference in power when charging using global operations, allowing for entanglement, compared to using local operations, keeping states separable at all times [4]. Researchers demonstrated that an N -fold quantum advantage can be achieved [3].

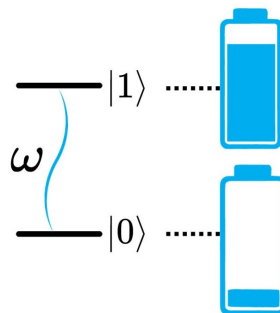


Figure 1.1.: A qubit can be used as a QB, where the $|0\rangle$ state is an empty battery, and the $|1\rangle$ state is a fully charged battery. The ω represents the Rabi frequency of the battery, which can be used to either charge or extract work from the QB.

A two-dimensional quantum-mechanical system is called a qubit, which has been widely explored and developed with the purpose of quantum computing. In the context of quantum computing, the discrete splitting of energy levels can be used to represent the computational basis. The ground state $|0\rangle$ represents 0-bit, and the first excited state $|1\rangle$ represents the 1-bit. In the context of quantum batteries, the energy difference of the $|0\rangle$ and $|1\rangle$ states can be used to store energy in a qubit. This is visualised in figure 1.1.

Since these early fundamental works, the research on QBs has been expanding

rapidly. Both qubits and quantum harmonic oscillators (QHO) can be used as QB systems [17]. The charging protocol has been explored, considering both direct charging via an external field as charger-mediated energy transfer [17]. Open system approaches have developed, where the QB is modelled in a more realistic environment, allowing for noise and decoherences [18]. This also led to proposals such as charging with linear feedback control [19]. Furthermore, the exact role of entanglement has been discussed and extended to the role of other quantum correlations, which can be measured by for example quantum discord [20].

In the previous years, the focus has shifted to the possibilities of practical implementations of quantum batteries. The first quantum advantage in an experimental setting was demonstrated with an organic microcavity [21]. This study shows a super-extensive power scaling with the number of organic molecules. Later, also a solid-state qubit as QB was shown to transfer work with the modes of an electromagnetic field [22]. In 2022, the first experimental implementation of a superconducting quantum battery was also achieved [23]. This was focused on the optimal charging of a single qubit as QB, whilst later work included a practical proposal for N transmon qubits capacitively coupled to a shared resonator [24]. This way, the quantum advantage can be practically implemented for transmon qubits.

Recently, Gemme *et al.* showed the implementation of a QB on the superconducting transmon qubits on the IBM Quantum Platform [25]. For the first time, this allows studying QB properties from a cloud-based quantum computer. This is beneficial for several reasons. Firstly, it makes it practically easier and more feasible to study QBs. Cloud computing allows for studying the QBs from anywhere in the world in well-established quantum hardware systems. The possibilities have also expanded since Qiskit Pulse [26] was released, allowing to modify the pulse shape. This involves a lower level of programming, which is often only possible on-site of the quantum computer. A relevant example of how this can be used is the qutrit QB implementation on the IBM Quantum Platform [27]. Secondly, investigating the opportunities of implementing QBs is particularly important for superconducting transmon qubits. This quantum hardware operates at low temperatures, meaning the energy costs are high and a reduction leads to significant improvements. Furthermore, superconducting transmon qubits are currently prime candidates for becoming the standard hardware platform of quantum computers. This makes improving their energy management increasingly relevant.

1.3. RESEARCH GOALS

The TU Delft has its own multi-hardware Quantum Technology platform, called "Quantum Inspire" [28], which is publicly accessible too. Starmon-5 is a quantum computer consisting of 5 superconducting transmon qubits [29], available on Quantum Inspire. The goal of this research is to investigate and characterise the performance of the superconducting transmon qubits of Starmon-5 as building blocks of a quantum battery and explore the opportunities and challenges of using transmon qubits in quantum computer hardware as QBs.

The goals of this thesis are:

1. To investigate and analyse the performance of transmon qubits of the Starmon-5 quantum processor of Quantum Inspire in the context of a quantum battery.
2. To characterise different superconducting transmon qubits as QBs, and compare them based on a framework of figures of merit.
3. To explore charger-mediated charging in a cloud-computing system.
4. To extend to $n \geq 2$ qubits, and explore the possibilities of the quantum advantage in the current superconducting quantum hardware.

The novelties of our work include the demonstration of charger-mediated energy transfer and parallel charging in superconducting transmon qubits.

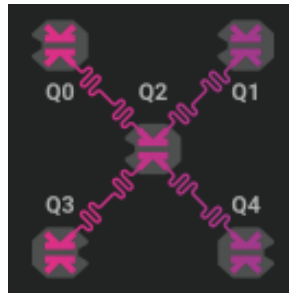


Figure 1.2.: Starmon-5 processor, Quantum Inspire. Obtained from reference [28].

1.4. THESIS STRUCTURE

This thesis is organised as follows.

- **Chapter 1** gives an introduction to the thesis. It states its background & relevance, presents the state-of-the-art research, and the goals of this research.
- **Chapter 2** provides a general overview of the theoretical framework of quantum batteries.
- **Chapter 3** shows the implementation and characterisation of a quantum battery on the Starmon-5 platform by Quantum Inspire.
- **Chapter 4** proposes using the CNOT gate to implement charger-mediated energy transfer in transmon quantum batteries. This system is implemented on the Starmon-5, and the results are shown and discussed.
- **Chapter 5** takes the first steps to implement a N -body quantum battery on the superconducting quantum platform. Parallel charging is implemented, whilst for collective charging it is argued that a different platform design is required.

- **Chapter 6** summarises the main conclusions of this research, and discusses the current limitations of QB implementation on the Starmon-5 processor along with an outlook for future work.

Appendix:

- *Appendix A* compares modular pulse shaping using Qiskit Pulse with the $R_x(\theta)$ gate implementation to charge QBs on the IBM Platform. This verifies the decision to use the $R_x(\theta)$ gate for QB implementation on Quantum Inspire.
- *Appendix B* shows preliminary results towards optimising the pulse for charging a QB. The optimisation is based on Krotov and implemented on IBM Quantum Hardware. No improvement is achieved at this stage.
- *Appendix C* includes the code developed for this thesis and provides instructions on implementing it. It can be used to replicate or extend the work of this thesis.
- *Appendix D* contains all data obtained during the cloud experiments to ensure data transparency.

2

THEORETICAL BACKGROUND

2.1. QUANTUM THERMODYNAMICS

2.1.1. WORK EXTRACTION

Thermodynamics is a field in physics that studies the relation of macroscopic properties such as energy, entropy, heat and work. It examines large-scale systems, where these properties emerge from the behaviour of smaller, microscopic units. This is described by statistical mechanics. In contrast, quantum thermodynamics investigates how thermodynamic quantities such as energy, entropy, heat and work operate in a finite, microscopic system. An example of such systems is the quantum battery (QB).

The first step towards the concept of a QB was the work by Allahverdyan *et al.* in 2004. This study investigates the maximal extractable work of a finite quantum system [2]. Suppose one has a finite quantum system, then its initial state can be described by a density operator $\hat{\rho}$. The system has an associated internal Hamiltonian, \hat{H} . An external time-dependent field $\hat{V}(t)$ is applied to cyclically drive the system, meaning that the final Hamiltonian returns to the state of the initial Hamiltonian. The total Hamiltonian is then given by,

$$\hat{H}(t) = \hat{H} + \hat{V}(t) \quad (2.1)$$

To ensure cyclicity, the time-dependent part of the Hamiltonian is turned on at $t = 0$, and returns to zero at the end of the process, $t = \tau$.

$$\hat{V}(t) = \begin{cases} \hat{V} & \text{if } 0 \leq t \leq \tau \\ 0 & \text{otherwise} \end{cases} \quad (2.2)$$

When the external field $\hat{V}(t)$ is turned on, the density matrix $\hat{\rho}(t)$ evolves via the Liouville-von Neumann equation [30]:

$$i\hbar \frac{\partial \hat{\rho}(t)}{\partial t} = [\hat{H}(t), \hat{\rho}(t)] \quad (2.3)$$

To ensure the unitary evolution of a finite quantum system, $\hat{\rho}(t)$ must evolve via unitary operations. In other words,

$$\hat{\rho}(t) = \hat{U}(t)\hat{\rho}\hat{U}(t)^\dagger \quad (2.4)$$

This unitary operator can be described by the time-ordered exponential of the integral of the Hamiltonian,

$$\hat{U}(\tau) = \hat{\mathcal{T}} \exp \left[-i \int_0^\tau dt \hat{H}(t) \right] \quad (2.5)$$

This makes the work extraction protocol from a finite quantum system fundamentally different from a generic thermodynamic system.

2.1.2. ERGOTROPY AND PASSIVE STATES

The internal energy associated with a certain density matrix and Hamiltonian is given by $\hat{E} = \text{tr}[\hat{\rho}\hat{H}]$, where tr is the trace of a matrix. The maximal extractable work at a specific time is the difference between the energy associated with the initial density matrix and the energy associated with the density matrix at time t .

$$W(t) = \text{tr}[\hat{\rho}\hat{H}] - \text{tr}[\hat{\rho}(t)\hat{H}] \quad (2.6)$$

The maximal extractable work of a finite quantum system is called ergotropy [2]. To define the ergotropy, the minimal accessible energy state must be found. This state is also called the passive state. A passive state is defined as a density state from which no more work can be extracted [31, 32]. For each initial density state $\hat{\rho}$, there is an associated passive state $\hat{\sigma}_\rho$, i.e.

$$\hat{\sigma}_\rho = \hat{U}_\rho \hat{\rho} \hat{U}_\rho^\dagger \quad (2.7)$$

Here \hat{U}_ρ is chosen such that the associated energy is minimised, i.e. $\hat{U}_\rho = \min[\text{tr}[\hat{U}\hat{\rho}\hat{U}^\dagger]]$ for all $\hat{U} \in \text{SU}(d)$.

The ergotropy can then be written as [2],

$$\mathcal{W} = \text{tr}[\hat{\rho}\hat{H}] - \text{tr}[\hat{\sigma}_\rho\hat{H}] \quad (2.8)$$

Here, the difference with macroscopic systems becomes non-trivial. In thermodynamics, the passive state is always the associated Gibbs state $\hat{\omega}_{\beta^*}$. A Gibbs state is the equilibrium state of a system at constant temperature. Being in equilibrium, its energy associated is minimised. The Gibbs state is defined as,

$$\hat{\omega}_{\beta^*} = \frac{e^{-\beta\hat{H}}}{Z}, \quad Z = \text{tr} \left[e^{-\beta\hat{H}} \right] \quad (2.9)$$

Here, Z is the partition function. Hence, the maximal extractable work of a macroscopic system is:

$$\mathcal{W}_{\text{th}} = E(\hat{\rho}) - TS(\hat{\rho}) + T \ln Z \quad (2.10)$$

For each state $\hat{\rho}$, there exists a unique Gibbs state $\hat{\omega}_{\beta^*}$ with the same amount of entropy, i.e. $S(\hat{\omega}_{\beta^*}) = S(\hat{\rho})$. Finite quantum systems are more constrained, in the sense that not only the entropy $S(\hat{\rho})$ must be preserved, but also the eigenvalues of $\hat{\rho}$. This means that the maximal extractable work given in equation (2.10) may not be available. In other words, the state $\hat{\omega}_{\beta^*}$ may not be reachable via unitary operations. This poses an upper bound on the ergotropy [1]:

$$\mathcal{W} \leq \text{tr}[\hat{\rho}\hat{H}] - \text{tr}[\hat{\omega}_{\beta^*}\hat{H}] \quad (2.11)$$

2.1.3. CHARGING, STORAGE, AND TRANSFER OF ENERGY

A good battery can (1) charge fast and efficiently, (2) store energy for an arbitrary amount of time, and (3) transfer energy to a consumption centre in a fast and useful manner. For practical implementation, the full process must be considered. This is visualised in figure 2.1. All three different processes can be studied and optimised. In this thesis, the focus is on the charging of the quantum battery.

Interestingly, the framework of charging a QB is simply the opposite of work extraction. Instead of extracting work by going from an active state to the passive state, $\text{tr}[\hat{\rho}\hat{H}] \rightarrow \text{tr}[\hat{\sigma}_{\rho}\hat{H}]$, we are interested in storing work by going from the passive state to the maximally active state: $\text{tr}[\hat{\sigma}_{\rho}\hat{H}] \rightarrow \text{tr}[\hat{\rho}\hat{H}]$. The unitary of charging is thus simply the hermitian conjugate of the unitary realising maximal work extraction, $\hat{U}_{\text{charging}} = \hat{U}_{\text{transfer}}^\dagger$.

The study of storing energy in a QB is different from the charging and discharging process. It focuses on avoiding dissipation of the active state, and thus creating stable QBs. The stability of the QB can be enhanced by for example sequential measurements to bring the QB back to the fully charged state [33], linear feedback control where the driving field amplitude is adjusted based on the dissipation [34], or using dark and bright states [23]. The study of the stability of QBs is not as far explored as the study of charging and energy transfer, this can be because the operating times of QBs are typically smaller than the relaxation time T_1 and dephasing time T_2 (see for example [25], [27]).

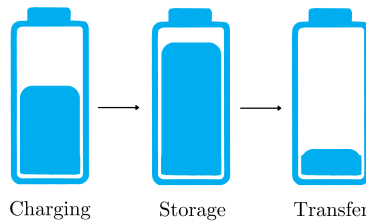


Figure 2.1.: The full process of a quantum battery: (1) charging, (2) storage of energy, and (3) transfer of energy.

2.2. QUANTUM BATTERY

2.2.1. ONE QUANTUM SYSTEM

A quantum battery can be defined as a d -dimensional quantum system [1]. The internal Hamiltonian can be expressed in full generality as follows,

$$\hat{H} = \sum_{j=1}^d \epsilon_j |\epsilon_j\rangle \langle \epsilon_j|, \quad \epsilon_j \geq \epsilon_{j+1} \quad (2.12)$$

The initial density state can be defined as,

$$\hat{\rho} = \sum_{k=1}^d r_k |r_k\rangle \langle r_k|, \quad r_k \leq r_{k+1} \quad (2.13)$$

The associated passive state is then,

$$\hat{\sigma}_\rho = \sum_{j=1}^d r_j |\epsilon_j\rangle \langle \epsilon_j| \quad (2.14)$$

Here, ϵ_j comes from the energy levels of the internal Hamiltonian in equation (2.12), and r_j comes from the energy levels of the initial density state in equation (2.13). As such, the passive state $\hat{\sigma}_\rho$ has the same eigenvalues as $\hat{\rho}$ but the set is re-ordered in non-increasing order with the energy states. This means that the lowest energy states get the highest occupation level, and vice versa. As such, the lowest final energy state is reached $E(\hat{\sigma}_\rho) = \sum_{j=1}^d r_j \epsilon_j$. The amount of extractable work for one QB is limited to the energy levels of the passive state. Importantly, there is no possibility of reaching the Gibbs state, defined in equation (2.9), when these eigenvalues do not match the eigenvalues of the passive state, given in equation (2.14).

2.2.2. AN ARRAY OF n QUANTUM SYSTEMS

Suppose instead of one quantum battery, we have n identical quantum batteries. Alternatively, it can be said that the QB consists of an array of multiple quantum systems. The Hamiltonian of the total system becomes,

$$\hat{H}_n = \sum_{j=1}^n \hat{H}_j \quad (2.15)$$

Here, \hat{H}_j are all independent copies of the single system Hamiltonian \hat{H} . This is where quantum phenomena start playing a non-trivial role. Although we take copies of identical states, the passive state of the total system $\hat{\sigma}_{\otimes(n)\rho}$ is not the same as the sum of all individual passive states $\otimes^{(n)} \hat{\sigma}_\rho$ [2].

$$\hat{\sigma}_{\otimes(n)\rho} \neq \otimes^{(n)} \hat{\sigma}_\rho \quad (2.16)$$

The passive state of the total system $\hat{\sigma}_{\otimes(n)\rho}$ can be called the completely passive state, while the passive state of an individual QB $\hat{\sigma}_\rho$ is referred to as simply the

passive state. The sum of n individual passive states is thus referred to $\otimes^{(n)}\hat{\sigma}_\rho$. When n increases, the completely passive state has increasingly more possibilities of assembling the Gibbs state given in equation (2.9). As such, the state gets closer and closer to the Gibbs state when n increases. For $n \rightarrow \infty$, the completely passive state asymptotically approaches the Gibbs state.

Consider the amount of work per QB, in a system of multiple QBs:

$$w_{\max}^{(n)} = \frac{1}{n} \left(\text{tr}[\otimes^{(n)}\hat{\rho}\hat{H}] - \text{tr}[\hat{\sigma}_{\otimes^{(n)}\hat{\rho}}\hat{H}] \right) \quad (2.17)$$

Taking the limit $n \rightarrow \infty$, it can be proven that the extractable work per copy approaches the thermodynamic limit [1]:

$$\lim_{n \rightarrow \infty} w_{\max}^{(n)} = \text{tr}[\hat{\rho}\hat{H}] - \text{tr}[\hat{\omega}_{\beta^*}\hat{H}] \quad (2.18)$$

A global unitary that acts on all copies can achieve this limit, meaning the unitary must be entangling [1, 2]. The main conclusion by Alicki *et al.* was therefore that more work can be extracted from the system due to entanglement [1]. Considering the same reversible work extraction from N identical non-interacting finite level systems, other researchers were able to show that the maximum work in equation (2.18) can also be reached by applying a sequential set of local operations [16]. This implies that entanglement is not a requirement for increasing the amount of extractable work [16].

2.2.3. ENTANGLEMENT BOOST OF POWER

Entanglement is not required to extract all available energy from the QB system, but instead, entanglement can be used to speed up the process [16]. This means that the power of a QB can be improved when entanglement creation is allowed [16]. A high-power battery has several benefits, for example, fast energy delivery is required for specific applications, which either require fast operation times or High-Load energy delivery. Additionally, high power can reduce heat generation, leading to higher efficiencies.

Let us first discuss how we can avoid entanglement creation. An indirect path can be used to avoid entanglement creation. This works as follows. Suppose we want to transpose a state $\hat{\rho}_\alpha = |i_1^\alpha i_2^\alpha \dots i_N^\alpha\rangle$ to a different state $\hat{\rho}_\beta = |i_1^\beta i_2^\beta \dots i_N^\beta\rangle$.

A visualisation of charging via the direct path is shown in figure 2.2a. Using the direct path, only one global operator is required:

$$|i_1^\alpha i_2^\alpha \dots i_N^\alpha\rangle \xrightarrow{\hat{U}^{\alpha\beta}} |i_1^\beta i_2^\beta \dots i_N^\beta\rangle \quad (2.19)$$

Using the indirect path, the same state can be reached using local operations, keeping the state separable at all times.

$$|i_1^\alpha i_2^\alpha \dots i_N^\alpha\rangle \xrightarrow{\hat{U}_1^{\alpha\beta}} |i_1^\beta i_2^\alpha \dots i_N^\alpha\rangle \xrightarrow{\hat{U}_2^{\alpha\beta}} |i_1^\beta i_2^\beta \dots i_N^\alpha\rangle \xrightarrow{\hat{U}_3^{\alpha\beta}} \dots \xrightarrow{\hat{U}_N^{\alpha\beta}} |i_1^\beta i_2^\beta \dots i_N^\beta\rangle \quad (2.20)$$

Hence, N local transposition unitaries must be applied. This is visualised in figure 2.2b.

The unitary for each transposition is then:

$$\hat{U}^{\alpha\beta} = \sum_{\mu \neq \alpha, \beta} |\mu\rangle\langle\mu| + |\alpha\rangle\langle\beta| + |\beta\rangle\langle\alpha| \quad (2.21)$$

This way, $|\alpha\rangle$ and $|\beta\rangle$ are swapped, whilst all other states are kept intact. The time-dependent unitary can then be written as

$$\hat{U}^{\alpha\beta}(t) = \sum_{\mu \neq \alpha, \beta} |\mu\rangle\langle\mu| + \hat{u}^{\alpha\beta}(t) \quad (2.22)$$

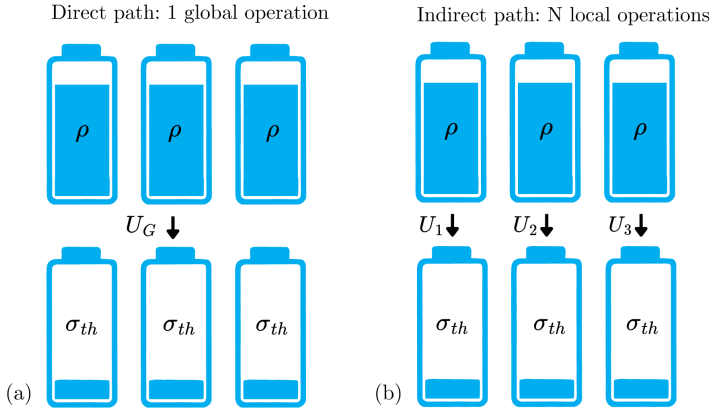


Figure 2.2.: Procedure of work extraction from a QB: direct path requires only applying one global unitary, whilst the indirect path requires N local unitary operations.

It is also possible to reduce the amount of entanglement required, without completely avoiding it. This way, the required amount of operations can also be reduced. The degree of entanglement can be characterised by the notion of l -separable states. Separable states are states which contain no entanglement. They may be written as:

$$|\psi\rangle = |\psi_1\rangle \otimes |\psi_2\rangle \otimes \dots \otimes |\psi_N\rangle \quad (2.23)$$

For any system, one can define the entropy vector $\vec{E}: E_1 \geq \dots \geq E_{2^{l-1}-1} \geq 0$. If the last $2^{l-1} - 1$ entries are 0, the state is said to be l -separable [35]. This means that it can be decomposed in pure states of at least l systems. It can be proven that the direct path can create genuinely multipartite entanglement, reducing the state to being ultimately 1-separable, whilst the indirect path allows the states to remain N -separable [16].

The time taken by each global operation is finite due to the quantum speed limit (QSL), which arises fundamentally due to Heisenberg's uncertainty principle [36].

Assuming that the time taken by each global operation is the same, this implies that the amount of time increases linearly with each operation required [16]. Hence, entanglement can boost the amount of energy acquired in a finite amount of time. In other words, there is an entanglement boost of power.

2.2.4. FASTER CHARGING: GLOBAL VERSUS LOCAL CHARGING

A specific protocol for global and local charging was proposed and denoted "Quantacell" [3]. The theoretical framework is the same as the aforementioned, except the focus is now on charging the battery. The desired action is then to go from the passive state to the maximally active state. As visualised in figure 2.3, two different ways of charging are considered:

1. Global charging. This follows the direct path. Global charging allows for entanglement to occur throughout the process of charging, but retains the purity of states between the initial and final states.
2. Parallel charging. This follows the indirect path. The states are now kept separable at all times in the process.

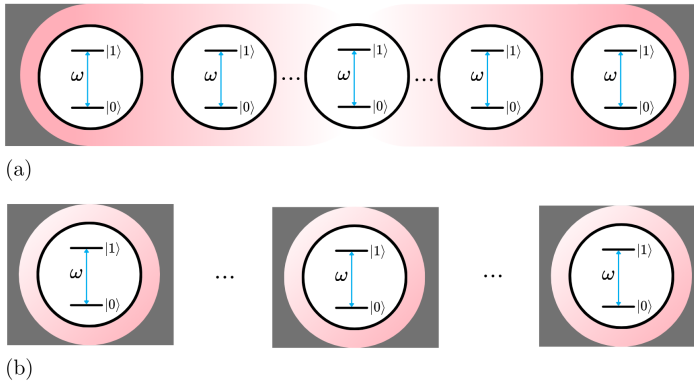


Figure 2.3.: An array of identical qubits, can be charged in two ways (a) Global charging, which can be practically achieved by a shared cavity [3]. Alternatively, the system can be locally charged, as shown in (b). This can be implemented by using an individual cavity for each qubit [3]. For superconducting transmon qubits, instead of a cavity, a shared or individual resonator can be used for the same purpose.

Using qubits, the available energy states are the $|0\rangle$ and $|1\rangle$ states, using the z-basis as the reference frame. The internal Hamiltonian of a single QB can be set at:

$$\hat{H} = |1\rangle\langle 1| \quad (2.24)$$

The internal Hamiltonian of an array of n copies is then,

$$\hat{H}^{(n)} = \sum_j |1\rangle_j \langle 1|_j \otimes_{k \neq j} \mathbb{1}^k \quad (2.25)$$

We want to go from a passive state to a maximally active state. Using the qubit states, optimal charging now involves the following process.

$$\begin{aligned} \hat{\sigma}_\rho &= |0\rangle^{(N)} \langle 0|^{(N)} \\ \hat{\rho}^* &= |1\rangle^{(N)} \langle 1|^{(N)} \\ \hat{\sigma}_\rho &\rightarrow \hat{\rho}^* \end{aligned} \quad (2.26)$$

The energy difference between the $|0\rangle$ and $|1\rangle$ state is set to be E_{\max} . Considering identical qubits, the total energy scales linearly, i.e. $E_{\max}^{(N)} = NE_{\max}$.

As discussed before, $\hat{H}(t) = \hat{H} + \hat{V}(t)$, where the time-dependent part of the Hamiltonian $\hat{V}(t)$ is given by equation (2.2). Notably, $\hat{V}(t)$ differs for global and parallel charging. The external driving field can be modulated by a parameter $\lambda(t)$, such that

$$\begin{aligned} \hat{V}(t) &= \lambda(t) \hat{V} \\ \lambda(t) &= \begin{cases} 1 & \text{if } 0 \leq t \leq \tau \\ 0 & \text{if else} \end{cases} \end{aligned} \quad (2.27)$$

Global charging can be achieved by choosing $\hat{V} = \hat{V}_{\text{global}}$:

$$\begin{aligned} \hat{V}_{\text{global}} &= E_{\max}^{(N)} \hat{\sigma}^{(N)} \\ &= E_{\max}^{(N)} (|1\rangle^{(N)} \langle 0|^{(N)} + |0\rangle^{(N)} \langle 1|^{(N)}) \end{aligned} \quad (2.28)$$

This requires a charging time $\tau_c = \frac{\pi}{2E_{\max}^{(N)}} = \frac{\pi}{NE_{\max}}$ [3]. Parallel driving can be accomplished by choosing:

$$\hat{V}_{\text{parallel}}^{(N)} = \sum_k E_{\max} (|0\rangle \langle 1| + |1\rangle \langle 0|) \otimes_{k \neq j}^N \mathbb{1} \quad (2.29)$$

This procedure requires a charging time $\tau_c = \frac{\pi}{2E_{\max}}$ [3]. In both cases, the amount of energy stored in total is the same. Hence,

$$P_{\text{global}} = NP_{\text{parallel}} \quad (2.30)$$

Global charging promises an N -fold advantage compared to parallel charging by using entanglement properties in the charging procedure [3]. Interestingly, the initial and final states are both pure states and thus remain separable. This result can be understood from the path taken in state space [3]. Global charging takes a path along the geodesic, i.e. the shortest path possible. This can be calculated for pure states via the Bures angle and is a constant value [37]. Parallel charging has a path length that scales with \sqrt{N} . As such, the path taken in state space is \sqrt{N} longer for parallel charging, resulting in an N -fold increase in charging time [3]. A numerical

analysis up to $N=4$ shows that the charging time decreases with $1/N$, which is in agreement with this theoretical framework, whilst the initial and final states indeed do not contain entanglement [3].

Although no entanglement is present in the final state, there can still be quantum correlations created throughout the process [20]. This can be represented by a quantity called the quantum discord, which is a measure of quantum correlations beyond entanglement. It was shown that although global charging avoids entanglement, the quantum discord does increase and is even required for maximal work extraction [20].

2.2.5. QUANTUM ADVANTAGE

The quantum advantage in battery power can be defined as [4],

$$\begin{aligned}\Gamma &= \frac{P_q}{P_c} \\ &= \frac{P_{\text{global}}}{P_{\text{parallel}}} = \frac{\tau_{\text{parallel}}}{\tau_{\text{global}}}\end{aligned}\tag{2.31}$$

where P_q is the power achievable via quantum processes, and P_c is the power achievable via classical processes. As discussed above, global charging can be considered a quantum process, whilst parallel charging is classical.

To achieve a quantum advantage, $\Gamma > 1$, entangling operations must take place [4]. The result of the previous section shows $\Gamma = N$. The authors also show that constraints can be posed on the global Hamiltonian to ensure that its structure remains similar to the parallel Hamiltonian, to avoid obtaining extra energy from the interactions [4]. Using the quantum speed limit [36], the quantum advantage is bound by $\Gamma \leq \sqrt{N}$ or $\Gamma \leq N$, depending on the explicit constraints imposed [4]. In this thesis, the least strict bound $\Gamma \leq N$ is used when discussing collective charging.

2.2.6. ROLE OF INTERACTION ORDER

Importantly, N -body interactions are difficult to realise in practical applications [4]. Suppose the physical system can achieve k -body interactions, where $2 \leq k \leq N$. It then directly interacts with $m \geq 1$ other quantum systems, here m is called the participation number. To show how this works, consider a 2-dimensional model with $k=2$, the maximum participation number is then all surrounding quantum systems, hence $m=8$.

For a generic charging procedure, the quantum advantage is then bound by [4],

$$\Gamma \leq \gamma[k^2(m-1) + k]\tag{2.32}$$

Here, γ is a constant. The quantum advantage is therefore typically limited by the interaction number k and participation number m , rather than its total number of systems N .

Considering a circuit-based charging procedure, the quantum advantage is bound even more tightly. It can be shown to be [4]:

$$\Gamma \leq \gamma k \quad (2.33)$$

This procedure is sketched for 2-body interactions in figure 2.4. This procedure is similar to what can be achieved in our circuit-based quantum computer, which allows for at most 2-body interactions.

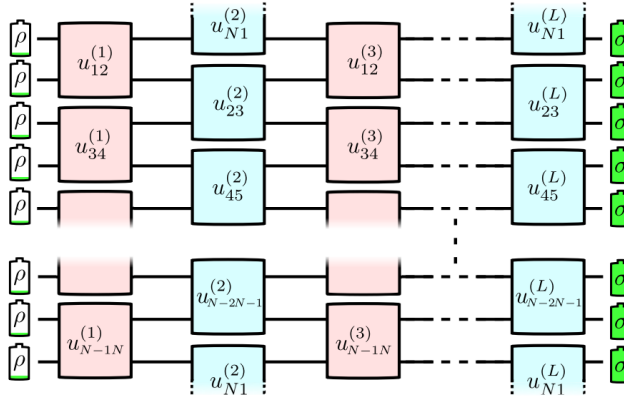


Figure 2.4.: Circuit-based quantum computing to charge a N -body QB using 2-qubit gates. Figure obtained from supplementary material [4].

2.3. TRANSMON THEORY

This section aims to give a basic understanding of superconducting transmon qubits and circuit quantum electrodynamics (circuit QED). This is important for understanding why and how transmon qubits are used in this study. It must be noted that both circuit QED and superconducting transmon qubits are entire research fields in themselves, so presented here is only a summary of relevant knowledge for this thesis. For the interested reader, we suggest reference [38] for an elaborate background on circuit QED, references [39] and [40] for background on superconducting transmon qubits, and reference [24] for the specific implementation of transmons as quantum batteries.

2.3.1. SUPERCONDUCTING TRANSMON QUBITS

Superconducting transmon qubits are one of the many quantum hardware platforms which are currently being explored for their usage in quantum technologies. Others include trapped ions [41], photons [6], quantum dots [42], and more. In this thesis, the focus is on using superconducting transmon qubits as QB. The main reason for this is the wide usage of transmon qubits for quantum technologies [43]. Transmons are one of the leading candidates for becoming the main qubits used in quantum computers and currently acquire a lot of attention in the field [39, 44]. For example, big industry players such as IBM and Google have both focused on fabricating large superconducting transmon circuits (433 qubits [45], and 53 qubits [46], respectively).

SUPERCONDUCTIVITY

Superconducting qubits are circuits made of superconducting materials. This means that the current in these materials experiences zero resistance, creating superconductivity. Operating in the superconducting regime, electrons are bound together to form a pair. These are called Cooper pairs. This is a quantum mechanical phenomenon due to electron-phonon interaction. Electrons are spin- $\frac{1}{2}$ particles, or fermions, and subject to Pauli's exclusion principle. This means that no two particles can be in an identical quantum state. Two electrons bound together as a Cooper pair then create a spin-1 quasiparticle, called a boson. Bosons are not subject to the Pauli exclusion principle restriction. Cooper pairs therefore all condense to the ground state energy, forming one common wave function to describe the state of all Cooper pairs together. This creates a larger energy gap to the first excited state, which avoids any small excitations. Therefore scattering of electrons does not occur, and the resistance becomes theoretically zero.

In the end, it thus becomes energetically favourable for the electrons to move together as Cooper pairs. As this pairing is rather weak, operating at low temperatures is required to avoid any thermal excitations to break the bond. This requires a cryogenic system to cool the system down. The search for room-temperature superconducting material is an active research field [47].

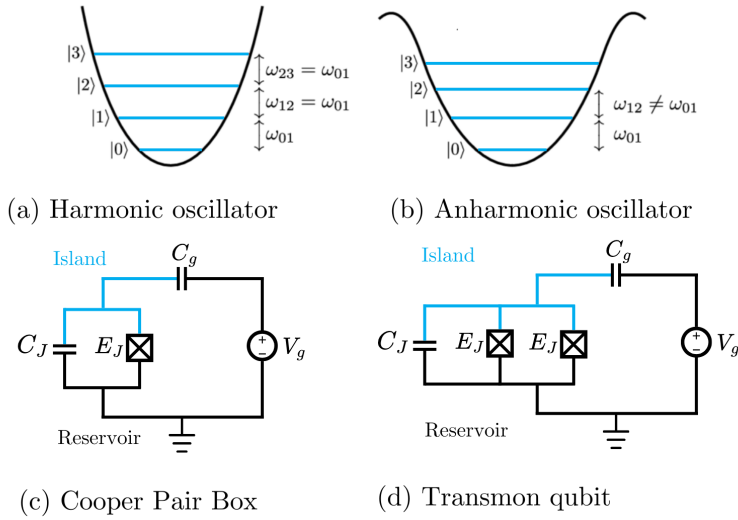


Figure 2.5.: Concepts of a superconducting qubit, (a) shows the energy splitting in a harmonic oscillator, whilst (b) shows the spectrum of an anharmonic oscillator. The circuitry of a Cooper Pair Box is shown in (c), and the circuitry composing a transmon qubit is shown in (d). The box with a cross "x" is the notation for a Josephson junction. The superconducting island is coloured in blue. Figures (a) and (b) are adapted from reference [48]. Figures (c) and (d) are adapted from reference [48].

COOPER PAIR BOX

How can quantum states be created using this superconducting material? A Josephson junction is a thin, insulating gap between two superconductors. This creates a barrier between the two superconductors. When the junction is small enough, the wavefunctions start to overlap. This allows for tunnelling of Cooper pairs through the junction, which can cause a current to flow even without applying a voltage.

The Josephson junction can be seen as a non-linear inductor. Combining the Josephson junction with a capacitor creates a Cooper Pair Box, which can be used to represent quantum states. This is shown in figure 2.5c. The Cooper Pair Box has two parts: a superconducting island (represented in blue), and a superconducting reservoir (represented in black). The quantum state is determined by the number of Cooper pairs tunnelling across the junction from the reservoir to the superconducting island. The quantum state can thus be written as,

$$\begin{aligned} |n\rangle &\rightarrow |0\rangle \\ |n+1\rangle &\rightarrow |1\rangle \end{aligned} \tag{2.34}$$

Here, n is the number of Cooper pairs on the island. The gate voltage can be used

to modify the quantum state. When an inductor and capacitor are placed in parallel, this creates an LC oscillator. In figure 2.5a, it is shown that this leads to equidistant energy levels. For driving a qubit, this is not ideal, as the same pulse ω_{01} driving the $|0\rangle \rightarrow |1\rangle$ transition, can be used to excite to higher energy states. These are energy states out of the computational basis and thus this leads to leakage. As the Josephson junction acts like a non-linear inductor, creating a cosine energy well. The spectrum then becomes anharmonic, see figure 2.5b. It is now possible to isolate the pulse ω_{01} driving the $|0\rangle \rightarrow |1\rangle$ transition, and thus, the system can operate as a qubit.

Lastly, a qubit which uses the difference in number of Cooper pairs as qubit states is called a charge qubit. It must be noted that more types of superconducting qubits exist, namely flux and phase qubits. Flux qubits use the direction of the flux and can also be used to represent two quantum states (clockwise, and counter-clockwise). Phase qubits use the phase difference of two superconducting wavefunctions to represent the quantum state. More information on those qubits can be found in reference [39].

TRANSMON QUBITS

The transmon qubit, first proposed in 2007 [40], is a type of charge qubit. The circuit of the Cooper Pair Box is modified by adding another capacitor in parallel, as visualised in figure 2.5d. Adding two Josephson junctions in parallel is called a SQUID, which stands for superconducting quantum interference device [49]. Compared to other charge qubits, using a SQUID instead of a single Josephson junction allows to shunt the noise better [40].

There are several benefits of using superconducting transmon qubits for quantum technologies. Firstly, the coupling of a superconducting qubit with the electromagnetic field is exceptionally strong compared to other hardware systems [50–52]. Furthermore, transmon qubits are relatively easy to fabricate through existing semiconductor fabrication processes [44]. This is also because the transmons are macroscopic quantum systems. Lastly, the scalability of transmon qubits is a great benefit as well [39, 40, 44]. The circuitry makes it relatively easy to scale up the number of qubits on a Quantum Processor Unit (QPU).

These benefits also apply to using the superconducting transmon qubit as QB. The choice to focus on superconducting transmon qubits for QBs in this thesis is two-fold. Firstly, superconducting transmon qubits hold great promise for quantum technologies. Creating battery systems of the same hardware as the computational qubits could ease the integration of a QB on the QPU. This can then help energy management at the quantum scale in order to reduce the macroscopic energy costs of the quantum computer. The application of transmon qubits extends quantum computing, and can also be useful for quantum memory [53] and quantum communication [54]. Secondly, also QuTech focuses on transmon qubits and has the openly accessible Starmon-5 available on Quantum Inspire. This makes it a pragmatic decision as well.

2.3.2. CIRCUIT QUANTUM ELECTRODYNAMICS

Quantum electrodynamics (QED) describes the fundamental interaction of light and matter in the quantum mechanical framework. The quantum dynamics of electromagnetic fields can be used for creating and manipulating quantum states. The most familiar description is cavity QED, where an atom is placed inside a cavity. The electromagnetic waves inside the cavity can be used to excite the atom to different energy levels. Circuit QED is an adaption to cavity QED. Here, instead of a cavity, a one-dimensional transmission drive line can be used to couple to an artificial atom. An example of this is the coupling of a transmon qubit to the microwave control line, enabling gate operations, or the coupling of a transmon qubit to a resonator for read-out. Both these processes occur in Starmon-5 [29].

TYPES OF QUANTUM SYSTEMS

Quantum states can be divided into two types: Fock states and coherent states. Fock states are mostly particle-like states, whilst coherent states are mostly wave-like states. Equation 2.12 denotes a quantum state in full generality. Here, we distinguish the quantum states as either a Two-Level-System (TLS) or a Quantum Harmonic Oscillator (QHO).

A TLS is a two-level system and behaves like a Fock state. The transmon qubit is designed to operate as a TLS. The internal Hamiltonian of a TLS is,

$$\hat{H}_{TLS} = \hbar\omega_{TLS} \frac{\hat{\sigma}_z}{2} \quad (2.35)$$

Here, $\hat{\sigma}_z$ is the Pauli-z matrix operating on the TLS. The convention in this framework is given by

$$\hat{\sigma}_z = \begin{bmatrix} 1 & 0 \\ 0 & -1 \end{bmatrix} \quad (2.36)$$

The QHO is a coherent state, typically, the internal Hamiltonian can be denoted by using the creation and annihilation operators of the field modes, \hat{a}^\dagger and \hat{a} , respectively.

$$\hat{H}_{QHO} = \hbar\omega_{QHO} \hat{a}^\dagger \hat{a} \quad (2.37)$$

JAYNES-CUMMINGS MODEL

The Jaynes-Cummings model describes the interaction between an atom and a single mode of a cavity [55]. Similarly, in circuit QED, it can also describe the interaction between a qubit and the modes in the microwave transmission line. The framework based on the Jaynes-Cummings model is as follows,

$$\begin{aligned} \hat{H}(t) &= \hat{H}_q + \hat{H}_t + \lambda(t) \hat{H}_I \\ \hat{H}_q &= \hbar\omega_q \frac{\hat{\sigma}_z}{2} \\ \hat{H}_t &= \hbar\omega_t \hat{a}^\dagger \hat{a} \\ \hat{H}_I &= g(\hat{a} \hat{\sigma}_+ + \hat{a}^\dagger \hat{\sigma}_-) \end{aligned} \quad (2.38)$$

Here, \hat{H}_q to the qubit Hamiltonian, H_t to the transmission line Hamiltonian, and \hat{H}_I to the interaction Hamiltonian. Furthermore, $\hat{\sigma}_\pm = \frac{1}{2}(\hat{\sigma}_x \pm i\hat{\sigma}_y)$. Lastly, g is the coupling strength between the qubit and field modes.

Note that we added the $\lambda(t)$ to make clear that in the context of QB charging the interaction only takes place when the classical control parameter $\lambda(t)$ turns on. In the context of QBs, The Jaynes-Cummings model provides a good description when the QB consists of one qubit, or when charging multiple qubits in parallel. In the case of parallel charging, the Jaynes-Cummings model applies to each qubit, as each qubit has its own resonator.

DICKE MODEL

The Dicke model describes the interaction between a set of N atoms with a single mode of a cavity [56]. Within the framework of circuit QED, the Dicke model can also be used to describe the interaction between the microwave transmission line and an array of qubits. For QBs, this model applies to the collective charging of a QB existing out of multiple quantum systems.

$$\begin{aligned}
 \hat{H} &= \hat{H}_r + \hat{H}_q + \lambda(t)\hat{H}_I \\
 \hat{H}_q &= \hbar\omega_q \sum_{i=1}^N \frac{\hat{\sigma}_z^{(i)}}{2} \\
 \hat{H}_t &= \hbar\omega_t \hat{a}^\dagger \hat{a} \\
 \hat{H}_I &= \frac{g^*}{\sqrt{N}} (\hat{a} + \hat{a}^\dagger) \sum_{i=1}^N \hat{\sigma}_x^{(i)}
 \end{aligned} \tag{2.39}$$

Here, g^* is the coupling strength in the Dicke model. Again, the parameter $\lambda(t)$ is added to make the context of QB charging clear. When the quantum battery is charged collectively, this model is a good description of the system. This is because N qubits interact with a single mode of the electromagnetic field. A description of the Dicke model as a QB can be found in reference [57], and shows an advantage of $\sim \sqrt{N}$ in power due to coherent interactions among the qubits. The theoretical framework for N superconducting transmon qubits charging collectively is fully described in reference [24]. The charging of a QB existing of transmon qubits is further elaborated in the next section, considering two different charging protocols.

2.4. CHARGING PROTOCOLS

All charging protocols can be broadly divided into two sub-categories: direct charging via a classical drive, and charger-mediated energy transfer from another quantum system. Both processes are visualised in figure 2.6, and discussed in the sections below.

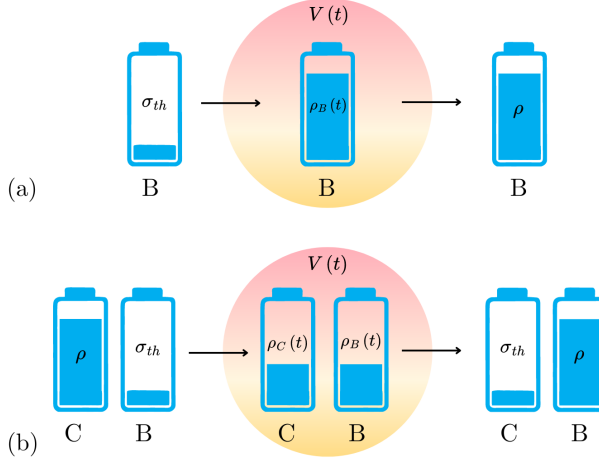


Figure 2.6.: Two different charging procedures: direct charging and charger-mediated energy transfer. Direct charging uses energy transfer from the external potential field. For charger-mediated charging, the energy transfer happens between two quantum systems and is catalysed by the external potential field.

2.4.1. DIRECT CHARGING

Direct charging means that the quantum battery is directly charged by an external field. This is the process that has been considered in this report so far. It is visualised in figure 2.6a.

The time-dependent Hamiltonian of direct charging can be written as,

$$\hat{H}(t) = H_{QB} + \hat{H}_D + \lambda(t)\hat{H}_I \quad (2.40)$$

Here, \hat{H}_{QB} stands for the Hamiltonian of the QB, \hat{H}_D is the Hamiltonian of the external drive field, and H_I denotes the interaction term between the two. Again, $\lambda(t)$ is the classical control parameter of the external field, which stays on during the time $t \in [0, \tau]$. When considering a system of multiple TLS, and allowing for nearest-neighbour interaction, the Hamiltonian becomes the following [24]:

$$\hat{H}_{QB}^{(N)} = \hbar\omega_{QB} \sum_{i=1}^N \frac{\hat{\sigma}_z^{(i)}}{2} + J \sum_{i=1}^{N-1} \hat{\sigma}_x^{(i)} \hat{\sigma}_x^{(i+1)} \quad (2.41)$$

Here, J is the nearest-neighbour interaction strength between the qubits. Similar to the Dicke model, the drive field Hamiltonian \hat{H}_D can be written as the Hamiltonian of the transmission line:

$$\hat{H}_D = \hbar\omega_D \hat{a}^\dagger \hat{a} \quad (2.42)$$

The interaction between the resonator and qubit is then given by [24],

$$\hat{H}_I = g \sum_{i=1}^N (\hat{a} + \hat{a}^\dagger) \hat{\sigma}_x^{(i)} \quad (2.43)$$

This can be considered for the transmon qubits in the Starmon-5 as well. Direct charging was also used in the first experimental realization of a superconducting transmon qubit as a quantum battery [23]. Furthermore, Gemme *et al.* also show direct charging of the batteries on IBM quantum hardware [25, 27]. To extend this work to collective charging of an array of transmon qubits, a proposal was made for a N transmon qubit-resonator system [24]. To the best of our knowledge, collective charging of transmon qubits has not yet been demonstrated in experimental conditions.

2.4.2. CHARGER-MEDIATED ENERGY TRANSFER

The other charging protocol is charging-mediated energy transfer [17]. There are two quantum systems: a charger, and a battery. The energy is transferred from the charger to the battery and may be facilitated by an external drive field. Charger-mediated energy transfer is visualised in figure 2.6b. Its time-dependent Hamiltonian can be written as [17],

$$\hat{H}(t) = \hat{H}_{QB} + \hat{H}_C + \lambda(t) \hat{H}_I \quad (2.44)$$

Here, the internal Hamiltonian \hat{H} contains both the QB and charger Hamiltonian, $\hat{H} = \hat{H}_B + \hat{H}_C$. \hat{H}_I resembles the interaction Hamiltonian.

Charger-mediated energy transfer was studied in the QHO and TLS [17]. Both TLS-TLS, TLS-QHO, and QHO-QHO combinations were considered, both in an ideal system which is exactly solvable [17], and a quantum open system [18]. We will discuss the TLS-TLS combination here, as this best represents two qubits on the Starmon-5 platform. The Hamiltonians of the QB and charger can be written as,

$$\begin{aligned} \hat{H}_{QB} &= \hbar\omega_0 \frac{\hat{\sigma}_z^{(QB)}}{2} \\ \hat{H}_C &= \hbar\omega_0 \frac{\hat{\sigma}_z^{(C)}}{2} \end{aligned} \quad (2.45)$$

Here, the QB and charger are assumed to be in resonance, i.e. $\omega_0 = \omega_{QB} = \omega_C$. The ideal initial and final states are,

$$\begin{aligned} \hat{\rho}_{\text{initial}}^{(QB)} &= |0\rangle \rightarrow \hat{\rho}_{\text{final}}^{(QB)} = |1\rangle \\ \hat{\rho}_{\text{initial}}^{(C)} &= |1\rangle \rightarrow \hat{\rho}_{\text{final}}^{(C)} = |0\rangle \end{aligned} \quad (2.46)$$

Equation (2.47) shows the interaction Hamiltonian \hat{H}_I that facilitates the processes described above.

$$\hat{H}_I = j(\hat{\sigma}_-^{(QB)}\hat{\sigma}_+^{(C)} + \hat{\sigma}_+^{(QB)}\hat{\sigma}_-^{(C)}) \quad (2.47)$$

Here, $\hat{\sigma}_z^{(QB,C)}$ are the Pauli matrices that act on the subspace of the quantum battery and charger, respectively. The constant j is the coupling strength between the charger and the battery. The interaction Hamiltonian H_I leads to so-called flip-flop behaviour. When the charger is discharged, the QB gets charged, and vice versa. This resembles the charger-mediated energy process implemented in chapter 4. Energy transfer takes place through Rabi oscillations. The time-dependent evolution of the total system is given by,

$$|\Psi(t)\rangle^{(QB,C)} = e^{-i\hbar\omega_0 t} [\cos(jt)|1\rangle_C|0\rangle_{QB} - i\sin(jt)|0\rangle_C|1\rangle_{QB}] \quad (2.48)$$

This leads to the figures of merit given in equation (2.49), where the stored energy is $E_s(\tau) = \langle\Psi(t)|\Psi(t)\rangle$, and charging power is $P(\tau) = \frac{E_s(\tau)}{\tau}$.

$$\begin{aligned} E_s(\tau) &= \hbar\omega_0 \sin^2(j\tau) \\ P(\tau) &= \hbar\omega_0 \frac{\sin^2(j\tau)}{\tau} \end{aligned} \quad (2.49)$$

The maximum stored energy is then achieved for $\tau_c = \frac{\pi}{2j}$ and yields $E_s = \hbar\omega_0$. This then gives the ideal power $P_s = \frac{2j}{\pi}\hbar\omega_0$. It is important to mention that these results only account for the ideal quantum battery. It could be that the internal Hamiltonian and interaction Hamiltonian do not commute, i.e. $[\hat{H}, \hat{H}_I] \neq 0$. This then means that for the non-commuting case, energy gets injected into the system via the external classical drive [17].

More properties can be studied that are important in a real quantum system, including energy fluctuations, the presence of loss and noisy mechanisms, and the influence of charging the charger with an external classical field [24]. Further work on charger-mediated energy transfer takes an open system approach [17]. The Gorini-Kossakowski-Sudarshan-Lindblad operator [58, 59] is used to account for coherent and dissipative contributions.

An important consideration taken in further work is the inclusion of the external drive field as part of the system Hamiltonian H , instead of merely part of the classical parameter $\lambda(t)$ [18, 60]. This is important as the full process is 1) charging the charger, and 2) energy transfer to the QB. The first step can influence the energy transfer in the second step. The ergotropy heavily depends on the way that the energy is injected into the charger during the first step [18]. Using a thermal bath at temperature T leads to a vanishing ergotropy [18]. Using a coherent driving field creates an ergotropy approximately equal to the stored energy [18]. This means all stored energy is extractable as work again. Using the *CNOT* gate in the Starmon-5 platform resembles using a charging pulse implemented by a coherent driving field rather than a thermal bath.

When considering a coherent driving field, the flip-flop behaviour occurs both between the drive field and charger, and charger and QB. The total system can then be written as,

$$\begin{aligned}
\hat{H}(t) &= \hat{H}_{QB} + \hat{H}_C + \hat{H}_D + \lambda(t)\hat{H}_I \\
\hat{H}_{QB} &= \hbar\omega_0 \frac{\hat{\sigma}_z^{(QB)}}{2} \\
\hat{H}_C &= \hbar\omega_0 \frac{\hat{\sigma}_z^{(C)}}{2} \\
\hat{H}_D &= \hbar\omega_0 \hat{a}^\dagger \hat{a} \\
\hat{H}_I &= j(\hat{\sigma}_-^{(QB)} \hat{\sigma}_+^{(C)} + \hat{\sigma}_+^{(QB)} \hat{\sigma}_-^{(C)}) + g(\hat{a} \hat{\sigma}_+ + \hat{a}^\dagger \hat{\sigma}_-)
\end{aligned} \tag{2.50}$$

The work on charger-mediated energy transfer exist out of numerical studies, see for example references [17, 18, 60, 61]. To our knowledge, there have been no experimental studies of charger-mediated energy transfer in quantum batteries.

2.5. OPTIMAL CHARGING

2.5.1. PULSE DESIGN

The charging protocol can be optimised by the pulse design of the external electric field, where $\epsilon(t) = \lambda(t)|V(t)|$. The ideal initial state of the QB is the $|0\rangle$ state. Suppose that instead, the initial state of the QB is given by,

$$|\Psi\rangle = \sqrt{a}|0\rangle + \sqrt{1-a}e^{-i\phi}|1\rangle \quad (2.51)$$

Gemme *et al.* showed that via the rotation wave approximation the energy of the system is determined by [25],

$$E(a, \phi, \theta) = \Delta \left[a \sin^2\left(\frac{\theta}{2}\right) + 2\sqrt{a}\sqrt{1-a} \sin(\theta) \sin\left(\frac{\theta}{2}\right) \cos\left(\frac{\theta}{2}\right) + (1-a) \cos^2\left(\frac{\theta}{2}\right) \right] \quad (2.52)$$

Here a and ϕ are the parameters that are determined by the initial state of the QB. The angle θ represents the total area of the pulse wavefront. It can be written as [25],

$$\theta(\tau) = \int_0^\tau \lambda(t) dt \quad (2.53)$$

Theoretically, the stored energy depends solely on the area of the pulse, independent of the specific shape of the pulse $\lambda(t)$ does not impact the stored energy [25]. The practical implementation shows that the function must be (1) fast decreasing and (2) not too narrow [25]. Otherwise, deviations to the ideal charging curve increase due to technical limitations.

Qiskit Pulse allows users to modify the pulse shape. This is not yet supported by Quantum Inspire, but can instead be studied on the IBM platforms.

2.5.2. QUANTUM OPTIMAL CONTROL

Optimal control theory provides a mathematical framework to find the best methods to control a system. Quantum Optimal Control (QOC) is a field that uses optimal control methods to enhance the functionalities of quantum systems. QOC designs the control fields, like electromagnetic pulses, to manipulate quantum systems in the preferred manner. Its primary goal is to find the best way to drive a quantum system to a desired final state while minimising errors and considering constraints. This is important because current Noisy Intermediate-Scale Quantum (NISQ) devices deviate from ideal quantum systems, and noise and decoherences from the environments start playing a role. Using QOC an optimal pulse can be designed that minimises those influences. Examples of what QOC can be used for are state preparation and gate implementation, hence, playing an important role in the path towards a universal quantum computer [62]. For an introductory overview of quantum optimal control, reference [63] is suggested. For more depth on the topic, we refer to the book in reference [64].

More specifically, the total Hamiltonian of a quantum system is given by, $\hat{H}(t) = \hat{H} + \hat{V}(t)$. One can then define $\hat{V}(t) = \lambda(t)\hat{H}_I = \sum_i \lambda_i(t)\hat{H}_i$, where \hat{H}_i are

the Hamiltonians, and $\lambda_i(t)$ are the control fields. For $\langle \hat{H}_i | i = 0, 1, \dots, N \rangle = SU(2^N)$, contains Lie closure and is therefore fully controllable.

The internal Hamiltonian \hat{H} itself can not be changed, and is set by the chosen system and hardware parameters. In reality, the ideal \hat{H} must be replaced by a Hamiltonian that includes all realistic terms, including noise and decoherence of the environment, and errors in the estimated parameters. We call this the real Hamiltonian \hat{H}' . The total Hamiltonian then becomes,

$$\hat{H}(t) = \hat{H}' + \sum_i \lambda_i(t)(\hat{H}_i + \hat{H}'_i) \quad (2.54)$$

The gate implemented in the real setting deviates from the ideal quantum gate. Using equation (2.5), the real gate implemented can be written as.

$$\hat{U}_{\text{gate}}(\tau) = \hat{\mathcal{T}} \exp -i \int_0^\tau dt \left(\hat{H}' + \sum_i \lambda_i(t)(\hat{H}_i + \hat{H}'_i) \right) \quad (2.55)$$

Here, $\hat{\mathcal{T}}$ is the time-ordered exponential. The goal is now to find the optimal control field $\lambda_i(t)$ such that the ideal final state can be reached in the best way possible.

An important elementary example of the use of QOC is the wide implementation of the Derivative Removal by Adiabatic Gate (DRAG) pulse [65]. Additionally to the standard Gaussian pulse, it includes a Gaussian derivative component. It is designed to avoid leakage to higher states, which becomes more prominent in systems with less anharmonicity. Another example includes the Weak Anharmonicity With Average Hamiltonian (WAHWAH) pulse [65], which especially has a large impact when dealing with more than one qubit to avoid leakage. Common QOC algorithms for optimising the pulse shape $\lambda(t)$ include Krotov [66], gradient ascent pulse engineering (GRAPE) [67] and chopped random basis optimisation (CRAB) [68, 69]. These methods are accessible via QuTip [70] in Python. They have been mostly utilised for numerical simulations. In 2022, with the development of Qiskit Pulse [26], the first demonstration of the usage of these QOC methods in real quantum hardware was shown on IBM Q hardware, improving the fidelity of the quantum gates [71].

QOC can also be used for the charging of QBs. In the same way that gates can be optimised, the unitary operator implementing the charging of the QB can be made more suitable for a realistic open-system setting. Until recently, only simple oscillatory charging fields were considered. The first application of QOC for QBs was based on the convergent iterative method [72]. The model considers charger-mediated energy transfer in an open dissipate system, and it was shown that both for TLS-TLS and QHO-QHO models the optimised pulse improves the charging power of the QB [72]. In particular, the energy cost of charging via the external classical drive can also be reduced significantly using the QOC pulse [72]. This energy cost is quantified as the integral of the field squared [72],

$$\mathcal{W}_\tau = \int_0^\tau dt |\lambda(t)|^2 \quad (2.56)$$

This method thus improves the efficiency of charging. This can be interesting from the Quantum Energy Initiative (QEI) perspective [9]. Further work uses a combined analytical-numerical approach based on Pontryagin's Minimum Principle [73]. This work considers both TLS and QHOs and optimises for both direct charging and charger-mediated energy transfer. The main recommendation is the usage of the Bang-Bang behaviour of the external drive $\hat{V}(t)$ as ideal for charging the QB [73].

Both studies consider open-loop optimisation methods. This means that the optimisation is done separately from the experiments, after which the optimised result can be implemented in an experiment. Recently, closed-loop optimisation of superconducting qubit gates was shown to reduce leakage, especially for fast-operating gates [74]. Closed-loop means that results from the experimental implementation of the pulse are used to optimise the pulse. In this way, the proposed algorithm simultaneously adapts the control parameters based on a cost function that considers the result from (experimentally implemented) randomised benchmarking [74]. As the focus of the field of QBs is largely on obtaining faster charging protocols, this optimised pulse shape can also be expected to aid QB charging.

2.6. FIGURES OF MERIT

There are several parameters related to studying the performance of a battery. It is interesting to determine the maximal amount of energy that can be stored on a QB. It is also crucial to be able to extract this as useful work. Then for practical applications, it is important to do this in the least amount of time, and hence, optimise its power.

For charging a QB, we consider the following figures of merit:

- η : Charging success rate. This depends on how many times the qubit successfully transitions to the maximally active state, the $|1\rangle$ state in our framework, and is compared to the total number of measurements.

$$\eta = \frac{E_s}{\Delta} = \frac{N_{|1\rangle}}{N_{|0\rangle} + N_{|1\rangle}} \quad (2.57)$$

- E_s : Total stored energy in the QB. The maximal stored energy depends on the resonance frequency of the transmon qubit, $\Delta = E_{|1\rangle \rightarrow |0\rangle} = \hbar\omega_0$. The total stored energy then depends on the charging success rate and the maximal value of stored energy,

$$E_s = \eta\Delta \quad (2.58)$$

Furthermore, it scales linearly with the amount of qubits in the transmon system: $E_s = NE_s^{(1)}$.

- τ : Charging time. This is the time it costs to fully charge the QB from its initial passive state. In this framework, the total pulse time of the charging pulse is taken as charging time.

$$\tau = \sum_i t_{\text{pulse}}^{(i)} \quad (2.59)$$

When using gate operations, the gate time is the same as the pulse time.

- P_c : Charging Power. The charging power depends on finding the aforementioned parameters,

$$P_c = \frac{E_s}{\tau} \quad (2.60)$$

3

QUANTUM BATTERY IMPLEMENTATION ON THE QUANTUM INSPIRE

This chapter shows the results of the quantum battery (QB) implementation on the Starmon-5 device using Quantum Inspire. The charging of the QB is characterised by studying the state-to-state transfer from the passive state to the maximally active state using the native $R_x(\theta)$ gate. The results are promising, showing a charging ratio of 97% on average. This leads to an average stored energy of $E_s = 23\mu\text{eV}$ per qubit. The charging process takes $\tau = 20\text{ns}$, leading to an average charging power of 1.1eV/ms per qubit. Whilst qubit q_0 performs best in terms of the highest charging ratio, the qubit q_4 attains the highest amount of stored energy and charging power. This is because the energy level splitting is larger for this qubit, enabling one to store more energy in one qubit.

3.1. STARMON-5 IN QUANTUM INSPIRE

The Starmon-5 is a superconducting quantum processor consisting of 5 transmon qubits [29]. It is openly accessible via Quantum Inspire, an online environment for cloud-based quantum computing, created and designed by QuTech [28]. QuTech is a research institute of the TU Delft and TNO.

The Starmon-5 consists of 5 qubits: q_0 , q_1 , q_2 , q_3 , and q_4 . It is shaped in an X-coupling configuration, see figure 3.1. The single-qubit gates are implemented by the microwave control lines, each single-qubit takes 20ns. Two-qubit gates are implemented using the flux-control line and dedicated bus resonators between two qubits, which enable the nearest-neighbour coupling. The available two-qubit gate is the controlled-Z (CZ) gate, and takes 40ns. Furthermore, the readout is done by the dispersively-coupled shared resonator using the readout feedlines.

A native gate is a gate that can directly be implemented on the quantum processor, whilst all other gates must be decomposed into native gates. The topology of Starmon-5 leads to the native gates summarised in table 3.1. This forms a complete

set for the computational basis of quantum computing, meaning all other gates can be decomposed in combinations of the native gates.

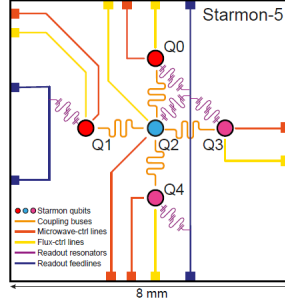


Figure 3.1.: Starmon-5 hardware platform. The platform consists of 5 superconducting transmon qubits, designed in an X-coupling configuration. Figure obtained from reference [29].

	Native gates	Duration (ns)
Single-qubit gates	X, Y, I, $R_x(\theta)$, $R_y(\theta)$, $R_z(\theta)$ X90, Y90, mX90, mY90	20
Two-qubit gates	CZ	40

Table 3.1.: Specifics of the native gates in Starmon-5 in Quantum Inspire. The native gates and single-qubit gate time of 20ns are obtained from [75]. The two-qubit gates complete within 40ns [76] (previously 60ns and 80ns [29]). *Notation:* X, Y stand for the Pauli-X,Y matrices, giving a π rotation around their respective axis. I is the identity matrix. $R_x(\theta)$ is a rotation of angle θ around the x-axis, X90 is a rotation of $\frac{\pi}{2}$ around the x-axis, mX90 is a rotation of $-\frac{\pi}{2}$ degrees around the X-axis. CZ stands for controlled-Z gate.

3.2. QUANTUM BATTERY FRAMEWORK

We implement here the most elementary case of a QB in Quantum Inspire. The QB consists of a single ($N = 1$) two-level ($d = 2$) quantum system. The energy is injected via direct charging. We consider the internal Hamiltonian to be:

$$\hat{H} = \hbar\omega_0 \frac{\hat{\sigma}_z}{2} \quad (3.1)$$

The QB has two energy levels ϵ_0 corresponding to $|0\rangle$, and ϵ_1 corresponding to $|1\rangle$. The ideal initial state is then,

$$\hat{\rho} = |0\rangle\langle 0| \quad (3.2)$$

And implicitly, the maximally active state is,

$$\hat{\rho}^* = |1\rangle\langle 1| \quad (3.3)$$

The ergotropy then becomes,

$$\mathcal{W} = \text{tr}[\hat{\rho}^* H] - \text{tr}[\hat{\sigma}_\rho \hat{H}] = \epsilon_1 - \epsilon_0 = \Delta \quad (3.4)$$

For the qubits, this energy difference can be found by the resonance frequency, $\Delta = \hbar\omega_0$. All Starmon-5 qubits have an individual resonance frequency of about 5–6GHz, of which the exact values can be found in table 3.2.

The external time-dependent field $V(t)$ must implement a rotation of π to facilitate the $|0\rangle \rightarrow |1\rangle$ transition employing direct charging. This can be implemented by creating a pulse via Qiskit Pulse, as done by Gemme *et al.* on IBM quantum devices [25]. In our case, we use:

$$V(t) = R_x(\theta(t)) \quad (3.5)$$

with $R_x(\theta(0)) = \mathbb{1}$ and $R_x(\theta(\tau)) = R_x(\pi) = X$. This decision is elaborated in the next section.

3.3. CHARGING VIA RX GATE

The current Starmon-5 backend does not support Qiskit Pulse, making it impossible to directly replicate the procedure used by Gemme *et al* [25]. However, native $R_x(\theta)$ gates can be used to study the charging of the QB. The native $R_x(\theta)$ gate is a DRAG pulse rather than a Gaussian, which was the pulse shape implemented in the study by Gemme *et al.* As discussed in section 2.5.2, the DRAG pulse is shaped like a Gaussian, but includes an additional Gaussian derivative component. It is designed to reduce the leakage outside of the computational basis. The framework in section 2.5.1 suggests that the charging depends on the total area applied, rather than the pulse shape, see equations (2.52) & (2.53). The work suggests that the pulse function has to be not too narrow and fast-decreasing. The DRAG pulse satisfies both criteria, which thus justifies using the native $R_x(\theta)$ gate to charge the QB.

To verify this, Appendix A contains our results for using the native $R_x(\theta)$ gates compared to the Gaussian pulse-shaped QB implementation on IBM Quantum Hardware. The charging curve and metrics of performance are comparable. The advantage of modular pulse shaping is that the charging time can be decreased arbitrarily, but as the single gates of the Quantum Inspire already have a low gate duration (20ns), this does not pose a constraint. Hence, we characterise the qubits on the Starmon-5 quantum processor as QBs based on charging via the $R_x(\theta)$ gate. This is visualised in figure 3.2.

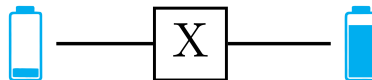


Figure 3.2.: The implementation of the X gate in Quantum Inspire facilitates direct charging of a QB.

3.4. QUANTUM BATTERY IMPLEMENTATION

A QB is implemented on the Starmon-5 processor using the native $R_x(\theta)$ gate. The result is shown in figure 3.3. There are 16 evenly-spaced intervals taken for $\theta \in [0, 2\pi]$. Each data point corresponds to the average outcomes corresponding to the amount of $|1\rangle$ state outcomes compared to the total of 1024 measurements. This procedure was repeated 20 times.

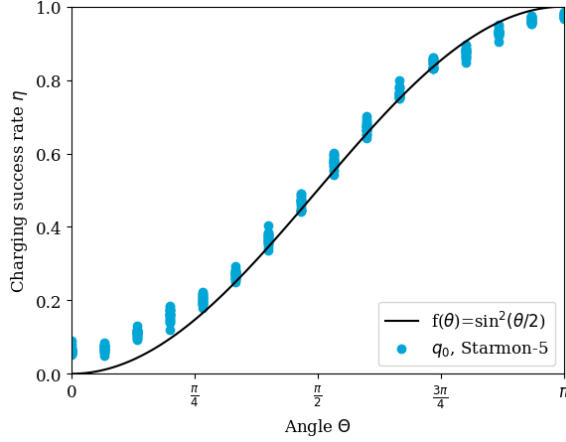


Figure 3.3.: Charging the QB on the Starmon-5. The charging success rate is given for different angles θ (also referred to as pulse area). The charging success rate represents the average energy in the qubit q_0 of the Starmon-5 in units of $\Delta = 26.55\text{eV}$. Blue dots: Each data point represents the average of 1024 measurements. Black line: The charging of an ideal QB, corresponding to $E(\theta) = \sin^2(\frac{\theta}{2})$

In figure 3.4, the mean values for each angle are shown including their standard error in black. As can be seen from the standard error, the amount of data $N = 20$ (each constituting the average of 1024 measurements) provides good precision and high reliability of the estimates. This is the amount of data points that were suggested as a good compromise between the quality of data and the time required to obtain the data [25]. We observe that $N = 10$ has a marginal effect on the mean value and standard errors. Hence, in section 3.5 we use $N = 10$ to compare the data of all qubits.

The real QB is prone to initialisation errors. The initialisation errors can be deducted from fitting the data to equation (2.52), instead of the ideal curve $E(\theta) = \sin^2(\frac{\theta}{2})$. This way, one can get the best estimates for a and ϕ , which can be substituted into equation (2.51) to get the initial wave function. The ideal values are $a = 1$, and $\phi = 0$. The best-fit values are found to be:

$$\begin{aligned} a &= 0.95829 \pm 0.00522 \\ \phi &= 0.12458 \pm 0.02902 \end{aligned} \tag{3.6}$$

The blue line in figure 3.4 represents the fit function, created by filling the best-fit values of a & ϕ into equation (2.52). It can be seen that this is well aligned with the mean value data points. The fit values in equation (3.6) are comparable with the work on IBM quantum batteries ($a^{(1)} = 0.981 \pm 0.003$, $\phi^{(1)} = 0.45 \pm 0.06$ for $\tau = 600\text{ns}$ and $a^{(2)} = 0.964 \pm 0.003$, $\phi^{(2)} = 0.30 \pm 0.06$ for $\tau = 130\text{ns}$ [25]). This lower value of a suggests a higher initialisation error. We suspect that it may also occur due to the reduced charging time in Quantum Inspire ($\tau = 20\text{ns}$ compared to $\tau = 135\text{ns}$), and thus show the deviation of the general charging curve rather than initialisation errors.

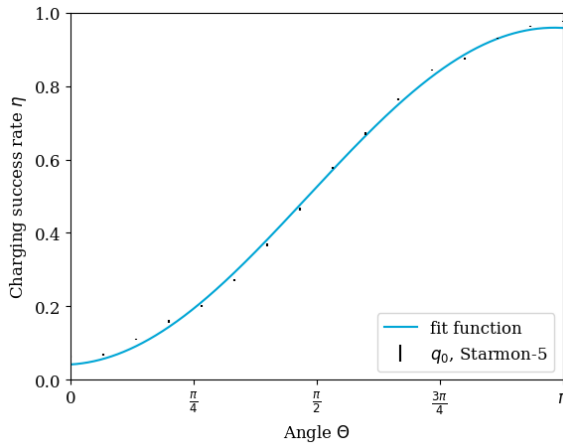


Figure 3.4.: Analysis of charging of the QB in Quantum Inspire (q_0 , Starmon-5). The mean value including error bars is shown in black. The fit function, using $a=0.958$, and $\phi= 0.125$ is shown in blue.

3.5. CHARGING OF Q0, Q1, Q2, Q3, Q4

Table 3.2 shows the data acquired for charging each qubit of the Starmon-5 platform individually. It can be observed that q_3 performs the best in terms of final stored energy, and fit value to the ideal curve. However, all qubits perform very comparably, and all show great promise for charging as QB.

The same fit function as given in section 3.4 is used for determining the charging trajectories of each qubit. These are plotted in figure 3.5. It can be observed that all trajectories are comparable as well.

It must be mentioned that there is a small difference in the circuit used for q_0 , as the data was acquired using `qc.measure_all()`. This measures all qubits simultaneously. For all other qubits, `qc.measure(qr[qubit], cr[qubit])` was used, which only measures the chosen qubit, and maps this qubit to a specific classical bit. This was suggested as it avoids possible cross-talk during measurement [76]. However, as q_0 went offline during the time of this study, it was not possible

to acquire the data again. As can be seen from table 3.2, the values of q_0 do not unexpectedly deviate from the other qubits, hence this dataset is used.

Qubit	ω_0 (GHz)	η	a	ϕ
q_0	6.420	0.974	0.958	0.126
q_1	6.522	0.956	0.971	-0.994
q_2	5.699	0.975	0.989	-0.105
q_3	5.042	0.984	0.992	-0.097
q_4	4.905	0.945	0.974	-0.128

Table 3.2.: Experimental values for all 5 qubits in Starmon-5, Quantum Inspire. The resonance frequencies ω_0 were acquired from Quantum-Inspire, the charging success rate η , and fit data a and ϕ were all acquired from the experimental data.

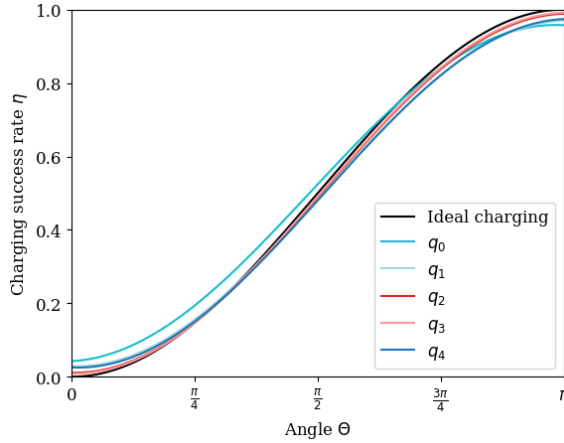


Figure 3.5.: Charging trajectories for all five qubits of Starmon-5, Quantum Inspire.

3.6. FIGURES OF MERIT

The figures of merits were found for each qubit, and are presented in in table 3.2. The qubits q_0 and q_1 store the largest amount of energy. The charging time is the gate time of a single-qubit gate, $\tau=20\text{ns}$. As the charging time is the same for all qubits, the charging power scales linearly with the energy stored in the QB E_s . Hence, in terms of charging power, qubits q_0 and q_1 also give the best performance.

3.7. DISCUSSION

In this chapter, the implementation of a quantum battery on the Starmon-5 of the Quantum Inspire platform was shown.

Qubit	$E_s(\mu\text{eV})$	$\tau(\text{ns})$	$P_c(\text{eV/ms})$
q_0	25.9	20	1.30
q_1	25.8	20	1.29
q_2	23.0	20	1.15
q_3	20.5	20	1.03
q_4	19.2	20	0.959

Table 3.3.: Figures of merit for all 5 qubits in Starmon-5, Quantum Inspire.

CHARGING SUCCESS RATE.

We find that the charging success rate (η) of the Starmon-5 qubits is $\eta = 0.967$ on average. It can be concluded from the data that qubit q_3 performs the best in terms of charging success rate, with $\eta = 0.984$. These results are comparable with previously obtained results for the Armonk processor of the IBM quantum platform, where $\eta > 0.95$ was obtained [25].

STORED ENERGY

The stored energy (E_s) depends on the charging success rate and the resonance frequency. The difference in resonance frequencies is larger than the difference in success rate, and thus the resonance frequency dominates which qubit effectively stores the most energy. For the Starmon-5 processor, this is qubit q_0 , which stores $E_s = 26.6\mu\text{eV}$. The average stored energy of all qubits is $E_s = 22.9\mu\text{eV}$. This is slightly higher than the previously obtained result, which can be calculated to have a stored energy of $E_s = 20.6\mu\text{eV}$ [25]. Further work charges a qutrit on the IBM quantum platform, leading to an increase of stored energy, which can be calculated to be $E_s = 36.1\mu\text{eV}$ based on the results in reference [27]. This can be explained as here transitions are driven to the second energy state $|2\rangle$ by exploiting the possibilities of Qiskit Pulse. As Quantum Inspire does not yet support Qiskit Pulse, our work focuses on operations within the computational basis.

INITIALISATION ERRORS

The fit function to the stored energy of the QB, as given in equation (2.52), also shows that the same qubit is also subject to the lowest initialisation errors, $1 - a = 0.023$. However, this does not hold in full generality: it was concluded by Gemme *et al.* that initialisation errors lead to a counter-intuitive improvement in the charging of the QB [25]. We expect based on the theoretical framework discussed in section 2.1.3 that these initialisation errors will lead to a decrease in the ergotropy. Using cyclic operations, initialisation errors can reduce the available work as the process is subject to the conservation of eigenvalues.

CHARGING TIME

The charging time of our qubits is set to $\tau=20\text{ns}$, whilst previous work shows a minimal pulse time of $\tau=30\text{ns}$ ¹[27] and $\tau=135\text{ns}$ [25]. Thus, our implemented charging times are shorter than previously reported charging times. We expect that this is a result of using the native $R_x(\theta)$ gate, which uses the DRAG pulse, a well-known optimised pulse shape for reducing leakage to higher computational subspaces. Gemme *et al.* instead designed their pulse shape based on Gaussian shapes [25, 27].

CHARGING POWER

Our results lead to an average charging power of $P_c=1.14\text{eV/ms}$, with a maximum power of $P_c=1.30\text{eV/ms}$ for qubit q_0 . The charging power of q_0 is better than the QB with the highest charging success rate q_3 due to the larger transition energy. This again emphasises the importance of the transition energy when deciding which qubit to use as a quantum battery. Our values are an improvement compared to the work on the Armonk processor, which can be calculated to have a maximum power of $P_c=0.145\text{eV/ms}$ (mainly due to the higher charging time) based on the results in reference [25]. Interestingly, our charging power is in fact higher than the charging power of the qutrit implementation on IBM hardware, which can be calculated to be $P_c=1.20\text{eV/ms}$ [27]. This is due to a combination of a lower charging success rate and a higher charging time of the qutrit.

¹Simulations of the theoretical behaviour show that the QB is already charged for $E=0.95\Delta$ at time $t=\frac{2}{3}\tau$ [27]. Thus, although the pulse time is set at 30ns, the authors use a charging time of 20ns. We do not take this into account for our results, and therefore also use $\tau=30\text{ns}$ to ensure a fair comparison of the studies. Another argument for not taking this into account is that the energy decomposition always requires the full pulse time, even if the battery is already charged at an earlier stage.

4

CHARGER-MEDIATED ENERGY TRANSFER IN QUANTUM INSPIRE

The quantum battery (QB) in Quantum Inspire is charged via charger-mediated energy transfer. Another quantum system is initialised in the maximally active state, and acts as the charger. An external pulse facilitates the transfer of energy from the charger to the quantum battery. The unitary gate that is used for this is the two-qubit CNOT gate. This is not a native gate for the Starmon-5 processor, leading to an increase in the charging time from 20ns for direct charging to 120ns for charger-mediated energy transfer. The qubit q_2 is taken as the charger, whilst the other qubits (q_1, q_3, q_4) are used as the QBs. The data shows a minimal effect on the success rate of charging. As the charging time is increased significantly, the charging power also decreases noticeably. Charger-mediated energy transfer is therefore mainly recommended to be used for specific applications.

4.1. CHARGER MEDIATED ENERGY TRANSFER FRAMEWORK

Charger-mediated energy transfer means that the quantum battery is charged via another quantum system, referred to as the charger. For the full description, see section (2.4.2). In Quantum Inspire, we study the energy transfer between two qubits. The charger and quantum battery can be described via their density matrix and initial Hamiltonian:

$$\begin{aligned} \text{Charger: } \quad & \hat{\rho}_C, \hat{H}_C \\ & E_C(t) = \text{tr}[\hat{H}_C \hat{\rho}_C(t)] \end{aligned} \tag{4.1}$$

$$\begin{aligned} \text{Battery: } \quad & \hat{\rho}_{QB}, \hat{H}_{QB} \\ & E_{QB}(t) = \text{tr}[\hat{H}_{QB} \hat{\rho}_{QB}(t)] \end{aligned} \tag{4.2}$$

As the charging occurs between the $|0\rangle$ and $|1\rangle$ states of the superconducting transmon qubits in Starmon-5, both the charger and the battery are TLS. To maximally extract work from the charger, it is initialised in the $|1\rangle$ state, whilst the

QB is initialised in the $|0\rangle$ state. This means the initial state of the total system becomes,

$$\hat{\rho}_{C,QB}(0) = |1\rangle\langle 1|_C \otimes |0\rangle\langle 0|_{QB} \quad (4.3)$$

The initial energy levels are ϵ_0 corresponding to the energy of the state $|0\rangle$, and ϵ_1 corresponding to the state $|1\rangle$, and $\epsilon_0 = -\epsilon_1 = \hbar\omega_0$ where ω_0 is the resonance frequency of the QB. For ideal charging, the aim for the final state is:

$$\hat{\rho}_{C,QB}(\tau) = |0\rangle\langle 0|_C \otimes |1\rangle\langle 1|_{QB} \quad (4.4)$$

We are looking to implement a unitary operator that facilitates this via,

$$\hat{U}\hat{\rho}(0) = \hat{\rho}(\tau) \quad (4.5)$$

4

4.2. CNOT GATE FOR ENERGY TRANSFER

Ideally, a native two-qubit gate operation is used to facilitate the charger-mediated energy transfer, as this allows for minimising the charging time and input pulses. The Starmon-5 only has the CZ gate as a native two-qubit gate, which implements a phase flip. This does not directly lead to a change in the energy state of the qubits. Thus, we must look at different two-qubit gates that can be decomposed into the CZ gate and native single-qubit gates.

SWAP GATE

At first sight, the SWAP gate seems an ideal candidate for charger-mediated energy transfer: it implements the desired transfer of states, whilst keeping the quantum states separable at all times. See equation (4.6). It swaps the states of the two quantum systems, which can be seen as energy transfer from the charger to the battery and vice versa.

$$\text{SWAP} = \begin{bmatrix} 1 & 0 & 0 & 0 \\ 0 & 0 & 1 & 0 \\ 0 & 1 & 0 & 0 \\ 0 & 0 & 0 & 1 \end{bmatrix} \quad (4.6)$$

However, the SWAP gate is decomposed into 3 CNOT gates [77]¹. The CNOT gate itself also implements the transition from the ideal initial state in equation (4.3) to the ideal final state in equation (4.4). It is only when initialisation errors occur that the CNOT gate does not implement the ideal protocol, and may also act as an entangling gate. This may pose constraints on the ergotropy [2]. Due to the large difference in charging time, the CNOT gate is used for charger-mediated energy transfer.

¹This leads to a total of 6 Hadamard gates, decomposed of 12 native single qubit gates, and 2 CZ gates. The total charging time becomes 280ns.

CNOT GATE

The CNOT operation is given in equation (4.7). Choosing the charger as a control qubit, and ensuring the QB starts in the ground state, the CNOT gate can be used to transfer the energy from the charger to the battery.

$$\text{CNOT} = \begin{bmatrix} 1 & 0 & 0 & 0 \\ 0 & 1 & 0 & 0 \\ 0 & 0 & 0 & 1 \\ 0 & 0 & 1 & 0 \end{bmatrix} \quad (4.7)$$

The CNOT gate is not a native gate of the Starmon-5 processor, see table 3.1 for all native gates. The gate must thus be decomposed into several native gates. The native 2-qubit gate of Quantum Inspire is the CZ gate. The CNOT gate can be created from the following scheme:

1. Hadamard gate H on the charger qubit
 - X on the charger qubit
 - Y90 on the charger qubit
2. CZ gate between the charger and battery qubit
3. Hadamard gate H on the charger qubit
 - X on the charger qubit
 - Y90 on the charger qubit

This leads to a total charging time of 120ns (4 native single-qubit gates, 1 native two-qubit gate). This is a large limitation of the current hardware for the implementation of charger-mediated energy transfer.

CZ GATE

The CZ gate can be implemented on a superconducting quantum processor [78, 79]. When a CZ gate is applied to a target and control qubit, the target qubit acquires a phase based on the phase of the control qubit. The control and target qubit must have a shared coupling resonator. To implement the CZ gate, the frequencies of the two qubits must be in resonance. As can be seen from table 3.2, the resonance frequencies of all qubits vary slightly. The resonance frequency can be modified by changing the flux in the SQUID loop of the qubit. Hence, by changing the voltage on the flux bias line, the frequency of the target qubit can be brought in resonance with the control qubit. By operating near the avoided crossings of the $|11\rangle$ and $|02\rangle$ states, the change in phase starts to accumulate. It is important that the crossing to the $|02\rangle$ does not take place, as this state is out of the computational basis.

The CZ gate is implemented by varying the detuning slowly with a ramp time t_R and interaction time t_I [78]. Entangling evolution is allowed to occur during t_I , but afterwards, the system returns to its original state. This is complementary to how charger-mediated energy transfer of a QB is described to take place (see section 2.4.2).

In terms of external driving, only one flux pulse is required to implement the CZ gate. As described above, by adding two Hadamards the CNOT gate can be created. This facilitates our implementation of charger-mediated energy transfer in transmon qubits.

CNOT GATE FOR ENERGY TRANSFER

Figure 4.1 shows the circuit for charger-mediated energy transfer in Quantum Inspire. To study the dependence on the angle $\theta(t)$, the $R_x(\theta)$ gate is first implemented on the control qubit (q_2), after which the CNOT is applied between the control qubit and target qubit (q_1 , q_3 , or q_4). Note that the CNOT gate is in reality decomposed into the native gates.

4

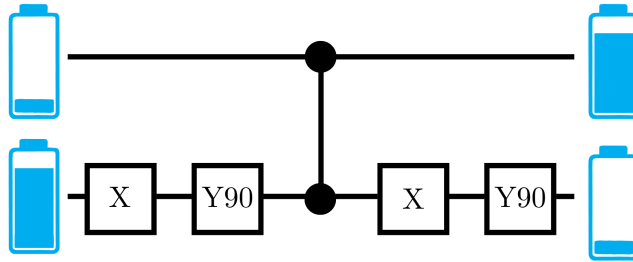


Figure 4.1.: The implementation of the CNOT gate in Quantum Inspire facilitates charger-mediated energy transfer of a QB. The CNOT gate decomposition of native gates is shown: X-Y90-CZ-X-Y90.

4.3. CHARGER-MEDIATED ENERGY TRANSFER IMPLEMENTATION

One qubit (q_2) acts as a charger, whilst another qubit (q_1 , q_3 or q_4) acts as a QB. We choose this scheme as qubit q_2 is connected with all other qubits via shared resonators, which can be seen in figure 3.1. Charger-mediated energy transfer is implemented by using the CNOT gate. The charging of the battery qubits is shown in figure 4.2. Again, the charging data closely adheres to the ideal charging curve. The relevant values of the charging success rate can be found in table 4.1. The charging from q_2 to q_3 seems to perform best, both in terms of charging success rate (η) and closest fit to the ideal charging curve (a, ϕ). The fit variables are used to visualise all charging trajectories in figure 4.3.

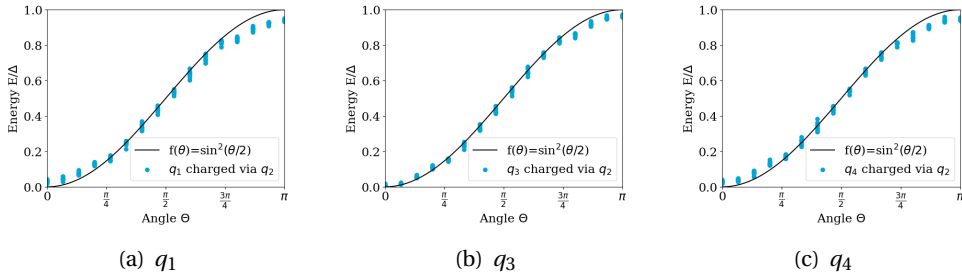


Figure 4.2.: Charger-mediated energy transfer in Quantum Inspire, data plots. The q_2 qubit functions as the charger, whilst the other qubits (a) q_1 , (b) q_3 , and (c) q_4 are implemented as quantum batteries.

Qubit	ω_0 (GHz)	η	a	ϕ
$q_1 q_2$	6.522	0.940	0.954	-0.0823
$q_3 q_2$	5.042	0.966	0.980	-0.0951
$q_4 q_2$	4.905	0.948	0.960	-0.0479

Table 4.1.: Experimental values for all 5 qubits in Starmon-5, Quantum Inspire. The resonance frequencies ω_0 were acquired from Quantum-Inspire, the percentage of full charging E/Δ , and fit data a and ϕ were all acquired from the data presented in figure 4.3.

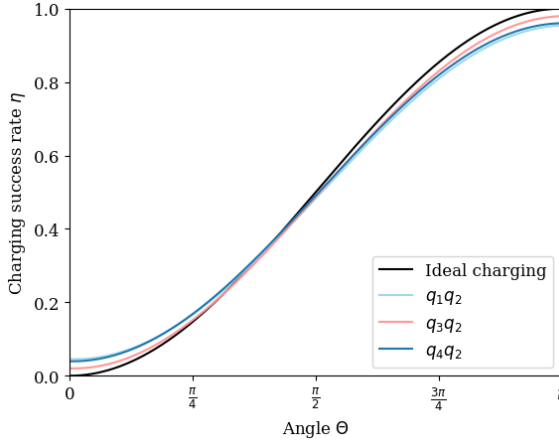


Figure 4.3.: The fit functions of all charger-mediated energy transfer trajectories, $q_1 q_2$, $q_3 q_2$ and $q_4 q_2$.

4.4. FIGURES OF MERIT

The figures of merit for charger-mediated energy transfer in Quantum Inspire can be found in table 4.2. The amount of stored energy is $22.7\mu\text{eV}$ on average. The

total charging time takes 120ns, as this is the total operation time to implement a CNOT gate. This is a 6-fold increase compared to direct charging. Lastly, the average charging power of charger-mediated energy transfer is 0.18eV/ms. It is not yet possible to replicate the theoretical improvement of the charging power of charger-mediated energy transfer [60] due to the technical constraints of current operational specifics.

Qubit	$E_s(\mu\text{eV})$	$\tau(\text{ns})$	$P_c(\text{eV/ms})$
q_1	25.4	120	0.211
q_3	20.1	120	0.168
q_4	19.2	120	0.160

Table 4.2.: Figures of merit for charger-mediated charging in the Starmon-5 processor. All qubits functioning as QB (q_1, q_3, q_4) are charged via charger q_2 .

4

4.5. DISCUSSION

Charger-mediated energy transfer was implemented utilising a CNOT gate between two qubits in Starmon-5.

CHARGING SUCCESS RATE

The charging success rate (η) has an average of 0.951, making it comparable with both our results of direct charging ($\eta=0.967$) and existing literature ($\eta > 0.95$). It was initially expected to be slightly less efficient since the CNOT gate requires multiple gate operations, consisting of multiple single-qubit gates, and a two-qubit gate. This can lead to more errors throughout the charging process, hence reducing the success rate of charging. Fortunately, this only has a marginal effect in reality.

STORED ENERGY

Charger-mediated energy transfer leads to an average stored energy of $E_s = 21.6\mu\text{eV}$, which is very comparable to the ideal amount of stored energy $E_s = 22.7\mu\text{eV}$. The stored energy is also almost the same as for direct charging, which is on average $E_s = 21.8\mu\text{eV}$ for q_1, q_3 and q_4 . This shows promising results of the effectiveness of implementing a CNOT gate for charger-mediated energy transfer in superconducting transmon qubits.

INITIALISATION ERRORS

The same qubits are initialised in the same way as during direct charging, yet the initialisation error is here estimated to be $1 - a = 0.034$ on average. It is higher compared to direct charging of these qubits ($1 - a = 0.021$). This suggests that this value does not only represent initialisation errors but is indeed also influenced by the rest of the charging curve.

CHARGING TIME

The charging time was determined to be $\tau=120\text{ns}$ based on the operation time of the native gates composing the CNOT gate. This is a 6-fold increase compared to direct charging and thus poses a large constraint on using charger-mediated energy transfer. The reason is clear: the CNOT gate is not a native gate operation and is decomposed into 4 native single-qubit gates and the native two-qubit gate.

The IBM quantum platform does have hardware available for which the CNOT gate is native. However, the total gate time is not reduced compared to the CNOT implementation on Quantum Inspire. For example, on IBM Cairo the minimal CNOT gate duration is 167ns (q_5, q_8). This is a higher charging time than the CNOT gate in Quantum Inspire. We conclude that it is a crucial job to improve this quantity for the use of superconducting transmon hardware for charger-mediated energy transfer.

Furthermore, we have chosen not to take the initialisation of the charger into account. One could therefore take also the charging of the charger qubit into account for the total charging time, meaning $\tau=\tau_{CNOT} + \tau_{R_x} = 140\text{ns}$. This results in a 7-fold increase and does not change the implications. In both cases, the charging time is a lot longer compared to the case of direct charging. Another reason to not take the initialisation time into account is also that one may want to have a waiting time between initialising and transferring the energy.

CHARGING POWER

Subsequently, the charging power is also significantly reduced due to the higher charging time. The average charging power is now 0.18eV/ms , which is again 6 times smaller than the direct charging of the qubits.

OTHER REMARKS

A critical question to ask is whether the energy is transferred from the charger to the battery when using the CNOT gate. Although the external field is used to bring the qubits in resonance, it is likely that also some energy is contributed from this external field. This requires further investigation. Interestingly, it was shown that in an open quantum system, the CNOT gate can be used for work and heat conversion, effectively acting as a quantum engine or quantum refrigerator [80]. Better insight into the exact process of energy transfer is required here. This can be used to design a pulse that ensures the energy transfer solely takes place between the charger and battery.

5

CHARGING OF MULTIPLE QUBITS

A quantum battery consisting of 4 superconducting qubits is charged using parallel charging. This is implemented by applying the $R_x(\theta)$ gate on all qubits simultaneously. The figures of merit are effected as follows. The stored energy increases linearly with the amount of qubits. Comparing the parallel charging of the qubits to the separate charging of each qubit, the total energy remains approximately the same. The charging time is only 20ns, as the charging occurs simultaneously. This leads to a 4-fold increase in power compared to individual charging, as can be expected from $N=4$ qubits. Collective charging giving the full quantum advantage can currently not be implemented on the Starmon-5 processor due to the lack of multi-qubit coupling. The possibility of exploiting nearest-neighbour coupling for a quantum advantage of $\Gamma \propto 2$ is discussed. For future design of quantum processors, adding a shared resonator to the architecture of the qubits may allow to achieve the N -fold quantum advantage.

5.1. PARALLEL CHARGING

5.1.1. PARALLEL CHARGING FRAMEWORK

Parallel charging means that local operations are used on each qubit to bring them to the fully charged state. It is a classical process. Considering identical qubits, the total amount of energy is expected to increase linearly with the number of qubits. This is referred to as an extensive process.

The framework is the same as for direct charging, except the charging is applied to all qubits simultaneously. This means that our internal Hamiltonian for 4 qubits is given by,

$$\hat{H} = \sum_i^{N=4} \hbar \omega_0^{(i)} \frac{\hat{\sigma}_z^{(i)}}{2} \quad (5.1)$$

The passive state can be given by,

$$\hat{\sigma}_\rho = |0\rangle\langle 0|^{\otimes N} \quad (5.2)$$

And the maximally active state becomes,

$$\hat{\rho} = |1\rangle\langle 1|^{\otimes N} \quad (5.3)$$

The ergotropy is then given by $\mathcal{W} = \sum_i^{N=4} \Delta_i$. In a similar way as done in chapter 3, the $R_x(\theta)$ gate is used to charge each qubit individually. For complete charging, this results in $R_x(\pi)=X$. The gates are applied simultaneously, leading to the parallel charging of an array of 4 qubits on the Starmon-5 processor.

5.1.2. PARALLEL CHARGING USING RX GATES

We implement this on the quantum computer by simultaneously applying the $R_x(\theta)$ gate on all qubits. The gate implementation is visualised in figure 5.1. Parallel implementation of gates can negatively impact the figures of merit due to cross-talk between the qubits, depending on the performance of the quantum device. It is relevant to study this phenomenon for superconducting transmon qubits to estimate the potential for scalability.

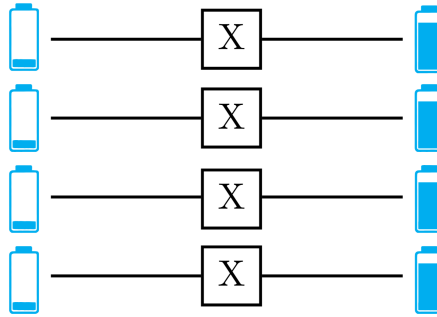


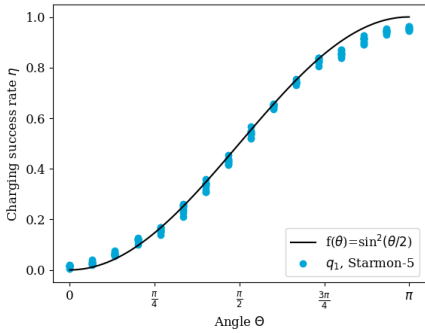
Figure 5.1.: The implementation of multiple X gates in Quantum Inspire facilitates parallel charging of multiple qubits as QB.

5.1.3. PARALLEL CHARGING IMPLEMENTATION

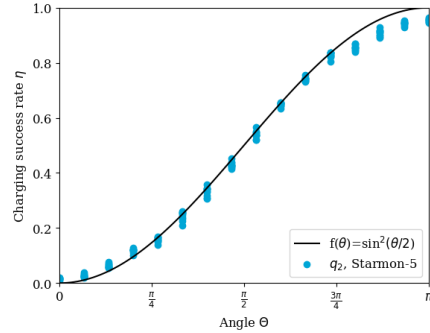
The experimental data is shown in figure 5.2. Note that although the data is shown separately, the qubits are all charged simultaneously during the same process. The relevant parameters are given in table 5.1. Using the fit functions of each qubit, figure 5.3 shows the charging trajectories of the qubits.

5.1.4. FIGURES OF MERIT

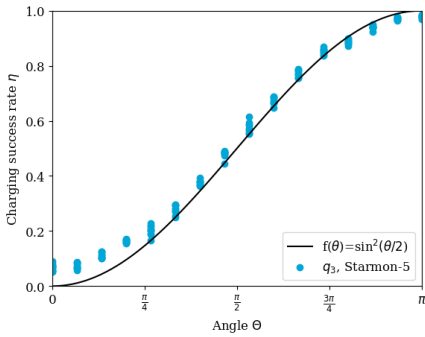
The figures of merit can be found in table 5.2. The total stored energy $E_s = 88.2\mu\text{eV}$. The total charging time of four qubits in parallel is the same as the charging time of one qubit, $\tau=20\text{ns}$. This leads to a relatively high charging power of $P_c=4.41\text{eV/ms}$.



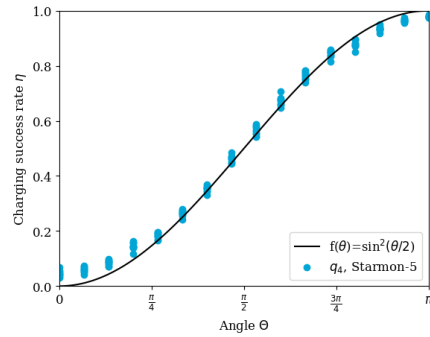
(a)



(b)



(c)



(d)

Figure 5.2.: Parallel charging of four qubits on the Quantum Inspire platform using the $R_x(\theta)$ gate. The charging curves are shown of qubits (a) q_1 , (b) q_2 , (c) q_3 , and (d) q_4 . Blue points indicate the raw data from experiments, and the black line indicates the ideal charging curve.

Qubit	ω_0 (GHz)	η	a	ϕ
q_1	6.522	0.955	0.972	-0.0857
q_2	5.699	0.978	0.960	0.168
q_3	5.042	0.979	0.970	0.0973
q_4	4.905	0.934	0.966	-0.195

Table 5.1.: Experimental values of charging qubits q_1 , q_2 , q_3 , q_4 from the Starmon-5 processor in parallel.

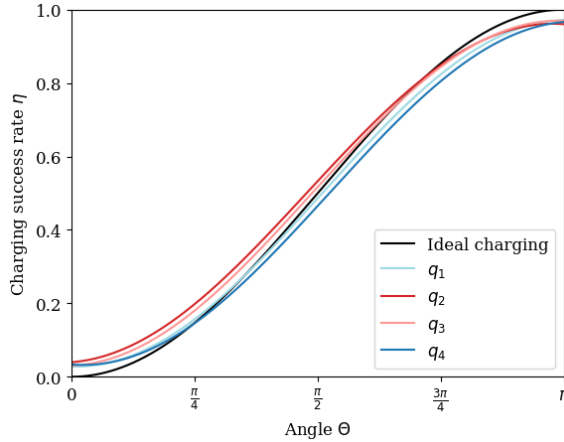


Figure 5.3.: The charging curves of all available qubits (q_1 , q_2 , q_3 and q_4) on the Starmon-5 processor when being charged in parallel. The charging curve is based on the fit function of equation (3.6), and the experimental data given in table 5.1.

Qubits	E_s (μeV)	τ (ns)	P_c (eV/ms)
$q_1 q_2 q_3 q_4$	88.2	20	4.41

Table 5.2.: Figures of merit for parallel charging of 4 qubits on Starmon-5, Quantum Inspire.

5.1.5. DISCUSSION

Parallel charging in the transmon qubits of Starmon-5 shows promising results. Within error ranges, the total amount of energy stored is exactly N times as large as the energy stored in the individual qubits. This is promising for the scalability of qubits as QBs, even without exploiting the quantum advantage.

CHARGING SUCCESS RATE

The charging success rate is $\eta=0.96$ for the qubits on average. Again, this is a relatively good result, and comparable with the P_c success rate of direct

charging ($\eta = 0.967$), charger-mediated energy transfer ($\eta = 0.951$) and previously reported values in literature ($\eta > 0.95$)[25, 27].

STORED ENERGY

The amount of stored energy is the sum of energy stored in each qubit, which becomes $E_s = \sum_{i=1}^{i=4} E_s^{(i)} = 88.2 \mu\text{eV}$ for parallel charging of the QB. The maximum available stored energy is $E_s = 91.7 \mu\text{eV}$. The total of the stored energy of the four qubits when charged individually with direct charging is $\sum_{i=1}^{i=4} E_s^{(i)} = 88.4 \mu\text{eV}$. Hence, the results are again comparable.

INITIALISATION ERRORS

The initialisation error during parallel charging is $1 - a = 0.033$ on average. This value is similar to previously found values, although it differs slightly again ($1 - a = 0.022$ for direct charging, $1 - a = 0.034$ for charger-mediated energy transfer).

CHARGING TIME

The gates can be applied in parallel, leading to a charging time of $\tau = 20\text{ns}$ for charging all the qubits. This is a useful result as the charging time thus does not increase when the number of quantum systems is increased. This is a strong argument for charging multiple qubits in parallel.

CHARGING POWER

The charging power now improves significantly, $P_c = 4.4\text{eV/ms}$. This is a 4-fold improvement compared to the direct charging of a single qubit, which is logical based on the array of $N = 4$ qubits being charged in parallel. This suggests that the QB implementation using transmon qubits is scalable. Even without making use of the quantum advantage, it is possible to store more energy in the system without increasing the charging time, and thus increase the charging power linearly.

OTHER REMARKS

The study of parallel charging shows promising results for the scalability of using superconducting transmon qubits as QB. However, it must be noted that no quantum advantage is implemented here. This can only be done when charging the qubits collectively. The next section discusses this in more depth.

5.2. COLLECTIVE CHARGING

Collective charging of finite quantum systems allows one to obtain a quantum advantage in power, see section 2.2.4 for the full description of this phenomenon. To collectively charge an array of multiple qubits, it is a necessity to be able to drive them with a shared pulse. Otherwise, entanglement can not be used to shorten the path, and therefore speed up the charging process. The Quantum Inspire has shared bus resonators between two qubits but does not contain a shared resonator between all qubits. The purpose of Quantum Inspire is quantum computing. Since the current native gate operations create a complete set for quantum computation, there is no need to complicate the system with multi-qubit resonators. Unfortunately, this means that it may not be possible to achieve collective charging on the Quantum Inspire platform.

The same applies to the QB implementation on the IBM Quantum Platform. The implementation of native multi-qubit gates can also be beneficial for quantum computing and is an active field of research. For example, reference [81] demonstrates an experimental platform allowing for native three-qubit gate operations. The following section first discusses the possibilities with two-qubit gates and then discusses experimental platforms that may allow to one obtain the quantum advantage in power for superconducting transmon qubits.

5

5.2.1. NEAREST-NEIGHBOUR COUPLING

The Quantum Inspire platform does have 2-qubit shared resonators, between q_2 and q_0, q_1, q_3, q_4 . Hence, This can theoretically be used to gain a quantum advantage of $\Gamma \propto 2$. We have come up with three proposals that could potentially implement this on the current quantum processor of the Starmon-5.

1. Bring qubits in resonance using the flux pulse. Charge them together via a pulse on the microwave control of one of the qubits. It must be explored whether the shared resonator can allow to drive both qubits simultaneously to the excited state using a single-qubit microwave line.
2. Bring qubits in resonance using the flux pulse. Charge one qubit to the $|2\rangle$ state using the single-qubit microwave transmission line, and allow the shared resonator to drive the $|02\rangle \rightarrow |11\rangle$ transition. The challenge is to design a pulse that drives this transition uniquely.
3. Bring the qubits in resonance by a flux pulse. Directly charge them via an excitation of the resonator mode. However, we expect it to be challenging to excite the two-qubit resonator directly.

These proposals have the disadvantage that in either way at least two pulses are required. This limits the implementation of the quantum advantage again. However, bringing the qubits in resonance may also be considered part of the initialisation process. It then becomes interesting to explore whether the duration of the second pulse can be shortened.

We suggest further research in using two-qubit gates to attain a 2-fold quantum advantage. This would be a huge step forward. These tasks may be implemented by using Qiskit Pulse. This is currently not possible on Quantum Inspire, but we expect this to become available soon.

5.2.2. MULTI-QUBIT COUPLING

Transmons can be collectively charged by having a shared resonator. When all qubits are identical, the one resonator mode can be used to drive all qubits collectively to the excited state. Alternatively, flux pulses on the qubits can be used to bring all qubits in resonance, and then charge them collectively using the shared resonator. This may become energetically expensive. A collective mode has been found that excites an array of non-identical transmon qubits coupled to a shared resonator [82]. This may be a more efficient way of charging the superconducting transmon qubits collectively. We recommend future research to investigate the usage of the collective mode for collective charging of transmon qubits.

Aside from a shared resonator, also shared microwave transmission lines can be used to collectively charge the qubits. The framework of this is the same: instead of coupling to a resonator mode, the transmons couple to a mode of the microwave transmission line. A shared microwave may become available in quantum computers as it also allows for multiplexing, decreasing the number of cables required [10]. We also suggest active research in this direction, as it specifically focuses on the alignment with quantum computing platforms.

6

CONCLUSIONS AND OUTLOOK

6.1. CONCLUSION

This study characterises the superconducting transmon qubits of Starmon-5 as quantum batteries (QBs), demonstrating comparable performance to recently published work on IBM Quantum Hardware [25]. Additionally, the implementation of charger-mediated energy transfer between two qubits, and parallel charging of four qubits is implemented on the Starmon-5 platform. Charger-mediated energy transfer uses the CNOT gate, which significantly increases the charging time. Nonetheless, this charging protocol holds promise for specific applications where the quantum state must be preserved. Furthermore, the successful implementation of parallel charging of the qubits of the Starmon-5 was shown. The energy stored scales proportional to the number of qubits, whilst the charging time remains the same. This results in a linear increase in power with the number of qubits. While parallel charging is a classical process in nature, our results indicate the scalability of transmon qubits as QBs. The quantum advantage predicts an additional N -fold scaling in charging power, but its realisation requires a collective resonator in the transmon circuit design, which is currently unavailable on the accessible hardware. Future research is recommended to focus on experimentally verifying the quantum advantage in superconducting transmon qubits. Finally, the importance of optimising pulse design is emphasised. This can enhance the performance of charging superconducting transmon qubits as QB. Especially for charger-mediated energy transfer and two-qubit interactions for a quantum advantage in power, this can be revolutionary. Overall, the implementation of superconducting transmon qubits as QBs holds great promise and can help us towards a more sustainable future.

6.2. FUTURE OUTLOOK

The interest in QBs is motivated by (1) the fundamental understanding of quantum thermodynamics, (2) the ever-decreasing size of electronic devices, and (3) the potential to improve future applications, especially those focused on sustainability. This research shows promising results for the performance of superconducting transmon qubits as a QB. Superconducting transmon qubits are leading candidates for large-scale quantum computing, yet the energy consumption of these quantum computers is concerning [83].

The study of QB implementation in superconducting qubits is aligned with the future application of QBs in quantum technologies, which we expect to have a positive effect on their energy consumption. This extends from quantum computing to other quantum technologies, such as quantum metrology and quantum communication.

QUANTUM ADVANTAGE

Collective charging can not yet be implemented on Starmon-5, due to the lack of a shared resonator or a collective microwave control line. Hence, no quantum advantage was attained. Similar platforms which are publicly available all do not have a shared resonator. This is because, for quantum computing purposes, a shared resonator creates extra noise and errors. Furthermore, a universal quantum computer can be created from single- and two-qubit gates, hence it is not a necessity. It can be interesting to investigate experimental platforms that contain a shared resonator as QB (e.g. [82]) such that the quantum advantage can be shown for transmon qubits.

The two-qubit resonators between q_2q_1 , q_2q_3 , q_2q_4 , could theoretically be exploited to gain a quantum advantage in power of $\Gamma=2$, as was shown in figure 2.4. However, the pulse to generate the interactions between the resonators currently takes at least 40ns, and additionally does not implement the state transfer that leads to the collective charging of two qubits.

6

PULSE DESIGN

We emphasise the importance of pulse design for the practical implementation of quantum batteries in superconducting transmon qubits. This has relevance for all ways of charging the QB. As the protocol charger-mediated energy transfer currently has the highest charging time, pulse design can especially help reduce this quantity. Ideally, a fast single pulse can facilitate the energy transfer from the charger to the quantum battery. In that case, charger-mediated energy transfer may start to speed up the energy-transfer time, as theoretically predicted by reference [60]. Additionally, further investigations can focus on the pulse that achieves collective charging of two qubits, to attain a quantum advantage in power of $\Gamma=2$.

Using pulse design, energy states outside of the computational basis become accessible. A qutrit QB was characterised in IBM Quantum Hardware [27]. Using all d levels of the transmon can help with storing larger quantities of energy in quantum systems.

QUANTUM OPTIMAL CONTROL

Quantum Optimal Control (QOC) has great potential for improving the figures of merit of quantum batteries. There are numerous of QOC techniques, as discussed in section 2.5.2. Whilst QOC has been widely applied for quantum computing, there have only been two numerical studies about QOC for QBs [72, 73]. The next step is to implement these optimised pulses on real quantum hardware. Intrigued by this principle, we performed a preliminary optimisation to charge a QB and implemented this on IBM Quantum Hardware using Qiskit Pulse. The first results can be found in Appendix B, and show the optimisation of state-to-state transfer pulse for a TLS based on the Krotov method [66]. It must be noted that these are the first results and aim to provide a sketch of how

this can be implemented for a QB, rather than an actual improvement of the pulse compared to standard Gaussian or DRAG pulses ($\eta = 0.908$ for the optimised pulse). We suggest further work in this area. Additionally, closed-loop optimisation can greatly help with reducing the charging time. Recent work uses this technique to reduce gate times of superconducting transmon qubits below 10ns [74]. It is suggested that this is also explored for QB charging.

RESOURCE COST AND MNR EFFICIENCY

It is important to not only consider the metrics of performance but also the resource cost that comes with achieving them [10]. The implementation of charger-mediated energy transfer using the CNOT gate takes 4 microwave line pulses and one flux line pulse. As transferring these signals to the quantum chip costs energy, this protocol is a lot less energy efficient than direct charging of a QB. Optimising the pulse using QOC for QBs was shown to reduce the energy cost of the classical drive field [72]. We recommend further work to take the resource cost into account and explore the possibility of quantifying this for charging protocols based on the Metric-Noise-Performance framework proposed in reference [10].

FULL CHARGING PROCESS

In this thesis, the charging process of superconducting transmon qubits was studied. To fully implement a transmon qubit as QB, also the storage and work extraction must be studied. This is important for the real impact of QBs. In terms of the transfer of energy, it can be expected that the procedure of charger-mediated energy transfer can be also used to transfer energy from the quantum battery to a consumption centre. Both energy storage and energy transfer require further investigations in real quantum hardware, this is crucial for the practical implementation of QBs.

QUANTUM HARDWARE

It could also be interesting for future research to focus on different quantum hardware systems and characterise which quantum systems are best to use for specific applications. For example, the aim could be to store as much energy as possible whilst still operating in the quantum regime. In that case, it is beneficial to choose a hardware platform with high energy splitting, or accessible higher energy levels. When the purpose is instead to store quanta of energy that are exactly the amount required at the consumption centre, it makes sense to use the same hardware platform as that of the consumption centre. When a fast operation time and high power are a priority, one must choose a platform that easily enables the quantum advantage. For example, the quantum advantage has already been experimentally observed in organic microcavities [21], as it is more inherent to this hardware platform than it is to for example superconducting transmon qubits. Lastly, quantum systems can also be specifically designed with the purpose of a quantum battery. As an example, the anharmonic energy spectrum is preferred for quantum computing, but quantum batteries may benefit from a harmonic energy spectrum instead. This can then allow more of the same energy quanta to be stored in one QB, which could be used for multiple consumption centres.

QUANTUM METRICS FOR QB IMPLEMENTATION

Implementation of QBs on different platforms results in many figures of merit and other considerations to be taken into account when comparing quantum devices: the stored energy, efficiency, charging time, and charging power, but also scalability and alignment with applications. It may thus become useful to develop a framework of quantum metrics specifically tailored towards the implementation of a QB. This can be done in a similar way as what is done for quantum computing, see for example reference [84]. It may also be beneficial to translate the quantum metrics used for quantum computing to QBs. Some examples of quantum metrics that can also say something about the performance of a QB are single-qubit gate fidelity, cross-talk, relaxation time, decoherence time, quantum volume, and the Q-factor.

SUSTAINABLE QUANTUM TECHNOLOGIES

It must be mentioned that the energy scale at which quantum phenomena occur is extremely small, in this study an energy quantum of about $20\mu\text{eV}$ is achieved by fully charging a qubit. Therefore, we do not expect daily technologies to be charged by QBs, as this would require an enormous amount of quantum systems. Instead, we envision the direct application of QBs to be in superconducting transmon quantum computers. For example, fabricated qubits that do not perform well enough for quantum computation could be used as quantum batteries. This way, energy management inside the quantum computer can be improved. This can reduce the energy requirements on the quantum scale, which may result in a macroscopic energy reduction. In the future, QBs can help to create sustainable quantum technologies.

BIBLIOGRAPHY

- [1] R. Alicki and M. Fannes. “Entanglement boost for extractable work from ensembles of quantum batteries”. In: *Physical Review E* 87.4 (2013). ISSN: 1539-3755. DOI: [10.1103/physreve.87.042123](https://doi.org/10.1103/physreve.87.042123). URL: <https://dx.doi.org/10.1103/physreve.87.042123>.
- [2] A. E. Allahverdyan, R. Balian, and T. M. Nieuwenhuizen. “Maximal work extraction from finite quantum systems”. In: *Europhysics Letters* 67 (2004), pp. 565–571. DOI: [10.1209/epl/i2004](https://dx.doi.org/10.1209/epl/i2004). URL: <https://dx.doi.org/10.1209/epl/i2004>.
- [3] F. C. Binder, S. Vinjanampathy, S. V. Modi, Kavan, and J. Goold. “Quantacell: powerful charging of quantum batteries”. In: *New Journal of Physics* 17 (2015). DOI: [10.1088/1367-2630/17](https://dx.doi.org/10.1088/1367-2630/17). URL: <https://dx.doi.org/10.1088/1367-2630/17>.
- [4] F. Campaioli, F. A. Pollock, F. C. Binder, L. Céleri, J. Goold, S. Vinjanampathy, and K. Modi. “Enhancing the Charging Power of Quantum Batteries”. In: *Physical Review Letters* 118.15 (2017). ISSN: 0031-9007. DOI: [10.1103/physrevlett.118.150601](https://dx.doi.org/10.1103/physrevlett.118.150601). URL: <https://dx.doi.org/10.1103/physrevlett.118.150601>.
- [5] D. o. E. United Nations and S. A. -. S. Development. *Transforming our world: the 2030 Agenda for Sustainable Development*. General Assembly. 35. URL: <https://sdgs.un.org/2030agenda>.
- [6] S. Krastanov, M. Heuck, J. H. Shapiro, P. Narang, D. R. Englund, and K. Jacobs. “Room-temperature photonic logical qubits via second-order nonlinearities”. In: *Nature Communications* 12.1 (2021). ISSN: 2041-1723. DOI: [10.1038/s41467-020-20417-4](https://dx.doi.org/10.1038/s41467-020-20417-4). URL: <https://dx.doi.org/10.1038/s41467-020-20417-4>.
- [7] L. Henriët, L. Beguin, A. Signoles, T. Lahaye, A. Browaeys, G.-O. Reymond, and C. Jurczak. “Quantum computing with neutral atoms”. In: *Quantum* 4 (2020), p. 327. ISSN: 2521-327X. DOI: [10.22331/q-2020-09-21-327](https://dx.doi.org/10.22331/q-2020-09-21-327). URL: <https://dx.doi.org/10.22331/q-2020-09-21-327>.
- [8] L. Childress and R. Hanson. “Diamond NV centers for quantum computing and quantum networks”. In: *MRS Bulletin* 38.2 (2013), pp. 134–138. ISSN: 0883-7694. DOI: [10.1557/mrs.2013.20](https://dx.doi.org/10.1557/mrs.2013.20). URL: <https://dx.doi.org/10.1557/mrs.2013.20>.
- [9] A. Auffèves. “Quantum Technologies Need a Quantum Energy Initiative”. In: *PRX Quantum* 3.2 (2022). ISSN: 2691-3399. DOI: [10.1103/prxquantum.3.020101](https://dx.doi.org/10.1103/prxquantum.3.020101). URL: <https://dx.doi.org/10.1103/prxquantum.3.020101>.

- [10] M. Fellous-Asiani, Jing, Y. Thonnart, Hui, Robert, and A. Auffèves. “Optimizing resource efficiencies for scalable full-stack quantum computers”. In: *arXiv pre-print server* (2022). DOI: [arxiv:2209.05469](https://arxiv.org/abs/2209.05469). URL: <https://arxiv.org/abs/2209.05469>.
- [11] “Thermodynamics in the Quantum Regime”. In: *Fundamental Theories of Physics* (2018). ISSN: 0168-1222. DOI: [10.1007/978-3-319-99046-0](https://doi.org/10.1007/978-3-319-99046-0). URL: <https://dx.doi.org/10.1007/978-3-319-99046-0>.
- [12] J. Millen and A. Xuereb. “The rise of the quantum machines”. In: *Physics World* (2016), pp. 23–26. DOI: [10.1088/2058-7058/29/1/30](https://doi.org/10.1088/2058-7058/29/1/30).
- [13] J. Millen and A. Xuereb. “Perspective on quantum thermodynamics”. In: *New Journal of Physics* 18 (2017). DOI: [10.1088/1367-2630/18](https://doi.org/10.1088/1367-2630/18). URL: <https://dx.doi.org/10.1088/1367-2630/18>.
- [14] H. T. Quan, Y.-x. Liu, C. P. Sun, and F. Nori. “Quantum thermodynamic cycles and quantum heat engines”. In: *Phys. Rev. E* 76 (3 2007), p. 031105. DOI: [10.1103/PhysRevE.76.031105](https://doi.org/10.1103/PhysRevE.76.031105). URL: <https://link.aps.org/doi/10.1103/PhysRevE.76.031105>.
- [15] N. Linden, S. Popescu, and P. Skrzypczyk. “How Small Can Thermal Machines Be? The Smallest Possible Refrigerator”. In: *Physical Review Letters* 105.13 (2010). ISSN: 0031-9007. DOI: [10.1103/physrevlett.105.130401](https://doi.org/10.1103/physrevlett.105.130401). URL: <https://dx.doi.org/10.1103/physrevlett.105.130401>.
- [16] K. V. Hovhannisyanyan, M. Perarnau-Llobet, M. Huber, and A. Acín. “Entanglement Generation is Not Necessary for Optimal Work Extraction”. In: *Physical Review Letters* 111.24 (2013). ISSN: 0031-9007. DOI: [10.1103/physrevlett.111.240401](https://doi.org/10.1103/physrevlett.111.240401). URL: <https://dx.doi.org/10.1103/physrevlett.111.240401>.
- [17] G. M. Andolina, D. Farina, A. Mari, V. Pellegrini, V. Giovannetti, and M. Polini. “Charger-mediated energy transfer in exactly solvable models for quantum batteries”. In: *Physical Review B* 98.20 (2018). ISSN: 2469-9950. DOI: [10.1103/physrevb.98.205423](https://doi.org/10.1103/physrevb.98.205423). URL: <https://dx.doi.org/10.1103/physrevb.98.205423>.
- [18] D. Farina, G. M. Andolina, A. Mari, M. Polini, and V. Giovannetti. “Charger-mediated energy transfer for quantum batteries: An open-system approach”. In: *Physical Review B* 99.3 (2019). ISSN: 2469-9950. DOI: [10.1103/physrevb.99.035421](https://doi.org/10.1103/physrevb.99.035421). URL: <https://dx.doi.org/10.1103/physrevb.99.035421>.
- [19] M. T. Mitchison, J. Goold, and J. Prior. “Charging a quantum battery with linear feedback control”. In: *Quantum* 5 (2021), p. 500. ISSN: 2521-327X. DOI: [10.22331/q-2021-07-13-500](https://doi.org/10.22331/q-2021-07-13-500). URL: <https://dx.doi.org/10.22331/q-2021-07-13-500>.
- [20] G. L. Giorgi and S. Campbell. “Correlation approach to work extraction from finite quantum systems”. In: *Journal of Physics B: Atomic, Molecular and Optical Physics* 48.3 (2015), p. 035501. ISSN: 0953-4075. DOI: [10.1088/0953-4075/48/3/035501](https://doi.org/10.1088/0953-4075/48/3/035501). URL: <https://dx.doi.org/10.1088/0953-4075/48/3/035501>.

- [21] J. Q. Quach, K. E. McGhee, L. Ganzer, D. M. Rouse, B. W. Lovett, E. M. Gauger, J. Keeling, G. Cerullo, D. G. Lidzey, and T. Virgili. “Superabsorption in an organic microcavity: Toward a quantum battery”. In: *Science advances* 8.2 (2022). ISSN: 2375-2548. DOI: [10.1126/sciadv.abk3160](https://doi.org/10.1126/sciadv.abk3160).
- [22] I. S, M. Maffei, S, M. Pont, A. Harouri, Lema, A. itre, I. Sagnes, N. Somaschi, A. Auffèves, and P. Senellart. “Coherence-powered work exchanges between a solid-state qubit and light fields”. In: *arXiv pre-print server* (2022). DOI: [Nonearxiv : 2202.01109](https://arxiv.org/abs/2202.01109). URL: <https://arxiv.org/abs/2202.01109>.
- [23] C.-K. Hu, J. Qiu, P. J. P. Souza, J. Yuan, Y. Zhou, L. Zhang, J. Chu, X. Pan, L. Hu, J. Li, Y. Xu, Y. Zhong, S. Liu, F. Yan, D. Tan, R. Bachelard, C. J. Villas-Boas, A. C. Santos, and D. Yu. “Optimal charging of a superconducting quantum battery”. In: *Quantum Science and Technology* 7.4 (2022), p. 045018. ISSN: 2058-9565. DOI: [10.1088/2058-9565/ac8444](https://doi.org/10.1088/2058-9565/ac8444). URL: <https://dx.doi.org/10.1088/2058-9565/ac8444>.
- [24] F.-Q. Dou and F.-M. Yang. “Superconducting transmon qubit-resonator quantum battery”. In: *Physical Review A* 107.2 (2023). ISSN: 2469-9926. DOI: [10.1103/physreva.107.023725](https://doi.org/10.1103/physreva.107.023725). URL: <https://dx.doi.org/10.1103/physreva.107.023725>.
- [25] G. Gemme, M. Grossi, D. Ferraro, S. Vallecorsa, and M. Sassetti. “IBM Quantum Platforms: A Quantum Battery Perspective”. In: *Batteries* 8.5 (2022), p. 43. ISSN: 2313-0105. DOI: [10.3390/batteries8050043](https://doi.org/10.3390/batteries8050043). URL: <https://dx.doi.org/10.3390/batteries8050043>.
- [26] T. Alexander, N. Kanazawa, D. J. Egger, L. Capelluto, C. J. Wood, A. Javadi-Abhari, and D. C Mckay. “Qiskit pulse: programming quantum computers through the cloud with pulses”. In: *Quantum Science and Technology* 5.4 (2020), p. 044006. ISSN: 2058-9565. DOI: [10.1088/2058-9565/aba404](https://doi.org/10.1088/2058-9565/aba404). URL: <https://dx.doi.org/10.1088/2058-9565/aba404>.
- [27] G. Gemme, M. Grossi, S. Vallecorsa, M. Sassetti, and D. Ferraro. *Qutrit quantum battery: comparing different charging protocols*. Electronic Article. 22 pages, 11 figures. 2023. DOI: [10.48550/arXiv.2306.14537](https://arxiv.org/abs/2306.14537). URL: <https://ui.adsabs.harvard.edu/abs/2023arXiv230614537G>.
- [28] T. Last, N. Samkharadze, P. Eendebak, R. Versluis, X. Xue, A. Sammak, D. Brousse, K. Loh, H. Polinder, G. Scappucci, M. Veldhorst, L. Vandersypen, K. Maturová, J. Veltin, and G. Alberts. *Quantum Inspire: QuTech’s platform for co-development and collaboration in quantum computing*. Vol. 11324. SPIE Advanced Lithography. SPIE, 2020. URL: <https://doi.org/10.1117/12.2551853>.
- [29] Qutech. *Quantum Inspire Starmon-5 Fact Sheet*. 2022. URL: <https://qutech.nl/wp-content/uploads/2020/04/3.-Technical-Fact-Sheet-Quantum-Inspire-Starmon-5.pdf>.
- [30] “Wahrscheinlichkeitstheoretischer Aufbau der Quantenmechanik”. In: *Nachrichten von der Gesellschaft der Wissenschaften zu Göttingen, Mathematisch-Physikalische Klasse* (1927), pp. 245–272. URL: <http://dml.mathdoc.fr/item/GDZPPN002507277>.

- [31] W. Pusz and S. L. Woronowicz. “Passive states and KMS states for general quantum systems”. In: *Communications in Mathematical Physics* 58.3 (1978), pp. 273–290. ISSN: 0010-3616. DOI: [10.1007/bf01614224](https://doi.org/10.1007/bf01614224). URL: <https://dx.doi.org/10.1007/bf01614224>.
- [32] A. Lenard. “Thermodynamical proof of the Gibbs formula for elementary quantum systems”. In: *Journal of Statistical Physics* 19.6 (1978), pp. 575–586. ISSN: 0022-4715. DOI: [10.1007/bf01011769](https://doi.org/10.1007/bf01011769). URL: <https://dx.doi.org/10.1007/bf01011769>.
- [33] S. Gherardini, F. Campaioli, F. Caruso, and F. C. Binder. “Stabilizing open quantum batteries by sequential measurements”. In: *Physical Review Research* 2.1 (2020). ISSN: 2643-1564. DOI: [10.1103/physrevresearch.2.013095](https://doi.org/10.1103/physrevresearch.2.013095). URL: <https://dx.doi.org/10.1103/physrevresearch.2.013095>.
- [34] M. T. Mitchison, J. Goold, and J. Prior. “Charging a quantum battery with linear feedback control”. In: *Quantum* 5 (2021), p. 500. ISSN: 2521-327X. DOI: [10.22331/q-2021-07-13-500](https://doi.org/10.22331/q-2021-07-13-500). URL: <https://dx.doi.org/10.22331/q-2021-07-13-500>.
- [35] M. Huber, M. Perarnau-Llobet, and J. I. De Vicente. “Entropy vector formalism and the structure of multidimensional entanglement in multipartite systems”. In: *Physical Review A* 88.4 (2013), p. 042328. DOI: [10.1103/PhysRevA.88.042328](https://doi.org/10.1103/PhysRevA.88.042328). URL: <https://doi.org/10.1103/PhysRevA.88.042328>.
- [36] S. Deffner and S. Campbell. “Quantum speed limits: from Heisenberg’s uncertainty principle to optimal quantum control”. In: 50.45 (2017), p. 453001. DOI: [10.1088/1751-8121/aa86c6](https://doi.org/10.1088/1751-8121/aa86c6). URL: <https://dx.doi.org/10.1088/1751-8121/aa86c6>.
- [37] I. Bengtsson and K. Życzkowski. “Geometry of Quantum States: An Introduction to Quantum Entanglement”. In: *Geometry of Quantum States: An Introduction to Quantum Entanglement* (Jan. 2006). DOI: [10.1017/CB09780511535048](https://doi.org/10.1017/CB09780511535048).
- [38] W. Greiner and J. Reinhardt. *Quantum electrodynamics*. Springer Science & Business Media, 2008. DOI: <https://doi.org/10.1007/978-3-540-87561-1>.
- [39] T. E. Roth, R. Ma, and W. C. Chew. “An Introduction to the Transmon Qubit for Electromagnetic Engineers”. In: *arXiv pre-print server* (2021). DOI: [Nonearxiv:2106.11352](https://arxiv.org/abs/2106.11352). URL: <https://arxiv.org/abs/2106.11352>.
- [40] J. Koch, T. M. Yu, J. Gambetta, A. A. Houck, D. I. Schuster, J. Majer, A. Blais, M. H. Devoret, S. M. Girvin, and R. J. Schoelkopf. “Charge-insensitive qubit design derived from the Cooper pair box”. In: *Physical Review A* 76.4 (2007). ISSN: 1050-2947. DOI: [10.1103/physreva.76.042319](https://doi.org/10.1103/physreva.76.042319). URL: <https://dx.doi.org/10.1103/physreva.76.042319>.
- [41] J. I. Cirac and P. Zoller. “Quantum Computations with Cold Trapped Ions”. In: *Physical Review Letters* 74 (20 1995), pp. 4091–4094. DOI: [10.1103/PhysRevLett.74.4091](https://doi.org/10.1103/PhysRevLett.74.4091). URL: <https://link.aps.org/doi/10.1103/PhysRevLett.74.4091>.

- [42] D. Loss and D. P. Divincenzo. “Quantum computation with quantum dots”. In: *Physical Review A* 57.1 (1998), pp. 120–126. ISSN: 1050-2947. DOI: [10.1103/physreva.57.120](https://doi.org/10.1103/physreva.57.120). URL: <https://dx.doi.org/10.1103/physreva.57.120>.
- [43] S. Bravyi, O. Dial, J. M. Gambetta, D. Gil, and Z. Nazario. “The future of quantum computing with superconducting qubits”. In: *Journal of Applied Physics* 132.16 (2022), p. 160902. ISSN: 0021-8979. DOI: [10.1063/5.0082975](https://doi.org/10.1063/5.0082975). URL: <https://dx.doi.org/10.1063/5.0082975>.
- [44] X. Gu, A. F. Kockum, A. Miranowicz, Y.-x. Liu, and F. Nori. “Microwave photons with superconducting quantum circuits”. In: *Physics Reports* 718 (2017), pp. 1–102. ISSN: 0370-1573. DOI: <https://doi.org/10.1016/j.physrep.2017.10.002>. URL: <https://www.sciencedirect.com/science/article/pii/S0370157317303290>.
- [45] C. Hugh and C. Nay. *IBM unveils 400 qubit-plus quantum processor and next-generation IBM Quantum System Two*. Nov. 2022. URL: <https://newsroom.ibm.com/2022-11-09-IBM-Unveils-400-Qubit-Plus-Quantum-Processor-and-Next-Generation-IBM-Quantum-System-Two>.
- [46] F. Arute, K. Arya, R. Babbush, D. Bacon, J. C. Bardin, R. Barends, R. Biswas, S. Boixo, F. G. S. L. Brandao, D. A. Buell, B. Burkett, Y. Chen, Z. Chen, B. Chiaro, R. Collins, W. Courtney, A. Dunsworth, E. Farhi, B. Foxen, A. Fowler, C. Gidney, M. Giustina, R. Graff, K. Guerin, S. Habegger, M. P. Harrigan, M. J. Hartmann, A. Ho, M. Hoffmann, T. Huang, T. S. Humble, S. V. Isakov, E. Jeffrey, Z. Jiang, D. Kafri, K. Kechedzhi, J. Kelly, P. V. Klimov, S. Knysh, A. Korotkov, F. Kostritsa, D. Landhuis, M. Lindmark, E. Lucero, D. Lyakh, S. Mandrà, J. R. McClean, M. McEwen, A. Megrant, X. Mi, K. Michielsen, M. Mohseni, J. Mutus, O. Naaman, M. Neeley, C. Neill, M. Y. Niu, E. Ostby, A. Petukhov, J. C. Platt, C. Quintana, E. G. Rieffel, P. Roushan, N. C. Rubin, D. Sank, K. J. Satzinger, V. Smelyanskiy, K. J. Sung, M. D. Trevithick, A. Vainsencher, B. Villalonga, T. White, Z. J. Yao, P. Yeh, A. Zalcman, H. Neven, and J. M. Martinis. “Quantum supremacy using a programmable superconducting processor”. In: *Nature* 574.7779 (2019), pp. 505–510. ISSN: 0028-0836. DOI: [10.1038/s41586-019-1666-5](https://doi.org/10.1038/s41586-019-1666-5). URL: <https://dx.doi.org/10.1038/s41586-019-1666-5>.
- [47] B. Lilia, R. Hennig, P. Hirschfeld, G. Profeta, A. Sanna, E. Zurek, W. E. Pickett, M. Amsler, R. Dias, M. I. Erements, *et al.* “The 2021 room-temperature superconductivity roadmap”. In: *Journal of Physics: Condensed Matter* 34.18 (2022), p. 183002. DOI: [10.1088/1361-648X/ac2864](https://doi.org/10.1088/1361-648X/ac2864). URL: <https://dx.doi.org/10.1088/1361-648X/ac2864>.
- [48] A. F. Kockum and F. Nori. “Quantum Bits with Josephson Junctions”. In: Springer International Publishing, 2019, pp. 703–741. DOI: [10.1007/978-3-030-20726-7_17](https://doi.org/10.1007/978-3-030-20726-7_17). URL: https://dx.doi.org/10.1007/978-3-030-20726-7_17.
- [49] R. C. Jaklevic, J. Lambe, A. H. Silver, and J. E. Mercereau. “Quantum Interference Effects in Josephson Tunneling”. In: *Physical Review Letters* 12 (7 1964), pp. 159–160. DOI: [10.1103/PhysRevLett.12.159](https://doi.org/10.1103/PhysRevLett.12.159). URL: <https://link.aps.org/doi/10.1103/PhysRevLett.12.159>.

- [50] A. Frisk Kockum, A. Miranowicz, S. De Liberato, S. Savasta, and F. Nori. “Ultrastrong coupling between light and matter”. In: *Nature Reviews Physics* 1.1 (2019), pp. 19–40. ISSN: 2522-5820. DOI: [10.1038/s42254-018-0006-2](https://doi.org/10.1038/s42254-018-0006-2). URL: <https://dx.doi.org/10.1038/s42254-018-0006-2>.
- [51] A. Blais, R.-S. Huang, A. Wallraff, S. M. Girvin, and R. J. Schoelkopf. “Cavity quantum electrodynamics for superconducting electrical circuits: An architecture for quantum computation”. In: *Physical Review A* 69.6 (2004). ISSN: 1050-2947. DOI: [10.1103/physreva.69.062320](https://doi.org/10.1103/physreva.69.062320). URL: <https://dx.doi.org/10.1103/physreva.69.062320>.
- [52] C. K. Andersen and A. Blais. “Ultrastrong coupling dynamics with a transmon qubit”. In: *New Journal of Physics* 19.2 (2017), p. 023022. ISSN: 1367-2630. DOI: [10.1088/1367-2630/aa5941](https://doi.org/10.1088/1367-2630/aa5941). URL: <https://dx.doi.org/10.1088/1367-2630/aa5941>.
- [53] M. Reagor, W. Pfaff, C. Axline, R. W. Heeres, N. Ofek, K. Sliwa, E. Holland, C. Wang, J. Blumoff, K. Chou, M. J. Hatridge, L. Frunzio, M. H. Devoret, L. Jiang, and R. J. Schoelkopf. “Quantum memory with millisecond coherence in circuit QED”. In: *Physical Review B* 94.1 (2016). ISSN: 2469-9950. DOI: [10.1103/physrevb.94.014506](https://doi.org/10.1103/physrevb.94.014506). URL: <https://dx.doi.org/10.1103/physrevb.94.014506>.
- [54] N. Leung, Y. Lu, S. Chakram, R. K. Naik, N. Earnest, R. Ma, K. Jacobs, A. N. Cleland, and D. I. Schuster. “Deterministic bidirectional communication and remote entanglement generation between superconducting qubits”. In: *npj Quantum Information* 5.1 (2019). ISSN: 2056-6387. DOI: [10.1038/s41534-019-0128-0](https://doi.org/10.1038/s41534-019-0128-0). URL: <https://dx.doi.org/10.1038/s41534-019-0128-0>.
- [55] E. T. Jaynes and F. W. Cummings. “Comparison of quantum and semiclassical radiation theories with application to the beam maser”. In: *Proceedings of the IEEE* 51.1 (1963), pp. 89–109. ISSN: 0018-9219. DOI: [10.1109/proc.1963.1664](https://doi.org/10.1109/proc.1963.1664). URL: <https://dx.doi.org/10.1109/proc.1963.1664>.
- [56] R. H. Dicke. “Coherence in Spontaneous Radiation Processes”. In: *Physical Review* 93.1 (1954), pp. 99–110. ISSN: 0031-899X. DOI: [10.1103/physrev.93.99](https://doi.org/10.1103/physrev.93.99). URL: <https://dx.doi.org/10.1103/physrev.93.99>.
- [57] X. Zhang and M. Blaauboer. “Enhanced energy transfer in a Dicke quantum battery”. In: *Frontiers in Physics* 10 (2023). ISSN: 2296-424X. DOI: [10.3389/fphy.2022.1097564](https://doi.org/10.3389/fphy.2022.1097564). URL: <https://dx.doi.org/10.3389/fphy.2022.1097564>.
- [58] V. Gorini, A. Kossakowski, and E. C. G. Sudarshan. “Completely positive dynamical semigroups of N-level systems”. In: *Journal of Mathematical Physics* 17.5 (1976), pp. 821–825. ISSN: 0022-2488. DOI: [10.1063/1.522979](https://doi.org/10.1063/1.522979). URL: <https://doi.org/10.1063/1.522979>.
- [59] G. Lindblad. “On the generators of quantum dynamical semigroups”. In: *Communications in Mathematical Physics* 48.2 (1976), pp. 119–130. ISSN: 0010-3616. DOI: [10.1007/bf01608499](https://doi.org/10.1007/bf01608499). URL: <https://dx.doi.org/10.1007/bf01608499>.

- [60] A. Crescente, D. Ferraro, M. Carrega, and M. Sassetti. “Enhancing coherent energy transfer between quantum devices via a mediator”. In: *Physical Review Research* 4.3 (2022). ISSN: 2643-1564. DOI: [10.1103/physrevresearch.4.033216](https://doi.org/10.1103/physrevresearch.4.033216). URL: <https://dx.doi.org/10.1103/physrevresearch.4.033216>.
- [61] G. M. Andolina, D. Farina, A. Mari, M. Polini, and V. Giovannetti. “Charger-Mediated Quantum Batteries”. In: *Proceedings* 12.1 (2019). ISSN: 2504-3900. DOI: [10.3390/proceedings2019012060](https://doi.org/10.3390/proceedings2019012060). URL: <https://www.mdpi.com/2504-3900/12/1/60>.
- [62] C. P. Koch, U. Boscain, T. Calarco, G. Dirr, S. Filipp, S. J. Glaser, R. Kosloff, S. Montangero, T. Schulte-Herbrüggen, D. Sugny, and F. K. Wilhelm. “Quantum optimal control in quantum technologies. Strategic report on current status, visions and goals for research in Europe”. In: *EPJ Quantum Technology* 9.1 (2022). ISSN: 2662-4400. DOI: [10.1140/epjqt/s40507-022-00138-x](https://doi.org/10.1140/epjqt/s40507-022-00138-x). URL: <https://dx.doi.org/10.1140/epjqt/s40507-022-00138-x>.
- [63] J. Werschnik and E. K. U. Gross. “Quantum optimal control theory”. In: *Journal of Physics B: Atomic, Molecular and Optical Physics* 40.18 (2007), R175–R211. ISSN: 0953-4075. DOI: [10.1088/0953-4075/40/18/r01](https://doi.org/10.1088/0953-4075/40/18/r01). URL: <https://dx.doi.org/10.1088/0953-4075/40/18/r01>.
- [64] D. d’Alessandro. *Introduction to quantum control and dynamics*. CRC press, 2021. ISBN: 1000394999. DOI: [10.1201/9781003051268](https://doi.org/10.1201/9781003051268). URL: <https://doi.org/10.1201/9781003051268>.
- [65] F. Motzoi, J. M. Gambetta, P. Rebentrost, and F. K. Wilhelm. “Simple Pulses for Elimination of Leakage in Weakly Nonlinear Qubits”. In: *Physical Review Letters* 103.11 (2009). ISSN: 0031-9007. DOI: [10.1103/physrevlett.103.110501](https://doi.org/10.1103/physrevlett.103.110501). URL: <https://dx.doi.org/10.1103/physrevlett.103.110501>.
- [66] M. Goerz, D. Basilewitsch, F. Gago-Encinas, M. G. Krauss, K. P. Horn, D. M. Reich, and C. Koch. “Krotov: A Python implementation of Krotov’s method for quantum optimal control”. In: *SciPost Physics* 7.6 (2019). ISSN: 2542-4653. DOI: [10.21468/scipostphys.7.6.080](https://doi.org/10.21468/scipostphys.7.6.080). URL: <https://dx.doi.org/10.21468/scipostphys.7.6.080>.
- [67] N. Khaneja, T. Reiss, C. Kehlet, T. Schulte-Herbrüggen, and S. J. Glaser. “Optimal control of coupled spin dynamics: design of NMR pulse sequences by gradient ascent algorithms”. In: *Journal of Magnetic Resonance* 172.2 (2005), pp. 296–305. ISSN: 1090-7807. DOI: <https://doi.org/10.1016/j.jmr.2004.11.004>. URL: <https://www.sciencedirect.com/science/article/pii/S1090780704003696>.
- [68] P. Doria, T. Calarco, and S. Montangero. “Optimal Control Technique for Many-Body Quantum Dynamics”. In: *Physical Review Letters* 106.19 (2011). ISSN: 0031-9007. DOI: [10.1103/physrevlett.106.190501](https://doi.org/10.1103/physrevlett.106.190501). URL: <https://dx.doi.org/10.1103/physrevlett.106.190501>.
- [69] T. Caneva, T. Calarco, and S. Montangero. “Chopped random-basis quantum optimization”. In: *Physical Review A* 84.2 (2011). ISSN: 1050-2947. DOI: [10.1103/physreva.84.022326](https://doi.org/10.1103/physreva.84.022326). URL: <https://dx.doi.org/10.1103/physreva.84.022326>.

- [70] J. Johansson, P. Nation, and F. Nori. “QuTiP: An open-source Python framework for the dynamics of open quantum systems”. In: *Computer Physics Communications* 183.8 (2012), pp. 1760–1772. ISSN: 0010-4655. DOI: <https://doi.org/10.1016/j.cpc.2012.02.021>. URL: <https://www.sciencedirect.com/science/article/pii/S0010465512000835>.
- [71] E. S. Matekole, Y.-L. L. Fang, and M. Lin. “Methods and Results for Quantum Optimal Pulse Control on Superconducting Qubit Systems”. In: IEEE, 2022. DOI: [10.1109/ipdpsw55747.2022.00102](https://doi.org/10.1109/ipdpsw55747.2022.00102). URL: <https://dx.doi.org/10.1109/ipdpsw55747.2022.00102>.
- [72] R. R. Rodriguez, B. Ahmadi, G. Suarez, P. Mazurek, S. Barzanjeh, and P. Horodecki. *Optimal Quantum Control of Charging Quantum Batteries*. Electronic Article. Eq. 5 corrected, minor mistakes removed. 2022. DOI: [10.48550/arXiv.2207.00094](https://doi.org/10.48550/arXiv.2207.00094). URL: <https://ui.adsabs.harvard.edu/abs/2022arXiv220700094R>.
- [73] F. Mazzoncini, V. Cavina, G. M. Andolina, P. A. Erdman, and V. Giovannetti. “Optimal control methods for quantum batteries”. In: *Physical Review A* 107.3 (2023). ISSN: 2469-9926. DOI: [10.1103/physreva.107.032218](https://doi.org/10.1103/physreva.107.032218). URL: <https://dx.doi.org/10.1103/physreva.107.032218>.
- [74] M. Werninghaus, D. J. Egger, F. Roy, S. Machnes, F. K. Wilhelm, and S. Filipp. “Leakage reduction in fast superconducting qubit gates via optimal control”. In: *npj Quantum Information* 7.1 (2021). ISSN: 2056-6387. DOI: [10.1038/s41534-020-00346-2](https://doi.org/10.1038/s41534-020-00346-2). URL: <https://dx.doi.org/10.1038/s41534-020-00346-2>.
- [75] *Starmon-5: Operational Specifics*. 2024. URL: <https://www.quantum-inspire.com/kbase/starmon-5-operational-specifics/>.
- [76] G. R. Di Carlo. *Personal communication with Qutech*. 2024.
- [77] Y. Hardy and W. H. Steeb. “Decomposing the SWAP quantum gate”. In: *Journal of Physics A: Mathematical and General* 39.6 (2006), pp. 1463–1467. ISSN: 0305-4470. DOI: [10.1088/0305-4470/39/6/018](https://doi.org/10.1088/0305-4470/39/6/018). URL: <https://dx.doi.org/10.1088/0305-4470/39/6/018>.
- [78] F. W. Strauch, P. R. Johnson, A. J. Dragt, C. J. Lobb, J. R. Anderson, and F. C. Wellstood. “Quantum Logic Gates for Coupled Superconducting Phase Qubits”. In: *Physical Review Letters* 91.16 (2003). ISSN: 0031-9007. DOI: [10.1103/physrevlett.91.167005](https://doi.org/10.1103/physrevlett.91.167005). URL: <https://dx.doi.org/10.1103/physrevlett.91.167005>.
- [79] L. DiCarlo, J. M. Chow, J. M. Gambetta, L. S. Bishop, B. R. Johnson, D. I. Schuster, J. Majer, A. Blais, L. Frunzio, S. M. Girvin, and R. J. Schoelkopf. “Demonstration of two-qubit algorithms with a superconducting quantum processor”. In: *Nature* 460.7252 (2009), pp. 240–244. ISSN: 0028-0836. DOI: [10.1038/nature08121](https://doi.org/10.1038/nature08121). URL: <https://dx.doi.org/10.1038/nature08121>.
- [80] X.-T. Liang, J. Cheng, W.-Z. Zhang, and X. Leng. “Work and heat in quantum CNOT gate operations”. In: *The European Physical Journal D* 75.10 (2021). ISSN: 1434-6060. DOI: [10.1140/epjd/s10053-021-00270-w](https://doi.org/10.1140/epjd/s10053-021-00270-w). URL: <https://dx.doi.org/10.1140/epjd/s10053-021-00270-w>.

- [81] T. Roy, S. Hazra, S. Kundu, M. Chand, M. P. Patankar, and R. Vijay. “Programmable Superconducting Processor with Native Three-Qubit Gates”. In: *Physical Review Applied* 14.1 (2020). ISSN: 2331-7019. DOI: [10.1103/physrevapplied.14.014072](https://doi.org/10.1103/physrevapplied.14.014072). URL: <https://dx.doi.org/10.1103/physrevapplied.14.014072>.
- [82] K. V. Shulga, P. Yang, G. P. Fedorov, M. V. Fistul, M. Weides, and A. V. Ustinov. “Observation of a collective mode of an array of transmon qubits”. In: *JETP Letters* 105.1 (2017), pp. 47–50. ISSN: 0021-3640. DOI: [10.1134/s0021364017010143](https://doi.org/10.1134/s0021364017010143). URL: <https://dx.doi.org/10.1134/s0021364017010143>.
- [83] A. Auffèves. “Quantum Technologies Need a Quantum Energy Initiative”. In: *PRX Quantum* 3.2 (2022). ISSN: 2691-3399. DOI: [10.1103/prxquantum.3.020101](https://doi.org/10.1103/prxquantum.3.020101). URL: <https://dx.doi.org/10.1103/prxquantum.3.020101>.
- [84] W. van der Schoot, R. Wezeman, P. T. Eendebak, N. M. P. Neumann, and F. Phillipson. “Evaluating three levels of quantum metrics on quantum-inspire hardware”. In: *Quantum Information Processing* 22.12 (2023). ISSN: 1573-1332. DOI: [10.1007/s11128-023-04184-x](https://doi.org/10.1007/s11128-023-04184-x). URL: <https://dx.doi.org/10.1007/s11128-023-04184-x>.



MODULAR PULSE SHAPE COMPARED TO THE R_X GATE THE IBM QUANTUM PLATFORM

This appendix shows the implementation of the $R_x(\theta)$ gate and a modular Gaussian pulse which applies the same rotation angle θ on IBM Quantum Hardware. The results of the two procedures are comparable and verify the decision to use the $R_x(\theta)$ gate to charge qubits on Starmon-5.

A.1. MOTIVATION

The study of QB implementation on superconducting transmon qubits via the IBM Quantum Platform utilises Qiskit Pulse to design the specific pulse of the external field that drives the charging [25]. The pulse shape used is a Gaussian form, where the total area of the pulse determines the implemented rotation angle θ (as shown in equation 2.53). A rotation of angle $\theta = \pi$ typically corresponds to full charging of a QB. For a Gaussian pulse, both the standard deviation σ and amplitude \mathcal{N} can be varied to determine the total area θ . The study considers both options and finds very similar, though slightly varying results charging [25]. The conclusion is that the pulse must be (1) fast decreasing and (2) not too narrow [25].

Qiskit Pulse is not yet supported by Quantum Inspire. However, we argue that the $R_x(\theta)$ gate can adequately be used to study the charging of the qubits as QB. The $R_x(\theta)$ gate on IBM quantum platforms is typically optimised for the specific hardware. In Quantum Inspire, the $R_x(\theta)$ gate consists of a DRAG pulse, which is very similar to the Gaussian pulse but includes a derivative component, and is specifically designed to avoid leakage to higher states.

A.2. RESULTS

To compare the modular pulse shape with the build-in $R_x(\theta)$ gate, we study charging q_0 using both methods on the IBM Mumbai device. IBM Mumbai is a 27-qubit

device, which contains the Falcon r5.10 processor. Figure A.1a shows the charging using the $R_x(\theta)$ gate. This can be compared to figure A.1b where the modular pulse charging is shown. This pulse is a Gaussian, set up in the same way as employed by [25]. The total pulse time is set at $\tau = 30\text{ns}$, this pulse time minimises the charging time whilst still allowing for full charging [27]. The build-in $R_x(\theta)$ gate has a gate time of $\tau = 35.6\text{ns}$.

It can be seen that the charging scheme is very similar. Both methods acquire close to complete charging. In table A.1 the experimental values can be found, which shows that the $R_x(\theta)$ and modular pulse charging acquire the charging success rate of $\eta=0.979$ and $\eta=0.977$ respectively. Furthermore, the fit values are comparable too. This shows that the $R_x(\theta)$ gate can also be adequately used to charge the QB.

A difference that can be seen in the data points in figure A.1, the spread of using the modular pulse is larger. This can be seen from the average standard error. For charging using the modular pulse, the average the average standard error is $4.18 \cdot 10^{-3}$. Charging using the $R_x(\theta)$ gate has an average standard error of $3.5 \cdot 10^{-3}$. Yet both are relatively good values for the standard error.

For the IBM Mumbai, the X gate is a native operation, but the $R_x(\theta)$ gate is not. This poses no problem for full charging, but when studying the influence of the area θ it must be noted that the gate applied is not always a single pulse. It may be decomposed into multiple gates, leading to a higher charging time as well. However, for the Quantum Inspire, the $R_x(\theta)$ gate is a native operation and therefore only requires one applied pulse. As it does not affect the charging curve, it poses no problem, and the Quantum Inspire can only be expected to perform even better.

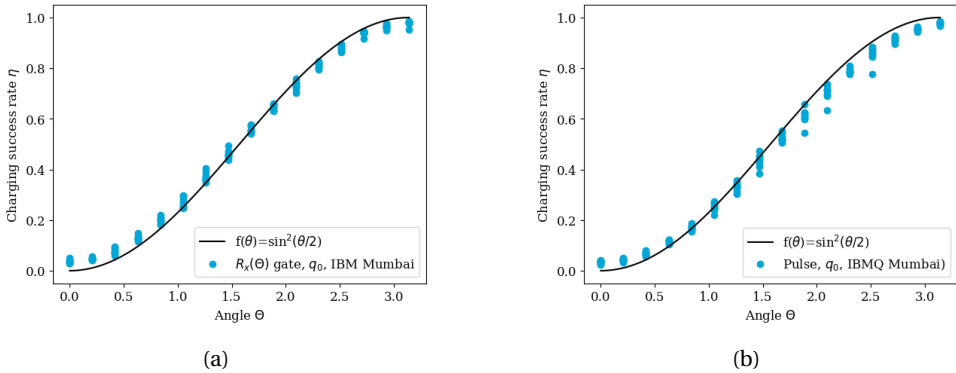


Figure A.1.: A comparison of the charging curve when using (a) the build-in $R_x(\theta)$ gate versus (b) modular pulse shaping in the IBM Mumbai device.

The fit function is plotted in figure A.2. This also shows that although the trajectories are slightly different, the final result is comparable. Additionally, the figures of merit are shown in table A.2. As the charging time of the modular pulse is set slightly lower than the gate time, the charging power of the modular pulse is higher. However, it does not have a major effect on the performance. On top of that, the $R_x(\theta)$ gate on the Starmon-5 has a gate time of 20ns, and can thus instead be

Process	ω_R (GHz)	η	a	ϕ
$R_x(\theta)$	5.071	0.979	0.967	0.0431
Pulse	5.071	0.977	0.964	-0.137

Table A.1.: Experimental values to compare different charging processes on IBM Mumbai. The resonance frequencies ω_R were acquired from IBM. The charging success rate $\eta = \frac{E}{\Delta}$, and fit data a and ϕ were all acquired from the experimental data.

expected to have an increased charging power. All in all, we conclude that the $R_x(\theta)$ gate can reliably be used to charge the QBs.

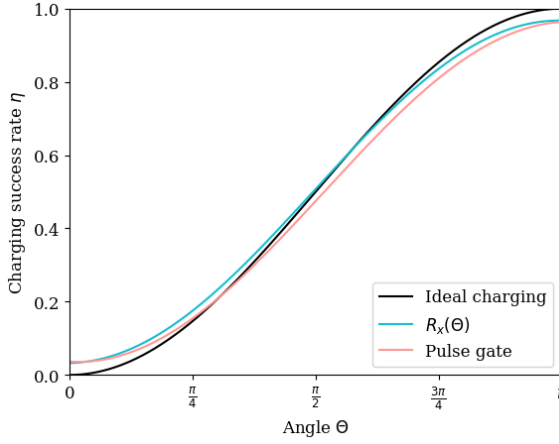


Figure A.2.: Charging trajectory of charging using the $R_x(\theta)$ gate (blue line), modular pulse shape (orange line), and ideal charging (black line). The trajectories are based on the fit values found from experimental data.

Process	E_s (μeV)	τ (ns)	P_c (eV/ms)
$R_x(\theta)$	20.5	35.6	0.576
Pulse	20.5	30	0.684

Table A.2.: Figures of merit for $R_x(\theta)$ gate versus the modular pulse Gaussian(θ) gate, implemented on IBM Mumbai.

B

TOWARDS OPTIMISING THE CHARGING PULSE OF A QUANTUM BATTERY

In this Appendix, a pulse optimisation for QB implementation is performed and implemented on the quantum processor of IBM Brisbane. It shows our first results. A charging rate of $\eta = 0.908$ is achieved, meaning it currently does not improve results compared to using a DRAG pulse or Gaussian pulse. The procedure can be used as inspiration, and further work in this direction is strongly encouraged.

A pulse optimisation for QB implementation is performed and implemented on real quantum hardware. The optimisation technique is called Krotov, and is accessible via the Krotov package [66] in QuTip [70]. An optimisation of state-to-state transfer of a two-level system (TLS) is done, meaning the following transition is optimised:

$$|0\rangle \xrightarrow{\text{pulse}} |1\rangle \quad (\text{B.1})$$

The X gate implements both $|0\rangle \rightarrow |1\rangle$ transfer and $|1\rangle \rightarrow |0\rangle$. Therefore, optimising for state-to-state transfer can be expected to perform better in the context of charging a QB. The quantum system used for the optimisation is TLS. As discussed in section 2.3, a transmon qubit can be approximated as a TLS. Whilst studies have previously shown the optimisation of a pulse for charging a QB, we implement the optimised pulse on real quantum hardware in the QB context using Qiskit Pulse.

B.1. STATE-TO-STATE TRANSFER

The pulse optimisation is shown in figure B.1. It must be emphasised that this optimisation is based on a [Krotov tutorial to optimise state-to-state transfer](#), with small changes to align it with our QB context and the IBM Brisbane device. A gate time of $\tau = 32\text{ns}$ was used. This was chosen as a competitive timeframe with the native X gate implementation, but still ensuring convergence of the optimisation.

Furthermore, the data points are aligned with the discretization of the IBM Quantum Hardware that was used, called IBM Brisbane. IBM Brisbane requires the pulse to take steps of 8, of which each step takes $dt=0.5\text{ns}$. The code of our optimisation is available on [GitHub](#).

B

The initial guess of the pulse is shown by the dashed line in figure B.1, and is a Blackman square function, ensuring a finite slope. The optimised pulse is shown by the bold black line in figure B.1, and shows a unique pulse which still resembles the square pulse, but also shows a damping oscillatory behaviour.

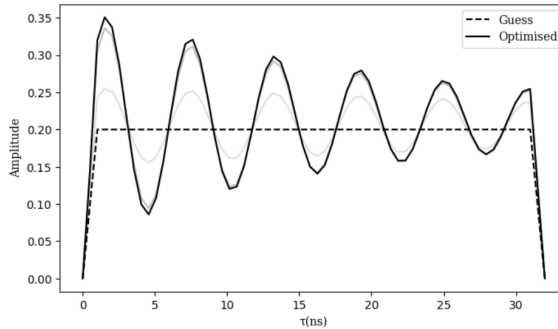


Figure B.1.: Optimisation of pulse using Krotov. The initial guess is a Blackman square, shown with dashed lines. The optimised pulse, shown by the solid line, adds a damped oscillatory behaviour.

Figure B.2 shows the dynamics of the population of states based on implementing the initial guess pulse (dashed line), and optimised pulse (solid lines). The colours represent whether the initial state was in the $|0\rangle$ state (pink) or in the $|1\rangle$ state (blue). The optimisation uses a convergence of 10^{-3} .

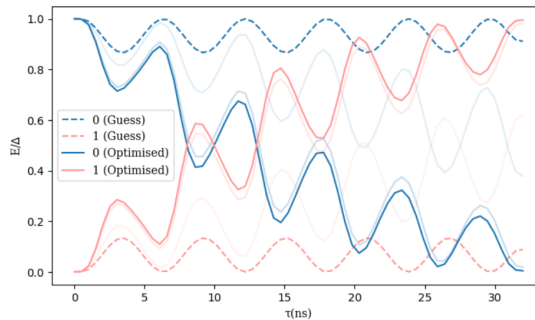


Figure B.2.: Dynamics of optimisation

Figure B.3 shows the pulse schedule of our optimised pulse for IBM Brisbane based on Qiskit Pulse. The results of implementing the optimised pulse on IBM Brisbane are shown in figure B.4. A total of $N=10$ experiments were performed, similar as

for all other datasets throughout this report. Each contains 1024 shots. The obtained data is shown in table D.16. This then leads to an average charging success rate of,

$$\eta = 0.908 \pm 0.004 \quad (\text{B.2})$$

It can therefore be concluded that the currently implemented protocol does not lead to an improvement in the charging of a QB. The charging success rate can be compared to values in Appendix A to conclude that the performance is worse than the native $R_x(\theta)$ gate or modular Gaussian implementation. This can be due to several reasons. Firstly, the transmon qubit is not an ideal TLS. Instead, it could be better to use the Hamiltonian of a transmon qubit, see for example [Kroto optimisation of an X-gate for transmon qubits](#). Secondly, the driving frequency was taken arbitrarily and can be edited to align with the specific qubit. In an ideal situation, a model of the specific device is used as Hamiltonian for the optimisation. Additionally, it must be ensured that the pulse does not vary too quickly for the IBM Quantum Hardware. It is also worth checking whether the pulse area converges to a value of $\theta = \pi$, and adjusting the amplitude accordingly.

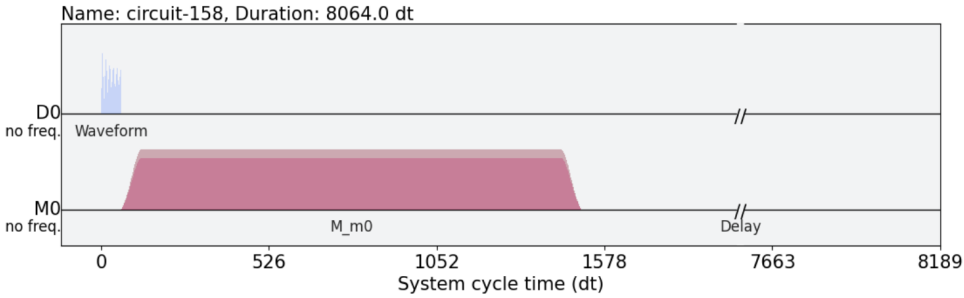


Figure B.3.: Pulse schedule of the optimised pulse ('Wavefront') and subsequent measurement ('M_{m0}') on IBM Brisbane using Qiskit Pulse.

B

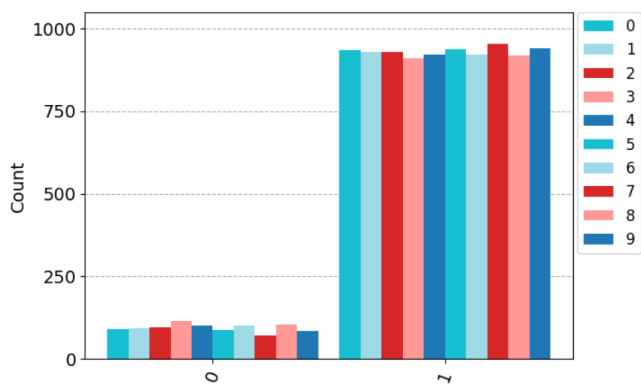


Figure B.4.: Results of the implementation of the optimised pulse on IBM Brisbane for $N = 10$ experiments, each containing 1024 shots.

C

CODE AND CIRCUITS

This appendix shows and discusses the code for the quantum battery (QB) implementation written for this thesis. It is written for the reader to get started with QB implementation on cloud computing from scratch, although prior knowledge of Qiskit is useful. It contains the code for chapters 3, 4 & 5, and Appendix A.

C.1. QISKIT, QUANTUM INSPIRE, AND IBM QUANTUM

This study has been conducted using Qiskit, the open-source software development toolkit for quantum computing, which uses Python as the programming language. Both IBM and Quantum Inspire devices support Qiskit. This makes Qiskit a good choice for this project, as it enables one to write the code in Qiskit and run it on the desired hardware.

To set everything up, it is important to have Python installed. We recommend using Anaconda, as this makes setting up an environment specifically for using the relevant quantum packages relatively easy. We use Jupyter Notebook to run the code in. After installing Anaconda and Jupyter Notebook, one needs to install the right packages for Qiskit, IBM Quantum and Quantum Inspire. To do so, open the Anaconda Prompt. The following code lines can be used as a guideline. One may also choose to set up two environments: one for IBM Quantum, and one for Quantum Inspire. For IBM Quantum, line 13 can be skipped. For Quantum Inspire, all packages need to be installed.

```
1  ## In Anaconda Prompt
2  # Create environment
3  conda create qiskit-env
4
5  #Activate environment
6  conda activate qiskit-env
7
8  # To install Qiskit
```

```

9  !pip install qiskit
10 !pip install qiskit-ibm-runtime
11
12 # To install IBM provider
13 !pip install qiskit-ibmq-provider
14
15 #To install Quantum Inspire
16 !pip install quantuminspire
17
18 # To start jupyter notebook
19 jupyter notebook
20

```

For using IBM Quantum, it is important to have an IBM account. This can easily be done on quantum.ibm.com. This automatically creates a unique API token, which is required to run experiments on IBM hardware from a Software Development Kit (SDK), Jupyter Notebook in our case. More information on how to set up your IBM account can also be found on their respective website.

```

1  # Save API token for IBM Quantum
2  from qiskit import IBMQ
3  IBMQ.save_account('API_token')

```

Similarly, to use Quantum Inspire, an account needs to be set up via quantuminspire.com. This generates an API token. To save your API token for future usage, one can run the following code in Jupyter Notebook:

```

1  # Save API token
2  from quantuminspire.credentials import save_account
3  save_account('API_token')

```

More information on setting up IBM Quantum and Quantum Inspire is available on their respective websites. There are also useful videos on Youtube for more guidance.

This should enable one to get started with the code of our study, which is shown and discussed in the sections below. Additionally, our Jupyter notebook files are accessible via the [GitHub](#).

C.2. DIRECT CHARGING OF A SINGLE QB IN QUANTUM INSPIRE

In this section, we provide an overview of the code used for direct charging of a single qubit in Quantum Inspire, as outlined in Chapter 3. The code segments shown

are relevant for all experiments conducted in Quantum Inspire, except the specific code segment in section C.2.3) and the circuit details in section C.2.4. The remaining parts must thus also be implemented for charger-mediated energy transfer and parallel charging. This is discussed further in section C.3 and section C.4.

C.2.1. PACKAGES

To start, one needs to import the relevant packages. This is shown below and is the same for all studies conducted in Quantum Inspire.

```

1  # Set up Quantum Inspire & import relevant packages
2  import numpy as np
3  import os
4
5  from qiskit import execute, QuantumCircuit, QuantumRegister, ClassicalRegister
6  from qiskit.tools.visualization import circuit_drawer, plot_histogram
7  from IPython.display import display, Math, Latex
8  import matplotlib.pyplot as plt
9  font = {'family': 'serif'}
10
11 from quantuminspire.credentials import get_authentication
12 from quantuminspire.api import QuantumInspireAPI
13 from quantuminspire.qiskit import QI
14
15 QI_URL = os.getenv('API_URL', 'https://api.quantum-inspire.com/')
16 authentication = get_authentication()
17 QI.set_authentication(authentication, QI_URL)
18 backend = QI.get_backend('Starmon-5')

```

C.2.2. FUNCTIONS

In Starmon-5, we always get 5-bit strings as output of counts. For example:

```
counts = '00001':1024, '00000':0
```

This occurs as for Starmon-5 we always need to define the circuit with 5 qubits (i.e. as `qc = QuantumCircuit(5,5)`). Hence, it is useful to define a function `finding_value()`. It takes the output from the experiment counts, and converts this into the charging success rate η . To do so, it also requires qubit and shots as input. Again, this function can be used for all experiments conducted in Quantum Inspire. See below.

```

1  #Define a function that returns the percentage of 1's states
2  #compared to the total number of states for the desired qubit.
3  def finding_value(counts,qubit,shots):

```

```

4     total = 0
5     if qubit == 0:
6         for binary_string, number in counts.items():
7             if binary_string[4] == '1':
8                 total += number
9     if qubit == 1:
10        for binary_string, number in counts.items():
11            if binary_string[3] == '1':
12                total += number
13    if qubit == 2:
14        for binary_string, number in counts.items():
15            if binary_string[2] == '1':
16                total += number
17    if qubit == 3:
18        for binary_string, number in counts.items():
19            if binary_string[1] == '1':
20                total += number
21    if qubit == 4:
22        for binary_string, number in counts.items():
23            if binary_string[0] == '1':
24                total += number
25    return total/shots

```

C.2.3. CODE

Here, we show the code used to perform the charging of battery q_0 on Starmon-5. The code can be used for the other qubits by simply changing the qubit number in line 4. This code was used for the data shown in chapter 3 specifically.

```

1     ##Direct charging of a single QB in Quantum Inspire
2
3     #Define the qubit, this has to be 0, 1, 2, 3, or 4 for Starmon-5
4     qubit=0
5
6     #Define the area with equidistant steps (n=16)
7     theta = np.linspace(0, np.pi, 16)
8
9     #Define the total number of shots per data point
10    shots = 1024
11
12    #Define the total number of runs
13    runs=10
14
15    y_values = []
16    data=[]

```

```

17
18 for i in range(runs):
19     for t in theta:
20         #Set up QuantumCircuit, this needs to be 5x5 for Starmon-5
21         qr = QuantumRegister(5)
22         cr = ClassicalRegister(5)
23         qc = QuantumCircuit(qr,cr)
24
25         #Charge the QB with specified area
26         qc.rx(t,qubit)
27
28         #Measure
29         qc.measure(qr[qubit],cr[qubit])
30
31         #Run on specified backend
32         job = backend.run(qc,shots)
33         counts = job.result().get_counts()
34
35         #Get results and append to the list
36         y = finding_value(counts,qubit,shots)
37         y_values.append(y)
38
39         #Store the total list in dataQ
40         data.append([y_values])
41
42         #Reset y_values for the next run
43         y_values=[]

```

C

When Starmon-5 is relatively busy, instead of running the code runs times in one go, it may be better to run the code instance by instance. This avoids losing the connection with Quantum Inspire, and stopping halfway through one run. However, instead of running the cell once, it has to be run ten times.

C.2.4. CIRCUIT

The corresponding circuit is shown in figure C.1. The $R_x(\theta)$ gate is applied to the defined qubit, and the corresponding measurement is performed. This is the circuit associated with chapter 3.

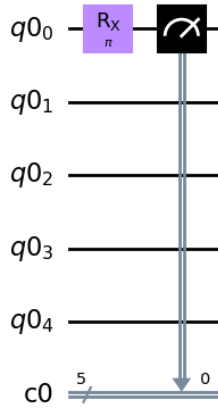


Figure C.1.: Circuit of QB implementation on Quantum Inspire. This shows the gate composition.

C.2.5. DATA PLOT

The code below can be used to plot the data in the same way as was done for figure 3.3 (and figure 4.2, and 5.2 for charger-mediated energy transfer and parallel charging, respectively).

```

1  ## Plot the data
2  # Generate the ideal curve function vlues
3  x_func = np.linspace(min(theta), max(theta), 100)
4  y_func = np.sin(x_func/2)**2
5
6  # Plot the ideal curve
7  plt.plot(x_func, y_func, color='black')
8
9  #Plot the data points
10 tud_color='#00A6D6'
11 for i in range(len(data)):
12     plt.scatter(theta,data[i],color=tud_color)
13
14 #Lay-out details
15 plt.xticks(fontname='serif')
16 plt.yticks(fontname='serif')
17 plt.xlabel("Angle  $\theta$ ",**font)
18 plt.ylabel("Energy E/ $\Delta$ ",**font)
19 plt.legend(["f( $\theta$ )=sin $^2(\theta/2)$ ", "Starmon-5, q=0"],
20           prop=font, loc="lower right")

```

```

21
22 plt.show()

```

C.2.6. DATA ANALYSIS

The code used for analysing our data is shown below. First, the data is converted to an array format and transposed. This means that each column now contains the values corresponding to a specific area, making it easier to calculate relevant properties such as the mean values, standard deviation, standard error, maximum values and minimum values. Note that the maximum value of the mean_values is used to define the optimal charging value of E/Δ . The standard error is used in the data plot of figure 3.4. The standard error and standard deviation of all data points are well within the statistical bounds.

```

1  #Transpose Data
2  dataT=np.array(data)
3  data = dataT.transpose()
4
5  #Mean Values
6  mean_values = []
7  for t in range(len(theta)):
8      mean_values.append(np.mean(data[t]))
9  print('Mean values:', mean_values)
10
11 #Standard Deviation
12 std_dev=[]
13 for t in range(len(theta)):
14     std_dev.append(np.std(data[t]))
15 print('Standard Deviation:', std_dev)
16
17 #Standard Error
18 std_err=[]
19 for t in range(len(theta)):
20     std_err.append(np.std(data[t]) / np.sqrt(np.size(data[t])))
21 print('Standard Error:', std_err)
22
23 #Maximum values
24 max_values = []
25 for t in range(len(theta)):
26     max_values.append(np.max(data[t]))
27 print('Maximum values:', max_values)
28
29 #Minimum values
30 min_values = []

```

```

31 for t in range(len(theta)):
32     min_values.append(np.min(data[t]))
33 print('Minimum values:',min_values)

```

C.2.7. FITTING THE DATA

This code derives the values given by equation 3.6, which are used for the fit function plotted in figure 3.4. The initial guess is set at [0.9999, 0]. This is because setting it at the actual ideal values [1, 0] gives an error in calculating the covariance, which is again used to find the best-fit values. Hence, the function `curve_fit()` starts malfunctioning. Setting the initial guess of a slightly below 1 solves this problem.

```

1  from scipy.optimize import curve_fit
2
3  def sin2_func(x, a,b):
4      y = a*np.sin(x/2)**2+2*np.sqrt(a)*np.sqrt(1-a)*np.sin(b)*np.sin(x/2)
5        *np.cos(x/2)+(1-a)*np.cos(x/2)**2
6      return y
7
8  guess = [0.9999, 0]
9  xdata=theta
10 ydata=mean_values
11
12 parameters, covariance = curve_fit(sin2_func, xdata, ydata, p0=guess)
13
14 fit_a = parameters[0]
15 fit_b = parameters[1]
16
17 SE = np.sqrt(np.diag(covariance))
18 SE_a = SE[0]
19 SE_b = SE[1]
20
21 print(F'The value of a is {fit_a:.5f} with standard error of {SE_a:.5f}.')
22 print(F'The value of phi is {fit_b:.5f} with standard error of {SE_b:.5f}.')

```

Below, the plotting of 3.4 is shown. It requires the fit parameters (`fit_a`, `fit_b`), the mean values (`mean_values`) and the standard error (`std_err`).

```

1  fit_sin2 = sin2_func(xdata, fit_a, fit_b)
2
3  plt.plot(xdata, fit_sin2 , '-', label='fit',color=tud_color)
4  plt.errorbar(theta, mean_values, yerr=std_err, fmt='none',ecolor='black')
5

```

```

6 plt.xticks(fontname='serif')
7 plt.yticks(fontname='serif')
8
9 plt.xlabel("Angle  $\Theta$ ",**font)
10 plt.ylabel("Energy E/ $\Delta$ ",**font)
11 plt.legend(["fit function", "Starmon-5, q=0"], prop=font, loc="lower right")

```

C.3. CHARGER-MEDIATED ENERGY TRANSFER IN QUANTUM INSPIRE

C

C.3.1. CODE

The code below was used for charger-mediated energy transfer based on the CNOT gate in Quantum Inspire. Note that the CNOT gate must always be applied between qubit q_2 and one of the other qubits, as only qubit q_2 shares resonators with the other qubits. If another qubit is chosen, the gate will be decomposed into several multiqubit gates, which significantly increases the charging time. The code for the data plot in section C.2.5, the data analysis in section C.2.6 and data fitting in section C.2.7 can also be used for the data obtained with this code.

```

1  ## Charger-mediated energy transfer in Quantum Inspire
2
3  #Define a charger and a battery (qubit)
4  #For Starmon-5, always choose qubit 2 as charger
5  charger=2
6  qubit=1
7
8  theta = np.linspace(0, np.pi, 16)
9  shots = 1024
10 runs = 10
11
12 y_values = []
13 data=[]
14
15 for i in range(runs):
16     for t in theta:
17         qr = QuantumRegister(5)
18         cr = ClassicalRegister(5)
19         qc = QuantumCircuit(qr,cr)
20
21         #Initialise the charger
22         qc.rx(t,charger)
23
24         #Perform energy transfer

```

```

25     qc.cnot(charger,qubit)
26
27     #Measure the qubit/battery
28     qc.measure(qr[qubit],cr[qubit])
29
30     #Run on desired backend
31     job = backend.run(qc,shots)
32     counts = job.result().get_counts()
33     y_values.append(finding_value(counts,qubit,shots))
34     data.append(y_values)
35     y_values=[]

```

C.3.2. CIRCUIT

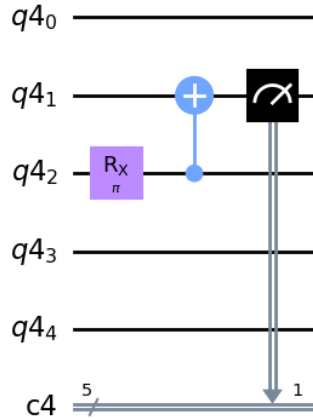


Figure C.2.: Circuit of Charger-mediated energy transfer using CNOT gate in Quantum Inspire. This shows the gate composition.

C.4. PARALLEL CHARGING IN QUANTUM INSPIRE

This code implements parallel charging of qubit q_0 , q_1 , q_2 , q_3 and q_4 . This is done by applying $R_x(\theta)$ gates simultaneously on all qubits. Note that at the time of performing the experiments, qubit q_0 was offline. Thus, chapter 5 does not contain data of qubit q_0 .

Again, the code for the data plot in section C.2.5, the data analysis in section C.2.6 and data fitting in section C.2.7 can also be used for the data obtained with this code.

C.4.1. CODE

```
1  ## Parallel charging in Quantum Inspire
2  qubit=[0,1,2,3,4]
3  theta = np.linspace(0, np.pi, 16)
4  shots = 1024
5  runs=10
6
7  data0=[]
8  data1=[]
9  data2=[]
10 data3=[]
11 data4=[]
12
13 q0_values=[]
14 q1_values=[]
15 q2_values=[]
16 q3_values=[]
17 q4_values=[]
18
19
20 for i in range(runs):
21     for t in theta:
22         #Set up Quantum Circuit
23         qc=QuantumCircuit(5)
24
25         #Charge all units of the QB
26         for q in qubit:
27             qc.rx(t,q)
28
29         #Measure all qubits
30         qc.measure_all()
31
32         #Run on desired hardware
33         job = backend.run(qc,shots)
34         counts = job.result().get_counts()
35
36         q0_values.append(finding_value(counts,0,shots))
37         q1_values.append(finding_value(counts,1,shots))
38         q2_values.append(finding_value(counts,2,shots))
39         q3_values.append(finding_value(counts,3,shots))
40         q4_values.append(finding_value(counts,4,shots))
41
42         data0.append(q0_values)
43         data1.append(q1_values)
```

```

44 data2.append(q2_values)
45 data3.append(q3_values)
46 data4.append(q4_values)
47
48 q0_values=[]
49 q1_values=[]
50 q2_values=[]
51 q3_values=[]
52 q4_values=[]

```

C.4.2. CIRCUIT

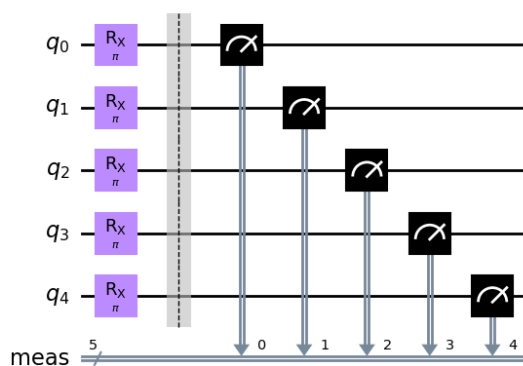


Figure C.3.: Circuit of parallel QB implementation on Quantum Inspire. This shows the gate composition.

C.5. MODULAR PULSE SHAPING COMPARED TO THE RX GATE ON THE IBM QUANTUM PLATFORM

This section provides the code to implement the $R_x(\theta)$ gate and the modular pulse shape on the IBM Quantum Platform. The modular pulse that is implemented is the Gaussian, and the standard deviation σ and coupling constant g are used to determine the amplitude. The coupling constant g is derived from the backend configuration, and the standard deviation σ is chosen based on the charging time $\tau=30\text{ns}$. The IBM Quantum Platform that was used is IBMQ Mumbai but can be changed to currently available platforms.

The code for the data plots in section C.2.5, the data analysis in section C.2.6 and data fitting in section C.2.7 was used for the data processing in Appendix A.

C.5.1. RX GATE

The $R_x(\theta)$ gate is implemented similarly as on Quantum Inspire, except the circuit is now run on the IBM Quantum Platform.

The data output from IBM Quantum is different as it gives counts with '0' or '1' as output. Therefore the function `finding_value()` is modified to account for this.

```

1 # Set up IBM Quantum & import relevant packages
2 from qiskit import IBMQ, QuantumCircuit, pulse, schedule, transpile
3 from qiskit.tools.jupyter import *
4
5 import matplotlib.pyplot as plt
6 import numpy as np
7 font = {'family': 'serif'}
8
9 from qiskit_ibm_provider import IBMProvider
10 provider = IBMProvider()
11 backend = provider.get_backend('ibmq_mumbai')

```

```

1 def finding_value(counts):
2     total=counts['1']+counts['0']
3     return (counts['1'])/total

```

```

1 theta = np.linspace(0, np.pi, 16)
2 shots = 1024
3 job_ID = []
4 qubit = 0
5
6 for t in theta:
7     circ=QuantumCircuit(1)

```

```

8     circ.rx(t,qubit)
9     circ.measure_all()
10    transpiled=transpile(circ,backend)
11    job=backend.run(transpiled,shots=1024)
12    job_ID.append(job.job_id())

```

```

1  values=[]
2  for i in job_ID:
3      retrieved_job=provider.backend.retrieve_job(i)
4      counts = retrieved_job.result().get_counts()
5      values.append(finding_value(counts))
6
7  data=[]
8  data.append(values)

```

C.5.2. MODULAR PULSE SHAPE

For the coming section, prior knowledge of Qiskit Pulse is recommended. Otherwise, it is advised to first do some of the tutorials provided in reference [26] before getting started with this code, specifically "[Calibrating qubits using Qiskit Pulse](#)". The set-up of this tutorial was also used to develop our code.

```

1  # Set up IBM Quantum & import relevant packages for Qiskit Pulse
2  from qiskit import IBMQ, pulse, schedule, transpile
3  from qiskit.circuit import QuantumCircuit, Gate, Parameter
4  from qiskit import pulse
5  from qiskit.pulse.library import Gaussian
6  from qiskit.tools.jupyter import *
7
8  import matplotlib.pyplot as plt
9  import numpy as np
10
11  IBMQ.load_account()
12  from qiskit_ibm_provider import IBMProvider
13  provider = IBMProvider()
14  backend = provider.get_backend('ibmq_mumbai')

```

```

1  # Set up relevant parameters
2  backend_config = backend.configuration()
3  dt = backend_config.dt
4  bc=backend.configuration().timing_constraints
5  acquire_alignment = bc['acquire_alignment']

```

```

6 granularity = bc['granularity']
7 pulse_alignment = bc['pulse_alignment']
8 lcm = np.lcm(acquire_alignment, pulse_alignment)
9 backend_defaults = backend.defaults()
10
11 def get_closest_multiple_of(value, base_number):
12     return int(value + base_number/2) - (int(value + base_number/2) % base_number)
13
14 # samples need to be multiples of 16
15 def get_closest_multiple_of_16(num):
16     return get_closest_multiple_of(num, granularity)
17
18 # Convert seconds to dt
19 def get_dt_from(sec):
20     return get_closest_multiple_of(sec/dt, lcm)
21
22 def finding_value(counts):
23     total=counts['1']+counts['0']
24     return (counts['1'])/total

```

```

1 # Specific to our experiment
2 drive_duration_sec = 30*ns
3 drive_sigma_sec = drive_duration_sec/8
4
5 hamil=backend_config.hamiltonian['vars']
6 g_coupling = hamil['omegad0']
7
8 def amp(theta,drive_sigma_sec,g_coupling):
9     result = theta/(np.sqrt(2*np.pi)*g_coupling*drive_sigma_sec)
10    return result

```

```

1 ## Code
2 theta = np.linspace(0, np.pi, 16)
3 y_values = []
4 job_ID=[]
5
6 for theta_round in theta:
7     drive_amp = amp(theta_round,drive_sigma_sec,g_coupling)
8
9     with pulse.build(backend=backend, default_alignment='sequential', name='QB Gate')
10    as QB_Gate:
11        drive_duration =
12            get_closest_multiple_of_16(pulse.seconds_to_samples(drive_duration_sec))

```

```

13     drive_sigma = pulse.seconds_to_samples(drive_sigma_sec)
14     drive_chan = pulse.drive_channel(qubit)
15     drive_amp = amp(theta_round,drive_sigma_sec,g_coupling)
16     pulse.set_frequency(freq, drive_chan)
17     #Pulse
18     pulse.play(pulse.Gaussian(duration=drive_duration,
19                             sigma=drive_sigma,
20                             amp=drive_amp,
21                             angle = theta_round,
22                             name='Quantum Battery Gate'), drive_chan)
23
24     circ = QuantumCircuit(1)
25     custom_gate = Gate('my_custom_gate',1,[])
26
27     circ.append(custom_gate,[0])
28     circ.measure_all()
29
30     circ.add_calibration(custom_gate, [0], QB_Gate)
31
32     circ_transpile = transpile(circ, backend)
33     circ_sched = schedule(circ_transpile, backend)
34
35     job = backend.run(circ_sched, shots=1024)
36     ID=job.job_id()
37     job_ID.append(ID)

```

```

1  #Storing data
2  values=[]
3  data=[]
4  for i in job_ID:
5      counts=provider.backend.retrieve_job(i).result().get_counts()
6      values.append(finding_value(counts))
7  data.append(values)

```

C.6. OPTIMISATION OF STATE-TO-STATE TRANSFER ON IBM BRISBANE

```
1  #Importing packages related to krotov optimisation
2  import os
3  import qutip
4  import numpy as np
5  import scipy
6  import matplotlib
7  import matplotlib.pyplot as plt
8  import krotov
9  from scipy.fftpack import fft
10 from scipy.interpolate import interp1d
11 import pickle
12
13 font = {'family':'serif'}
```

```
1  #importing qiskit & IBM packages
2  from qiskit import IBMQ, QuantumCircuit, pulse, schedule, transpile
3  #from qiskit.tools.monitor import job_monitor
4  from qiskit.visualization import plot_gate_map, plot_histogram
5  from qiskit.circuit import QuantumCircuit, Gate, Parameter
6  from qiskit.tools.jupyter import *
7
8  from qiskit_ibm_provider import IBMProvider
9  provider = IBMProvider()
10 backend = provider.get_backend('ibm_brisbane')
```

```
1  #IBM backend configurations
2  backend_config = backend.configuration()
3  dt = backend.dt
4  acquire_alignment = backend.configuration().timing_constraints['acquire_alignment']
5  granularity = backend.configuration().timing_constraints['granularity']
6  pulse_alignment = backend.configuration().timing_constraints['pulse_alignment']
7  lcm = np.lcm(acquire_alignment, pulse_alignment)
8  print(lcm)
9  backend_defaults = backend.defaults()
```

C.6.1. OPTIMISATION

```

1  #Two level Hamiltonian
2  def hamiltonian(omega=1, ampl0=0.2):
3      """Two-level-system Hamiltonian
4
5      Args:
6          omega (float): energy separation of the qubit levels
7          ampl0 (float): constant amplitude of the driving field
8      """
9      H0 = -0.5 * omega * qutip.operators.sigmaz()
10     H1 = qutip.operators.sigmaz()
11
12     def guess_control(t, args):
13         return ampl0 * krotov.shapes.flat_top(
14             t, t_start=0, t_stop=t_c, t_rise=0.3, func="blackman"
15         )
16
17     return [H0, [H1, guess_control]]
18
19 H = hamiltonian()

```

```

1  def get_closest_multiple_of(value, base_number):
2      return int(value + base_number/2) - (int(value + base_number/2) % base_number)
3
4  dt_ns=dt*1e9
5
6  #Choose your desired gate duration
7  desired_gate_duration_ns = 30
8
9  #Calculates the amount of data points in this gate_duration
10 desired_data_points = desired_gate_duration_ns/dt_ns
11
12 #Finding the closest values which are attainable on the Quantum Hardware
13 #Due to lcm
14 data_points = get_closest_multiple_of(desired_data_points,lcm)
15
16 #Real charging time in ns
17 t_c = data_points*dt_ns
18 print('The implemented gate duration is', t_c, 'ns')
19 print('(using', data_points, 'data points)')
20
21 #Create array of tlist

```

```

22 tlist = np.linspace(0, t_c, data_points)

```

```

1 def plot_pulse(pulse, tlist):
2     fig, ax = plt.subplots()
3     if callable(pulse):
4         pulse = np.array([pulse(t, args=None) for t in tlist])
5     ax.plot(tlist, pulse, color=tud_color)
6     ax.set_xlabel('t(ns)', font)
7     ax.set_ylabel('Amplitude', font)
8     plt.show(fig)
9 plot_pulse(H[1][1], tlist)

```

```

1 #Optimisation target
2 objectives = [
3     krotov.Objective(
4         initial_state=qutip.ket("0"), target=qutip.ket("1"), H=H
5     )
6 ]
7
8 objectives
9
10 def S(t):
11     """Shape function for the field update"""
12     return krotov.shapes.flattop(
13         t, t_start=0, t_stop=t_c, t_rise=0.3, t_fall=0.3, func='blackman'
14     )
15
16 pulse_options = {
17     H[1][1]: dict(lambda_a=5, update_shape=S)
18 }
19
20 proj0 = qutip.ket2dm(qutip.ket("0"))
21 proj1 = qutip.ket2dm(qutip.ket("1"))
22
23 guess_dynamics = objectives[0].mesolve(tlist, e_ops=[proj0, proj1])
24
25 def plot_population(result):
26     fig, ax = plt.subplots()
27     ax.plot(result.times, result.expect[0], label='0')
28     ax.plot(result.times, result.expect[1], label='1')
29     ax.legend()
30     ax.set_xlabel('Time', font)
31     ax.set_ylabel('population', font)

```

```

32     plt.show(fig)
33
34     plot_population(guess_dynamics)

```

```

1     ##Perform the optimisation
2     opt_result = krotov.optimize_pulses(
3         objectives,
4         pulse_options=pulse_options,
5         tlist=tlist,
6         propagator=krotov.propagators.expm,
7         chi_constructor=krotov.functionals.chis_ss,
8         info_hook=krotov.info_hooks.print_table(J_T=krotov.functionals.J_T_ss),
9         check_convergence=krotov.convergence.Or(
10            krotov.convergence.value_below('1e-3', name='J_T'),
11            krotov.convergence.check_monotonic_error,
12        ),
13        iter_stop=20,
14        store_all_pulses=True,
15    )
16
17    opt_result
18
19    plot_pulse(opt_result.optimized_controls[0], tlist)

```

```

1     opt_dynamics = opt_result.optimized_objectives[0].mesolve(
2         tlist, e_ops=[proj0, proj1])
3
4     plot_population(opt_dynamics)

```

```

1     tud_color='#00A6D6'
2     size = 20
3     def plot_iterations(opt_result):
4         """Plot the control fields in population dynamics over all iterations.
5
6         This depends on ``store_all_pulses=True`` in the call to
7         'optimize_pulses'.
8         """
9         fig, [ax_ctr, ax_dyn] = plt.subplots(nrows=2, figsize=(8, 10))
10        n_iters = len(opt_result.iters)
11        for (iteration, pulses) in zip(opt_result.iters, opt_result.all_pulses):
12            controls = [

```

```

13     krotov.conversions.pulse_onto_tlist(pulse)
14     for pulse in pulses
15 ]
16 objectives = opt_result.objectives_with_controls(controls)
17 dynamics = objectives[0].mesolve(
18     opt_result.tlist, e_ops=[proj0, proj1]
19 )
20 if iteration == 0:
21     ls = '--' # dashed
22     alpha = 1 # full opacity
23     ctr_label = 'Guess'
24     pop_labels = ['0 (Guess)', '1 (Guess)']
25 elif iteration == opt_result.iters[-1]:
26     ls = '-' # solid
27     alpha = 1 # full opacity
28     ctr_label = 'Optimised'
29     pop_labels = ['0 (Optimised)', '1 (Optimised)']
30 else:
31     ls = '-' # solid
32     alpha = 0.5 * float(iteration) / float(n_iters) # max 50%
33     ctr_label = None
34     pop_labels = [None, None]
35 ax_ctr.plot(
36     dynamics.times,
37     controls[0],
38     label=ctr_label,
39     color='black',
40     ls=ls,
41     alpha=alpha,
42 )
43 ax_dyn.plot(
44     dynamics.times,
45     dynamics.expect[0],
46     label=pop_labels[0],
47     color="#1F77B4", # colour blue
48     ls=ls,
49     alpha=alpha,
50 )
51 ax_dyn.plot(
52     dynamics.times,
53     dynamics.expect[1],
54     label=pop_labels[1],
55     color="#FF9896", # colour pink
56     ls=ls,
57     alpha=alpha,

```

```

58     )
59     ax_dyn.legend(prop=font)
60     ax_dyn.set_xlabel('t(ns)',**font)
61     ax_dyn.set_ylabel('E/\Delta$',**font)
62     ax_ctr.legend(prop=font,fontsize=size)
63     ax_ctr.set_xlabel('t(ns)',**font)
64     ax_ctr.set_ylabel('Amplitude',**font)
65     plt.show(fig)
66
67 plot_iterations(opt_result)

```

C.6.2. IMPLEMENTATION ON IBM QUANTUM PLATFORM

```

1  #specify desired qubit
2  qubit = 0
3  #to find the value from our data acquisition
4  def finding_value(counts):
5      total=counts['1']+counts['0']
6      return (counts['1'])/total
7
8  with pulse.build(backend=backend, default_alignment='sequential', name='QB Gate')
9      drive_chan = pulse.drive_channel(qubit)
10     # Drive pulse
11     pulse.play(pulse.library.Waveform(opt_pulse), drive_chan)
12
13     circ = QuantumCircuit(1)
14     custom_gate = Gate('my_custom_gate',1, [])
15     circ.append(custom_gate, [0])
16     circ.measure_all()
17
18     circ.add_calibration(custom_gate, [0], QB_Gate)
19
20     circ_transpile = transpile(circ, backend)
21     circ_sched = schedule(circ_transpile, backend)
22     circ_sched.draw()

```

```

1  job = backend.run(circ_transpile, shots=1024)

```

D

DATA

To ensure data transparency, this Appendix contains all data obtained during the experiments on Quantum Inspire. The data is used in chapter 3, 4, & 5. Each data cell contains an average of 1024 shots. The columns contain the $N = 10$ different charging trajectories, whilst each row represents the angle from $\theta \in (0, \pi)$ with steps of $\frac{\pi}{16}$.

D.1. DIRECT CHARGING OF A SINGLE QB

	η_1	η_2	η_3	η_4	η_5	η_6	η_7	η_8	η_9	η_{10}
0	0.0625	0.0547	0.0664	0.0557	0.0547	0.0527	0.0615	0.0635	0.0615	0.0586
$\frac{\pi}{16}$	0.0684	0.0576	0.0615	0.0762	0.0732	0.0586	0.0674	0.0664	0.0645	0.0762
$\frac{\pi}{8}$	0.1084	0.1094	0.1152	0.1123	0.1299	0.1182	0.1152	0.1211	0.1055	0.1191
$\frac{3\pi}{16}$	0.1689	0.1826	0.1729	0.1377	0.1611	0.1406	0.1377	0.1641	0.1836	0.1563
$\frac{\pi}{4}$	0.1973	0.2061	0.2217	0.2021	0.209	0.2148	0.2021	0.1963	0.1904	0.1992
$\frac{5\pi}{16}$	0.2793	0.251	0.2607	0.2695	0.2617	0.2852	0.2695	0.2773	0.2646	0.2793
$\frac{3\pi}{8}$	0.3682	0.3789	0.3691	0.3750	0.3799	0.3359	0.375	0.3535	0.3779	0.3545
$\frac{7\pi}{16}$	0.4912	0.4443	0.4717	0.4443	0.4854	0.4678	0.4443	0.4424	0.4453	0.4453
$\frac{\pi}{2}$	0.5635	0.6006	0.5703	0.5742	0.5908	0.5977	0.5742	0.5732	0.5518	0.585
$\frac{9\pi}{16}$	0.6523	0.6631	0.6719	0.6631	0.6533	0.6777	0.6631	0.6611	0.6729	0.6797
$\frac{5\pi}{8}$	0.7529	0.7578	0.7490	0.751	0.7627	0.7539	0.751	0.7822	0.7666	0.7588
$\frac{11\pi}{16}$	0.8564	0.8516	0.8320	0.8604	0.8350	0.8330	0.8604	0.8604	0.8340	0.8311
$\frac{3\pi}{4}$	0.8799	0.8955	0.8633	0.8555	0.8818	0.8613	0.8555	0.8867	0.8838	0.8857
$\frac{7\pi}{8}$	0.9277	0.9492	0.9277	0.9307	0.9297	0.9326	0.9307	0.9443	0.9238	0.9268
$\frac{15\pi}{16}$	0.9756	0.9668	0.957	0.9619	0.9561	0.957	0.9619	0.9717	0.9541	0.9561
π	0.9824	0.9727	0.9746	0.9766	0.9736	0.9727	0.9658	0.9727	0.9824	0.9688

Table D.1.: The dataset of direct charging of qubit q_0 in Starmon-5 on Quantum Inspire. This data was used for chapter 3, and plotted in figure 3.3.

0.0596	0.0693	0.0713	0.0596	0.0898	0.0547	0.0664	0.0791	0.0664	0.0605
0.0732	0.0508	0.0654	0.0771	0.0791	0.0859	0.0635	0.0762	0.0693	0.0693
0.1113	0.0977	0.1152	0.0967	0.0996	0.1133	0.1084	0.0938	0.1045	0.1143
0.1582	0.1729	0.1611	0.1211	0.1455	0.1729	0.1631	0.1611	0.1475	0.1494
0.1865	0.2197	0.1807	0.2148	0.1895	0.2070	0.1914	0.2090	0.1924	0.2012
0.2715	0.2725	0.2930	0.2725	0.2568	0.2705	0.2783	0.2539	0.2744	0.2627
0.3613	0.3594	0.3438	0.3643	0.3828	0.3555	0.3857	0.3633	0.3721	0.4033
0.4746	0.4639	0.4746	0.4521	0.4697	0.4912	0.4824	0.4756	0.4619	0.4473
0.5830	0.5781	0.5967	0.5801	0.5830	0.5742	0.5654	0.5547	0.5938	0.5781
0.6426	0.6943	0.6504	0.6650	0.6787	0.6719	0.6758	0.7021	0.6816	0.6650
0.7813	0.7793	0.7539	0.7510	0.7578	0.7988	0.7627	0.7588	0.7627	0.7764
0.8311	0.8438	0.8594	0.8506	0.8535	0.8340	0.8438	0.8359	0.8545	0.8447
0.8662	0.8760	0.8750	0.8604	0.8936	0.8770	0.8467	0.8789	0.8750	0.8750
0.9219	0.9229	0.9326	0.9268	0.9326	0.9336	0.9346	0.9365	0.9326	0.9053
0.9639	0.9609	0.9756	0.9521	0.9609	0.9707	0.9717	0.9678	0.9619	0.9619
0.9746	0.9707	0.9766	0.9688	0.9775	0.9756	0.9844	0.9775	0.9814	0.9795

Table D.2.: The second dataset of direct charging of qubit q_0 in Starmon-5 on Quantum Inspire. This data was used for chapter 3, and plotted in figure 3.3.

0.0215	0.0322	0.0127	0.0176	0.0186	0.0107	0.0234	0.0166	0.0186	0.0166
0.0273	0.0371	0.0244	0.0391	0.0205	0.0254	0.0313	0.0430	0.0244	0.0361
0.0732	0.0596	0.0791	0.0615	0.0693	0.0605	0.0527	0.0635	0.0625	0.0645
0.1260	0.1328	0.1250	0.1064	0.1357	0.1172	0.1143	0.1123	0.1104	0.1201
0.1650	0.1621	0.1738	0.1602	0.1660	0.1592	0.1650	0.1426	0.1563	0.1563
0.2129	0.2510	0.2227	0.2373	0.2422	0.2451	0.2178	0.2334	0.2510	0.2246
0.3242	0.3467	0.3545	0.3428	0.3174	0.3105	0.3223	0.3281	0.3193	0.3086
0.4404	0.4346	0.4316	0.4531	0.4297	0.4336	0.4375	0.4473	0.4111	0.4365
0.5039	0.5605	0.5205	0.5527	0.5283	0.5596	0.5352	0.5293	0.5361	0.5283
0.6455	0.6406	0.6582	0.6299	0.6436	0.6650	0.6357	0.6436	0.6279	0.6357
0.7285	0.7422	0.7236	0.7373	0.7422	0.7314	0.7236	0.7480	0.7432	0.7617
0.8203	0.8193	0.8154	0.8320	0.8193	0.8125	0.8291	0.8281	0.8330	0.8047
0.8438	0.8730	0.8506	0.8623	0.8428	0.8428	0.8350	0.8613	0.8525	0.8545
0.9248	0.9121	0.9111	0.9258	0.9082	0.9004	0.9111	0.8975	0.9190	0.9160
0.9443	0.9424	0.9521	0.9424	0.9424	0.9385	0.9424	0.9395	0.9521	0.9639
0.9570	0.9609	0.9619	0.9551	0.9424	0.9688	0.9541	0.9580	0.9521	0.9473

Table D.3.: The dataset of direct charging of qubit q_1 in Starmon-5 on Quantum Inspire. This data was used in chapter 3.

0.0039	0.0000	0.0019	0.0029	0.0029	0.0039	0.0029	0.0019	0.0009	0.0019
0.0156	0.0146	0.0215	0.0146	0.0205	0.0176	0.0195	0.0127	0.0244	0.0361
0.0479	0.0547	0.0459	0.0439	0.0566	0.0439	0.0566	0.0518	0.0439	0.0498
0.0996	0.1016	0.0957	0.1250	0.0947	0.0918	0.1084	0.1309	0.0947	0.1260
0.1514	0.1338	0.1504	0.1523	0.1514	0.1455	0.1377	0.1416	0.1377	0.1523
0.2148	0.2148	0.2188	0.2334	0.2383	0.2061	0.2412	0.2236	0.2324	0.2393
0.3506	0.3311	0.3154	0.3135	0.3506	0.3281	0.3516	0.3281	0.3330	0.3545
0.4434	0.4238	0.4473	0.4463	0.4463	0.4434	0.4424	0.4258	0.4150	0.4365
0.5449	0.5488	0.5400	0.5410	0.5703	0.5410	0.5830	0.5410	0.5273	0.5293
0.6367	0.6406	0.6553	0.6855	0.6631	0.6611	0.6299	0.6670	0.6602	0.6631
0.7480	0.7441	0.7705	0.7373	0.7646	0.7686	0.7686	0.7461	0.7510	0.7510
0.8281	0.8271	0.8369	0.8066	0.8369	0.8447	0.8408	0.8271	0.8486	0.8379
0.8633	0.8818	0.8867	0.8701	0.8418	0.8623	0.8623	0.8760	0.8750	0.8750
0.9258	0.9209	0.9336	0.9219	0.9297	0.9336	0.9277	0.9473	0.9258	0.9277
0.9648	0.9541	0.9619	0.9541	0.9590	0.9512	0.9697	0.9717	0.9766	0.9697
0.9727	0.9697	0.9775	0.9766	0.9658	0.9805	0.9756	0.9766	0.9736	0.9766

D

Table D.4.: The dataset of direct charging of qubit q_2 in Starmon-5 on Quantum Inspire. This data was used in chapter 3.

0.0156	0.0029	0.0019	0.0019	0.0039	0.0019	0.0117	0.0127	0.0019	0.0019
0.0156	0.0107	0.0137	0.0166	0.0176	0.0156	0.0088	0.0244	0.0127	0.0127
0.0488	0.0342	0.0449	0.0576	0.0654	0.0508	0.0566	0.0488	0.0508	0.0498
0.1250	0.1133	0.1318	0.1279	0.0898	0.1006	0.1182	0.0957	0.1123	0.1299
0.1582	0.1328	0.1289	0.1563	0.1582	0.1514	0.1514	0.1348	0.1113	0.1650
0.2236	0.2637	0.2383	0.2266	0.2236	0.2266	0.2285	0.2305	0.2451	0.2256
0.3145	0.3271	0.3174	0.3213	0.3447	0.3379	0.3311	0.3262	0.2979	0.3213
0.4512	0.4434	0.4365	0.4268	0.4668	0.4414	0.4160	0.4346	0.4453	0.4160
0.5508	0.5146	0.5801	0.5654	0.5557	0.5391	0.5332	0.5508	0.5605	0.5537
0.6631	0.6602	0.6543	0.6396	0.6621	0.6738	0.6621	0.6650	0.6416	0.6484
0.7461	0.7402	0.7559	0.7627	0.7529	0.7471	0.7607	0.7549	0.7725	0.7471
0.8467	0.8223	0.8320	0.8564	0.8467	0.8418	0.8340	0.8408	0.8330	0.8369
0.8877	0.8643	0.8936	0.8789	0.8750	0.8760	0.8623	0.8760	0.8633	0.8691
0.9395	0.9238	0.9365	0.9209	0.9443	0.9346	0.9346	0.9355	0.9326	0.9307
0.9658	0.9697	0.9648	0.9814	0.9717	0.9727	0.9727	0.9668	0.9766	0.9766
0.9854	0.9766	0.9854	0.9785	0.9873	0.9834	0.9873	0.9893	0.9736	0.9805

Table D.5.: The dataset of direct charging of qubit q_3 in Starmon-5 on Quantum Inspire. This data was used in chapter 3.

0.0166	0.0117	0.0117	0.0078	0.0068	0.0107	0.0049	0.0059	0.0107	0.0039
0.0088	0.0244	0.0273	0.0215	0.0166	0.0234	0.0225	0.0146	0.0234	0.0127
0.0469	0.0498	0.0547	0.0732	0.0586	0.0635	0.0498	0.0479	0.0459	0.0625
0.1182	0.0996	0.1172	0.1113	0.1309	0.1074	0.1084	0.1260	0.0996	0.1064
0.1484	0.1572	0.1279	0.1523	0.1445	0.1553	0.1348	0.1572	0.1621	0.1543
0.2236	0.2441	0.2314	0.2441	0.2324	0.2090	0.2217	0.2188	0.2432	0.2451
0.3164	0.3311	0.3164	0.3418	0.3564	0.3379	0.3174	0.3115	0.3340	0.3311
0.4316	0.4160	0.4248	0.4229	0.4404	0.4200	0.4102	0.4258	0.4092	0.4434
0.4932	0.5283	0.5674	0.5234	0.5410	0.5664	0.5352	0.5352	0.5557	0.5674
0.6523	0.6445	0.6270	0.6641	0.6270	0.6357	0.6338	0.6621	0.6221	0.6416
0.7246	0.7510	0.7324	0.7451	0.7314	0.7559	0.7539	0.7285	0.7598	0.7324
0.8164	0.8291	0.8203	0.7998	0.8164	0.8262	0.8076	0.8164	0.8154	0.8223
0.8486	0.8682	0.8281	0.8516	0.8555	0.8516	0.8613	0.8535	0.8730	0.8613
0.9219	0.9180	0.9043	0.9072	0.9004	0.9033	0.9092	0.9179	0.9150	0.9209
0.9434	0.9385	0.9512	0.9346	0.9365	0.9551	0.9424	0.9395	0.9424	0.9424
0.9531	0.9697	0.8213	0.9639	0.9570	0.9551	0.9619	0.9463	0.9697	0.9541

Table D.6.: The dataset of direct charging of qubit q_4 in Starmon-5 on Quantum Inspire. This data was used in chapter 3.

D.2. CHARGER-MEDIATED ENERGY TRANSFER

0.0283	0.0391	0.0283	0.0420	0.0283	0.0283	0.0342	0.0391	0.0195	0.0283
0.0449	0.0605	0.0293	0.0469	0.0605	0.0410	0.0410	0.0469	0.0479	0.0410
0.0850	0.0830	0.0693	0.0801	0.0938	0.0674	0.0781	0.0684	0.0732	0.0664
0.1230	0.1396	0.1377	0.1328	0.1260	0.1191	0.1299	0.1260	0.1279	0.1338
0.1504	0.1631	0.1650	0.1494	0.1494	0.1650	0.1777	0.1445	0.1729	0.1709
0.2383	0.2559	0.2539	0.2578	0.2148	0.2451	0.2441	0.2500	0.2500	0.2500
0.3711	0.3281	0.3555	0.3262	0.3594	0.3447	0.3223	0.3174	0.3340	0.3369
0.4326	0.4365	0.4219	0.4385	0.4590	0.4092	0.4395	0.4375	0.4473	0.4492
0.5303	0.5439	0.5429	0.5518	0.5361	0.5244	0.5381	0.5381	0.5283	0.5137
0.6484	0.6309	0.6406	0.6035	0.6201	0.6484	0.6377	0.6309	0.6377	0.6689
0.7188	0.7178	0.7461	0.7432	0.7363	0.7500	0.7295	0.7500	0.7500	0.6982
0.8135	0.8213	0.8213	0.7900	0.8271	0.8115	0.8135	0.8408	0.8203	0.8086
0.8418	0.8340	0.8496	0.8359	0.8223	0.8193	0.8291	0.8408	0.8281	0.8408
0.8965	0.8906	0.8936	0.8818	0.8896	0.8965	0.9102	0.9199	0.9004	0.8799
0.9219	0.9248	0.9297	0.9150	0.9287	0.9102	0.9307	0.9502	0.9219	0.9316
0.9375	0.9453	0.9326	0.9385	0.9326	0.9395	0.9512	0.9502	0.9375	0.9404

Table D.7.: The dataset of charger-mediated charging of charging qubit q_1 via qubit q_2 in Starmon-5 on Quantum Inspire. This data was used in chapter 4, and plotted in figure 4.2.

0.0098	0.0195	0.0059	0.0117	0.0127	0.0098	0.0049	0.0068	0.0059	0.0107
0.0176	0.0146	0.0146	0.0146	0.0166	0.0176	0.0156	0.0254	0.0186	0.0176
0.0605	0.0566	0.0508	0.0547	0.0508	0.0654	0.0576	0.0557	0.0625	0.0674
0.1094	0.1045	0.1006	0.1113	0.1211	0.1221	0.1221	0.1162	0.1113	0.1055
0.1465	0.1533	0.1602	0.1572	0.1582	0.1582	0.1426	0.1465	0.1514	0.1582
0.2354	0.2422	0.2490	0.2109	0.2314	0.2324	0.2275	0.2471	0.2520	0.2500
0.3252	0.3242	0.3379	0.3203	0.3545	0.3252	0.3203	0.3438	0.3291	0.3516
0.4180	0.4434	0.4580	0.4180	0.4434	0.4307	0.4248	0.4258	0.4141	0.4434
0.5508	0.5488	0.5498	0.5400	0.5586	0.5615	0.5146	0.5410	0.5391	0.5303
0.6445	0.6484	0.6416	0.6221	0.6797	0.6689	0.6494	0.6729	0.6406	0.7500
0.7451	0.7422	0.7305	0.7451	0.7588	0.7373	0.7490	0.7539	0.7412	0.8184
0.8418	0.8447	0.8291	0.8174	0.8232	0.8193	0.8652	0.8662	0.8506	0.8682
0.8555	0.8623	0.8633	0.8643	0.8594	0.8418	0.8281	0.8662	0.8506	0.9229
0.9170	0.9346	0.9072	0.8818	0.9287	0.9395	0.9580	0.9678	0.9541	0.9717
0.9463	0.9551	0.9512	0.9658	0.9492	0.9688	0.9746	0.9717	0.9639	0.9580

Table D.8.: The dataset of charger-mediated charging of charging qubit q_3 via qubit q_2 in Starmon-5 on Quantum Inspire. This data was used in chapter 4, and plotted in figure 4.2.

0.0391	0.0303	0.0352	0.0361	0.0312	0.0176	0.0234	0.0352	0.0352	0.0244
0.0420	0.0332	0.0488	0.0293	0.0371	0.0293	0.0420	0.0361	0.0469	0.0381
0.0820	0.0879	0.0752	0.0771	0.0869	0.0576	0.0615	0.0811	0.0762	0.0908
0.1436	0.1289	0.1396	0.1309	0.1260	0.1221	0.1543	0.1377	0.1230	0.1250
0.1846	0.1602	0.1787	0.1680	0.1738	0.1641	0.1719	0.1699	0.1602	0.1826
0.2559	0.2480	0.2646	0.2266	0.2637	0.2305	0.2637	0.2422	0.2637	0.2803
0.3096	0.3340	0.3311	0.3105	0.3848	0.3633	0.3457	0.3213	0.3301	0.3555
0.4580	0.4395	0.4541	0.4473	0.4287	0.4258	0.4541	0.4160	0.4492	0.4365
0.5508	0.5537	0.5391	0.5195	0.5410	0.5430	0.5488	0.5391	0.5371	0.5400
0.6357	0.6455	0.6670	0.6455	0.6484	0.6299	0.6465	0.6543	0.6445	0.6582
0.7568	0.7324	0.7188	0.7275	0.7227	0.7480	0.7354	0.7539	0.7520	0.7588
0.8164	0.8105	0.8125	0.8096	0.8105	0.8096	0.8115	0.8066	0.7910	0.8154
0.8701	0.8711	0.8604	0.8447	0.8584	0.8730	0.8281	0.8389	0.8408	0.8428
0.8965	0.9033	0.9082	0.9023	0.9033	0.8984	0.8926	0.9121	0.9141	0.9121
0.9414	0.9385	0.9590	0.9336	0.9336	0.9395	0.9307	0.9316	0.9424	0.9531
0.9551	0.9482	0.9414	0.9561	0.9453	0.9502	0.9385	0.9453	0.9453	0.9570

Table D.9.: The dataset of charger-mediated charging of charging qubit q_4 via qubit q_2 in Starmon-5 on Quantum Inspire. This data was used in chapter 4, and plotted in figure 4.2.

D.3. PARALLEL CHARGING

0.0146	0.0156	0.0186	0.0127	0.0166	0.0176	0.0059	0.0205	0.0146	0.0166
0.0254	0.0303	0.0391	0.0273	0.0215	0.0254	0.0332	0.0195	0.0264	0.0215
0.0566	0.0635	0.0762	0.0566	0.0605	0.0703	0.0674	0.0557	0.0654	0.0566
0.1211	0.1201	0.1113	0.1221	0.1191	0.1279	0.1191	0.1191	0.1191	0.1006
0.1543	0.1680	0.1631	0.1670	0.1572	0.1514	0.1504	0.1377	0.1650	0.1572
0.2549	0.2568	0.2383	0.2246	0.2471	0.2617	0.2559	0.2529	0.2100	0.2334
0.3408	0.3311	0.3330	0.3408	0.3584	0.3086	0.3066	0.3418	0.3438	0.3184
0.4190	0.4297	0.4297	0.4287	0.4404	0.4258	0.4531	0.4160	0.4375	0.4219
0.5195	0.5381	0.5215	0.5361	0.5664	0.5469	0.5361	0.5488	0.5459	0.5361
0.6348	0.6523	0.6553	0.6484	0.6504	0.6553	0.6533	0.6436	0.6416	0.6523
0.7402	0.7412	0.7354	0.7451	0.7549	0.7441	0.7383	0.7354	0.7412	0.7305
0.8262	0.8242	0.8379	0.8379	0.8379	0.8281	0.8213	0.8311	0.8057	0.8369
0.8525	0.8545	0.8701	0.8438	0.8555	0.8633	0.8486	0.8564	0.8691	0.8389
0.9170	0.9111	0.9150	0.8926	0.9014	0.9277	0.9141	0.8994	0.9111	0.8916
0.9541	0.9463	0.9385	0.9287	0.9463	0.9443	0.9443	0.9346	0.9424	0.9502
0.9600	0.9473	0.9482	0.9570	0.9619	0.9629	0.9541	0.9463	0.9521	0.9551

Table D.10.: The dataset of parallel charging of q_1 in Starmon-5 on Quantum Inspire. It contains the measurement data of qubit q_1 , when charged simultaneously with qubits q_2 , q_3 & q_4 . This data was used in chapter 5, and plotted in figure 5.2.

0.0723	0.0527	0.0635	0.0908	0.0713	0.0781	0.0742	0.0547	0.0557	0.0693
0.0850	0.0859	0.0566	0.0781	0.0664	0.0869	0.0684	0.0664	0.0713	0.0664
0.1055	0.1045	0.1133	0.1230	0.1123	0.1240	0.1006	0.1045	0.0996	0.1250
0.1553	0.1689	0.1602	0.1719	0.1680	0.1572	0.1660	0.1592	0.1660	0.1611
0.1660	0.2168	0.2021	0.2207	0.1895	0.1895	0.2041	0.2275	0.2100	0.2021
0.2510	0.2539	0.2715	0.2939	0.2949	0.2929	0.2832	0.2715	0.2803	0.2949
0.3760	0.3672	0.3936	0.3799	0.3789	0.3828	0.3643	0.3730	0.3701	0.3672
0.4443	0.4902	0.4795	0.4844	0.4854	0.4795	0.4883	0.4883	0.4736	0.4854
0.5557	0.5566	0.6152	0.5527	0.5703	0.5840	0.5723	0.5830	0.5625	0.5928
0.6729	0.6826	0.6846	0.6875	0.6660	0.6660	0.6875	0.6650	0.6748	0.6484
0.7852	0.7549	0.7705	0.7578	0.7793	0.7725	0.7832	0.7568	0.7871	0.7676
0.8535	0.8545	0.8584	0.8682	0.8584	0.8467	0.8408	0.8369	0.8604	0.8477
0.8809	0.9004	0.8984	0.8711	0.8877	0.8789	0.8838	0.8877	0.8916	0.8896
0.9385	0.9395	0.9404	0.9365	0.9414	0.9414	0.9492	0.9414	0.9473	0.9395
0.9658	0.9678	0.9736	0.9717	0.9688	0.9658	0.9766	0.9639	0.9746	0.9766
0.9785	0.9766	0.9824	0.9844	0.9707	0.9756	0.9775	0.9639	0.9639	0.9775

Table D.11.: The dataset of parallel charging of q_2 in Starmon-5 on Quantum Inspire. It contains the measurement data of qubit q_2 , when charged simultaneously with qubits q_1 , q_3 & q_4 . This data was used in chapter 5, and plotted in figure 5.2.

0.0430	0.0400	0.0313	0.0674	0.0410	0.0576	0.0508	0.0430	0.0518	0.0322
0.0576	0.0664	0.0508	0.0664	0.0518	0.0410	0.0605	0.0713	0.0742	0.0566
0.0869	0.0869	0.0908	0.0908	0.0957	0.0820	0.0723	0.0781	0.0713	0.0977
0.1406	0.1172	0.1387	0.1582	0.1406	0.1465	0.1641	0.1436	0.1426	0.1572
0.1797	0.1650	0.1836	0.1953	0.1963	0.1924	0.1680	0.1895	0.1797	0.1855
0.2695	0.2539	0.2656	0.2734	0.2412	0.2637	0.2734	0.2646	0.2617	0.2783
0.3584	0.3564	0.3564	0.3516	0.3457	0.3701	0.3633	0.3584	0.3320	0.3438
0.4717	0.4600	0.4531	0.4697	0.4629	0.4678	0.4443	0.4629	0.4854	0.4463
0.5635	0.5537	0.5830	0.5557	0.5879	0.5791	0.5674	0.5459	0.5420	0.5742
0.6641	0.6787	0.6738	0.6768	0.6738	0.6582	0.6465	0.7080	0.6572	0.6836
0.7520	0.7500	0.7822	0.7666	0.7598	0.7402	0.7754	0.7656	0.7832	0.7734
0.8164	0.8555	0.8477	0.8574	0.8535	0.8379	0.8467	0.8330	0.8496	0.8398
0.8779	0.8730	0.8936	0.8730	0.8789	0.8955	0.8516	0.8750	0.8955	0.8818
0.9424	0.9346	0.9287	0.9346	0.9346	0.9385	0.9346	0.9512	0.9189	0.9316
0.9756	0.9707	0.9551	0.9600	0.9697	0.9648	0.9609	0.9619	0.9629	0.9678
0.9746	0.9814	0.9775	0.9844	0.9785	0.9756	0.9814	0.9756	0.9805	0.9805

Table D.12.: The dataset of parallel charging of q_3 in Starmon-5 on Quantum Inspire. It contains the measurement data of qubit q_3 , when charged simultaneously with qubits q_1 , q_2 & q_4 . This data was used in chapter 5, and plotted in figure 5.2.

0.0059	0.0039	0.0039	0.0068	0.0039	0.0127	0.0107	0.0078	0.0049	0.0029
0.0195	0.0146	0.0185	0.0146	0.0215	0.0205	0.0205	0.0166	0.0156	0.0185
0.0479	0.0488	0.0488	0.0498	0.0605	0.0615	0.0703	0.0605	0.0381	0.0518
0.1094	0.0898	0.0918	0.1035	0.1025	0.1338	0.1162	0.1104	0.1104	0.1035
0.1377	0.1387	0.1504	0.1250	0.1523	0.1260	0.1611	0.1494	0.1455	0.1377
0.2432	0.2295	0.2207	0.2139	0.2363	0.2393	0.2285	0.2031	0.2041	0.2500
0.3174	0.3350	0.3223	0.3369	0.3154	0.2940	0.3047	0.2920	0.3037	0.3145
0.4180	0.3945	0.4424	0.4131	0.4316	0.4443	0.4170	0.4102	0.4229	0.4170
0.5107	0.5508	0.5156	0.5147	0.5605	0.5430	0.5195	0.5381	0.5283	0.5127
0.6270	0.6006	0.6426	0.6260	0.6406	0.6191	0.6504	0.6289	0.6025	0.6016
0.7031	0.7402	0.7295	0.7158	0.7227	0.7207	0.7178	0.7207	0.7051	0.7139
0.8105	0.8027	0.8135	0.8203	0.7998	0.8164	0.8027	0.7930	0.7852	0.8115
0.8203	0.8232	0.8564	0.8320	0.8369	0.8330	0.8369	0.8486	0.8369	0.8486
0.8770	0.8760	0.9014	0.8945	0.8926	0.8896	0.8877	0.9014	0.8906	0.8780
0.9287	0.9336	0.9346	0.9180	0.9072	0.9111	0.9307	0.9307	0.9199	0.9238
0.9336	0.9307	0.9492	0.9473	0.9482	0.9473	0.9521	0.9307	0.9053	0.9150

Table D.13.: The dataset of parallel charging of q_4 in Starmon-5 on Quantum Inspire. It contains the measurement data of qubit q_4 , when charged simultaneously with qubits q_1 , q_2 & q_3 . This data was used in chapter 5, and plotted in figure 5.2.

D.4. MODULAR PULSE SHAPED AND RX GATE ON IBM MUMBAI

0.0500	0.0391	0.0332	0.0459	0.0410	0.0371	0.0352	0.0293	0.0283	0.0303
0.0570	0.0479	0.0410	0.0488	0.0400	0.0449	0.0449	0.0439	0.0518	0.0488
0.0912	0.0762	0.0703	0.0586	0.0957	0.0781	0.0723	0.0674	0.0889	0.0713
0.1495	0.1318	0.1152	0.1201	0.1279	0.1406	0.1240	0.1240	0.1260	0.1309
0.2090	0.1836	0.1875	0.1826	0.2207	0.2002	0.2002	0.1895	0.2002	0.2100
0.2938	0.2510	0.2559	0.2979	0.2822	0.2725	0.2666	0.2471	0.2930	0.2520
0.3758	0.3574	0.3652	0.3887	0.4043	0.3711	0.3662	0.3486	0.3643	0.3564
0.4615	0.4473	0.4561	0.4609	0.4941	0.4502	0.4551	0.4717	0.4570	0.4365
0.5468	0.5527	0.5449	0.5742	0.5557	0.5566	0.5400	0.5723	0.5781	0.5518
0.6548	0.6563	0.6602	0.6299	0.6572	0.6445	0.6494	0.6318	0.6445	0.6348
0.7243	0.7246	0.7031	0.7383	0.7275	0.7139	0.7334	0.7578	0.7461	0.7422
0.8073	0.8184	0.8232	0.8018	0.8135	0.8193	0.8037	0.7959	0.8281	0.8184
0.8620	0.8730	0.8857	0.8916	0.8955	0.8818	0.8926	0.8936	0.8750	0.8721
0.9160	0.9473	0.9414	0.9424	0.9365	0.9443	0.9434	0.9424	0.9375	0.9365
0.9485	0.9639	0.9668	0.9648	0.9756	0.9580	0.9648	0.9678	0.9746	0.9580
0.9533	0.9854	0.9854	0.9766	0.9785	0.9814	0.9844	0.9785	0.9805	0.9824

Table D.14.: Data set of charging using the $R_x(\theta)$ gate implementation on q_0 of IBM Mumbai. This dataset was used for Appendix A.

0.0381	0.0234	0.0361	0.0381	0.0332	0.0273	0.0342	0.0381	0.0400	0.0332
0.0361	0.0400	0.0332	0.0518	0.0400	0.0420	0.0469	0.0449	0.0371	0.0479
0.0576	0.0625	0.0625	0.0684	0.0645	0.0654	0.0811	0.0713	0.0732	0.0723
0.1172	0.1211	0.1221	0.1230	0.1191	0.1133	0.1074	0.1143	0.1035	0.1064
0.1816	0.1758	0.1562	0.1631	0.1553	0.1797	0.1680	0.1670	0.1689	0.1885
0.2646	0.2402	0.2207	0.2529	0.2471	0.2686	0.2588	0.2500	0.2432	0.2734
0.3291	0.3252	0.3047	0.3135	0.3398	0.3301	0.3330	0.3467	0.3564	0.3398
0.4365	0.4521	0.3838	0.4326	0.4219	0.4424	0.4717	0.4111	0.4414	0.4521
0.5205	0.5195	0.5176	0.5527	0.5420	0.5156	0.5186	0.5283	0.5068	0.5186
0.6572	0.6074	0.6250	0.6162	0.5459	0.6016	0.6084	0.6191	0.6250	0.5977
0.6973	0.7305	0.6934	0.6904	0.6348	0.7109	0.7129	0.7158	0.7373	0.7080
0.8096	0.7822	0.7754	0.7988	0.7822	0.7822	0.7861	0.7852	0.7949	0.7891
0.8818	0.8506	0.8711	0.8828	0.7764	0.8740	0.8564	0.8613	0.8623	0.8438
0.8965	0.9082	0.9111	0.9219	0.8994	0.9150	0.9092	0.9092	0.9229	0.9219
0.9502	0.9512	0.9482	0.9434	0.9551	0.9551	0.9531	0.9629	0.9570	0.9541
0.9678	0.9785	0.9824	0.9805	0.9697	0.9756	0.9697	0.9805	0.9766	0.9746

Table D.15.: Data set of charging using the modular Gaussian pulse on qubit q_0 of IBM Mumbai. This dataset was used for Appendix A.

D.5. OPTIMISED PULSE ON IBM BRISBANE

D

Experiment	η
1	0.9111
2	0.9082
3	0.9062
4	0.8887
5	0.9004
6	0.9150
7	0.9004
8	0.9307
9	0.8975
10	0.9180

Table D.16.: Data set of the optimised pulse implemented on qubit q_0 of IBM Brisbane. This data is used in Appendix B.